CFD Modelling of a Rotary Lime Kiln

A Thesis submitted in partial fulfilment of the requirements for the Degree of a Master in Engineering specialising in Mechanical Engineering at the University of Canterbury

James Macphee

Department of Mechanical Engineering
University of Canterbury
Christchurch, New Zealand
January 2010

Acknowledgements

Firstly I would like to thank my supervisors, Mathieu Sellier and Mark Jermy, for the opportunity they gave me to undertake this project and the guidance and supported offered throughout it.

Thanks also go to my mentor Edilberto Tadulan, from McDonald's Lime, for his guidance and technical assistance provided during the project

I would like to thank the Foundation for Research, Science and Technology (FRST) for the Technology in Industry Fellowship (TIF), and subsequent financial assistance, granted which allowed me to undertake the project.

Special thanks goes to John and Karen Prescott for the hospitable accommodation they provided whilst I was working on site at McDonald's Lime in Otorohanga.

Finally, and most importantly, I would like to thank Mum and Dad for their continued, and generous, support of my education over the last 24 years. Without it this thesis would have never been possible.

Abstract

McDonalds Lime Ltd, situated in Otorohanga, New Zealand, operate two dry process rotary lime kilns producing burnt and hydrated lime for a range of industries including agriculture, roading, water treatment, gold mining and steel making. The following Technology in Industry Fellowship (TIF) funded Masters Project is structured around investigating the combustion characteristics of Kiln Two at McDonald's Lime Ltd using Computational Fluid Dynamics (CFD).

Numerical results obtained using the commercial CFD code FLUENT were first validated against experimental data from the International Flame Research Foundation's (IFRF) Furnace No.1. The validation study focussed on comparing the finite rate and mixture fraction/PDF approaches to combustion chemistry, as well as different methods for defining coal particle size distributions.

Numerical modelling of Kiln Two at McDonald's Lime Ltd began with full three-dimensional simulations, however due to their complexity and large computational times, two-dimensional axisymmetric models were primarily used for investigations. Comparisons were made between the two approaches. Investigations into the original pulverised coal fired system focussed on how the kiln aerodynamics and heat transfer properties were affected by changes to the coal and air inlet properties. The performance of a recently installed waste oil firing system was also investigated, with results showing that firing the kiln with a 25% thermal substitution of oil is the most efficient mode of operation. As the investigations focussed on the combustion characteristics the effects of the reacting limestone bed were ignored in all simulations.

CFD modelling of the combustion characteristics within a large scale rotary kiln proved to be an extremely complex task. The work presented in this thesis has, however, provided some promising results which will assist kiln operators understand the effects of changing different operating parameters, and ultimately enable McDonald's Lime to reduce their operating costs and environmental impact. Furthermore, the project has laid the foundation for further investigations into the combustion of waste fuels in rotary kilns.

Table of Contents

1 Introduction

As global warming continues to impact on the environment within which we live, the burning of fossil fuels as a source of energy is being placed under increased political and social scrutiny. As a result, industrial users of fossil fuels are being forced to either scale back consumption, or find ways to reduce total CO_2 emissions, while maintaining current production rates. Concurrently, there continues a global push towards recycling used products in order to prevent the waste of potentially useful materials and reduce the consumption of fresh raw materials, energy usage and water pollution from land fill.

These factors, combined with the ever-increasing cost of fossil fuels, have lead to significant research into combustion systems over the last decade. Many industries have moved to firing waste products, particularly biomass and waste oil, as a substitute for common fossil fuels such as coal. Meanwhile advanced technologies such as Computational Fluid Dynamics are being used to improve designs in an effort to increase combustion efficiency and reduce pollutant emissions.

McDonalds Lime Ltd situated in Otorohanga, New Zealand consumes a significant amount of coal during its production of various lime products. Originally founded in 1865 on the Otago Peninsula, McDonalds Lime are today located in the Waitomo region and part owned by Holcim (NZ Limited and New Zealoand Steel. McDonalds Lime operate New Zealands largest limestone quarry at the 67 hectare Oparure site which feeds the two largest rotary kilns in the country at their Otorohanga plant. The Oparure operation excavates high grade calcium-rich limestone from the ground before passing it through a series of crushing and screening operations, the details of which depend on the final product type. Much of the lime is transported to the Otorohanga complex for production into burnt and hydrated lime. McDonalds Lime has a wide customer base that includes the agricultural, mining, timber, water treatment,

manufacturing, steel refining and roading industries, both within New Zealand and around the pacific. The work of this thesis focuses on the combustion processes occurring within the larger of McDonalds Lime's two kilns, Kiln Two.

Figure 1: McDonalds Lime Ltd's Oparuare quarry (top) and Otorohanga plant (bottom).

1.1 Rotary Lime Kilns

A rotary lime kiln, as demonstrated in Figure 2, is essentially a long, direct-contact, counter-flow heat exchanger. The kiln is slightly sloped and rotates about its axis at approximately 1 RPM. Primary air and fuel enters through the burner pipe with additional hot secondary combustion air entering through the kiln hood. Raw limestone is fed from the elevated end and slowly moves down the kiln by the combined effects of gravity and rotation, before dropping out at the hot burner end into a cooler. The endothermic reaction (Eq. 1) that takes place in the kiln uses the hot flowing gases to decompose raw limestone ($CaCO_3$) and form calcium oxide, CaO, otherwise known as burnt lime. Hydrated lime can

then be formed through a strongly exothermic reaction by adding water to the burnt lime (Eq. 2).

$$CaCO_3 + heat \rightarrow CaO + CO_2 \quad (1)$$

$$CaO + H_2O \rightarrow Ca(OH)_2 \quad (2)$$

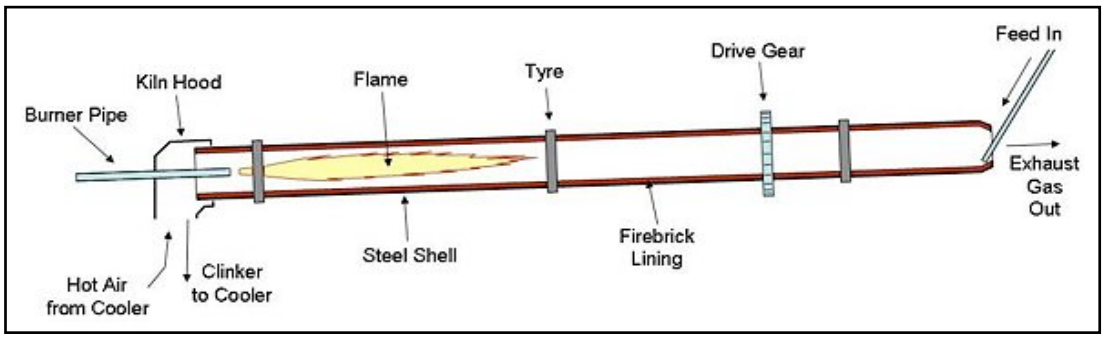

Figure 2: Schematic of a rotary lime kiln *(Wikipedia, 2009)*.

Figure 3: Kiln Two at McDonalds Lime.

Kiln Two at McDonalds Lime is approximately 50 metres long and until recently has been solely fired using pulverised coal. The kiln produces approximately 300 tonnes of burnt lime per day requiring in excess of 200 tonnes of coal. The kiln was installed at McDonalds Lime in the early 1980s, however since then it has undergone a number of changes, the most notable being the addition of a

KVS preheater which preheats the incoming raw limestone using kiln exhaust gases.

1.2 Previous Research

Fuel and Combustion Technologies (FCT) have previously investigated the operation of Kiln Two at McDonald's Lime. The initial study by FCT (FCT, 1997a) found that the previous Atritor coal mill provided inadequate primary air velocities and a coarse coal grind which resulted in flame impingement on the refractory wall, fires in the coal ductwork, an undesirable heat transfer pattern, and the formation of an ash ring in the kiln. FCT conducted a further series of acid/alkali scale model experiments and confirmed the need for improvements in the burner design (FCT, 1997b). The experiments suggested that a high momentum burner placed in the correct location would overcome poor aerodynamics and prevent flame impingement. The replacement of the Atritor mill with a higher capacity Raymond Mill led to a significant improvement in the kiln operation by reducing many of the undesirable phenomena that were occurring. While less prominent than in the past, ash rings unfortunately continue to form in the McDonalds kiln, leading to several hours of downtime each week as they are removed.

1.3 Current Research

With the ever-increasing cost of raw coal, the associated transport costs of imported low sulphur coal, and the global desire to recycle waste materials McDonalds Lime have turned to waste oil, primarily from ship slops, as a way to reduce the thermal cost of producing lime. McDonald's Lime have recently implemented a waste oil firing system, which involved placing a lance down the centre of the existing single tube burner pipe in Kiln Two. On the end of the lance is a Laval Nozzle which sprays vaporised waste oil into the kiln as a substitution for a proportion of the pulverised coal. McDonalds Lime would like to investigate the performance of this oil-fired system using CFD.

Additionally the company would like to investigate the performance of the original coal fired system and further investigate the formation of ash rings and remedy any combustion processes that may be assisting in their formation. Finally McDonalds Lime would like to improve the overall combustion efficiencies of their kiln and reduce greenhouse gas emissions. Much of the latter is, however, outside the scope of the current project.

To achieve the objectives detailed above, McDonald's Lime have turned to numerical modelling for assistance. Numerical methods such as Computational Fluid Dynamics (CFD) allow the testing of many variable combustion parameters that are either impossible to test on full-scale equipment, or time consuming, expensive and inaccurate with small-scale experiments. CFD has gained widespread recognition as a useful tool for studying pulverised coal flames, especially for bitumous coals (Bosoaga et al., 2006). The use of CFD allows the analysis of a system involving heat transfer, fluid flow, combustion, turbulence and pollutant emissions and thus is obviously an attractive solution for investigating the combustion characteristics of the McDonald's Lime kiln.

The research presented in this thesis uses the commercial CFD code FLUENT (v6.3 and v12) to investigate the steady state combustion characteristics of Kiln Two at McDonalds Lime, both for the original coal firing system and a hybrid coal and oil firing system. FLUENT contains a number of sub-models to account for the processes occurring during coal combustion. These include heating, devolatilization, and volatile and char combustion, together with the transport of spherical coal and ash particles. The outcome of the numerical modelling aims to provide a detailed understanding of the combustion processes occurring in Kiln Two for both firing systems. Aspects of the original coal firing system such as recirculation and its effect on the ash ring will be investigated, as well as the effects of coal flow rate on temperature profile. Modelling of the oil firing system ultimately aims to illustrate the design characteristics required for the coal and oil fired systems to operate with the same characteristics.

Chapter Two of this thesis details the scope and objectives of the project while Chapter Three provides a review of previous research into rotary lime kilns and combustion related issues including burner design, combustion aerodynamics, heat transfer processes and recent multidimensional modelling work. Chapter Four describes the methodology of Computational Fluid Dynamics. Chapter Five investigates the accuracy of using FLUENT for combustion modelling using a validation study of the International Flame Research Foundations (IFRF) Furnace No.1. Chapter Six lays out the operating conditions the McDonalds Lime Kiln Two and Chapter Seven then investigates the performance of two and three dimensional modelling approaches for Kiln Two. Chapter Eight details the results of coal-only modelling of the McDonalds kiln while Chapter Nine presents results for the hybrid coal and oil fired kiln. Chapter Ten presents conclusions and recommendations that have been drawn from the presented results and finally Chapter Eleven suggests future work that could be undertaken.

2 Scope and Objectives

As has been outlined in the previous chapter, McDonald's Lime wishes to use numerical modelling as a tool for optimizing the design and operation of one of their coal fired, rotary lime kilns. The aim of the current research is to develop numerical models of Kiln Two using the commercial CFD code, FLUENT, and subsequently assist kiln operators, engineers and management at McDonald's Lime to improve the efficiency of their operation. The work presented in this thesis focuses on the flame characteristics and the changes that arise by adjusting various operating parameters. With the aid of numerical tools such as FLUENT, the scope of the project has the potential to be much greater and therefore it is important to define the objectives of the present study. Those objectives are achieved in the scope of the following steps:

- Conduct a validation study to determine the accuracy of FLUENT for investigating combustion characteristics.
- Develop a three-dimensional numerical model of Kiln Two at McDonald's Lime based on the normal operating conditions.
- Investigate changes to the operating parameters of the current coal fired kiln and how these changes may influence ash ring formation, operating costs and the environmental impact.
- Develop a numerical model to investigate the performance of Kiln Two when fired with a partial fuel substitution of waste oil.

It is worth noting aspects that are outside the scope of the present study.

- Modelling heat transfer through the kiln walls.
- Modelling the chemical decomposition of the reacting limestone bed and the subsequent release of CO_2.

3 Literature Review

The following chapter presents a brief synopsis of current literature available on rotary kilns and associated components. Much of the material researched throughout this project relates to rotary cement kilns, a key piece of equipment used during cement production. While the reactions and characteristics of the bed are very different, the flame aerodynamics and heat transfer processes occurring in a cement kiln are very similar to those in a lime kiln.

3.1 Combustion Aerodynamics

Combustion involves the exothermic oxidation of a fuel, during which it undergoes a series of steps (FCT, 1997a).

MIXING – IGNITION – CHEMICAL REACTION – DISPERSAL OF PRODUCTS

In most reactions the rate of the mixing process is much slower than the final three steps. Therefore, to ensure an efficient combustion process, adequate air must be supplied to the fuel stream to obtain fast and effective mixing of the two reactants before ignition occurs. The rate, and amount, of mixing thus controls the overall rate of combustion, which explains the commonly heard expression, "If it's mixed, it's burnt".

While adequate air must be supplied to ensure efficient mixing with the fuel stream, the amount of air supplied must be carefully controlled. Any excess air added to the kiln must be heated to the kiln back-end temperature, reducing the kiln efficiency and causing unnecessary heat loss through the flue gases. More significantly however is that the increased airflow through the cooler causes a reduction in the secondary air temperature and consequently flame temperatures, meaning that even more fuel is required to heat the bed to the required temperature. Overall, the total increase in fuel consumption is much

greater than that required to simply heat the excess air to the back end temperature (Figure 4).

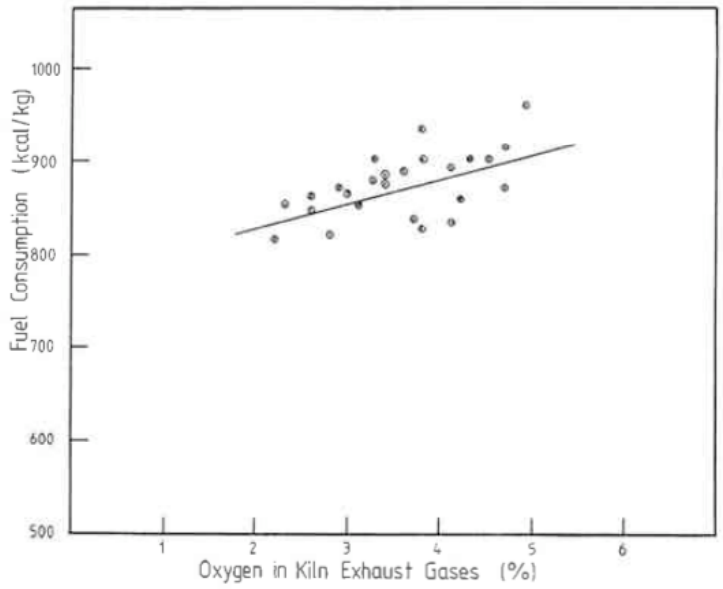

Figure 4: Effect of excess air on fuel consumption *(Mullinger, 1987).*

Meanwhile, if low levels of oxygen are supplied incomplete combustion will occur, which again means additional fuel is required to achieve the required heat transfer to the calcinating bed. The heat loss through the flue gases also increases with low excess oxygen levels due to the incomplete combustion of carbon. Figure 5 demonstrates how the supplied oxygen level affects the heat losses of a rotary kiln. An efficient kiln/burner will obtain minimum heat loss with low levels of excess oxygen.

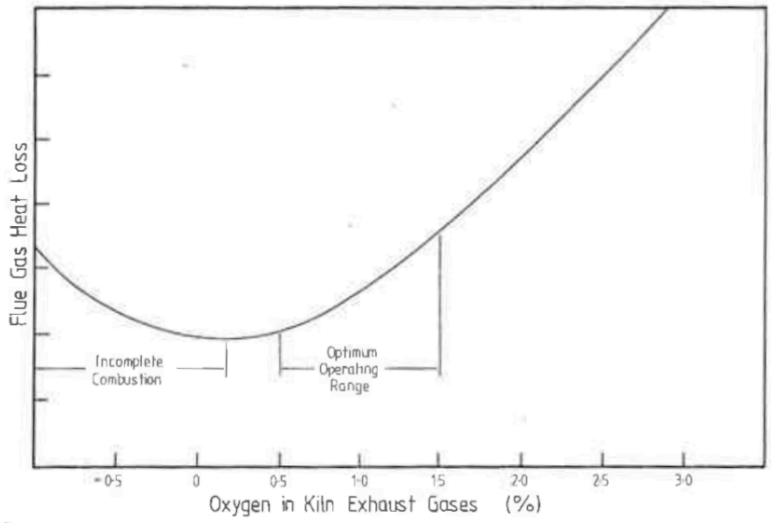

Figure 5: Effects of kiln oxygen on flue gas heat loss *(Mullinger, 1987).*

The mixing of fuel and air in a rotary kiln burner like that at McDonald's Lime occurs by entrainment of secondary air into the primary air and fuel jet. An additional stream of swirling air can also be used to promote turbulent mixing. The secondary air entering through the firing hood typically has momentum at least one order of magnitude lower than the fuel jet (Georgallis, 2004). The shear between the two streams causes the secondary stream to be accelerated to the velocity of the fuel jet causing it to expand outwards. This process continues until the momentum of the fuel jet is the same as its surroundings. If, however, the fuel jet has a momentum in excess of what is required for the complete entrainment of the secondary air stream, recirculation of combustion gases can occur as is demonstrated in Figure 6. This phenomenon is a good indication that the mixing process is complete and can prevent the flame from impinging on the kiln wall, a process that can cause damage to the refractory and excess heat transfer to the bed.

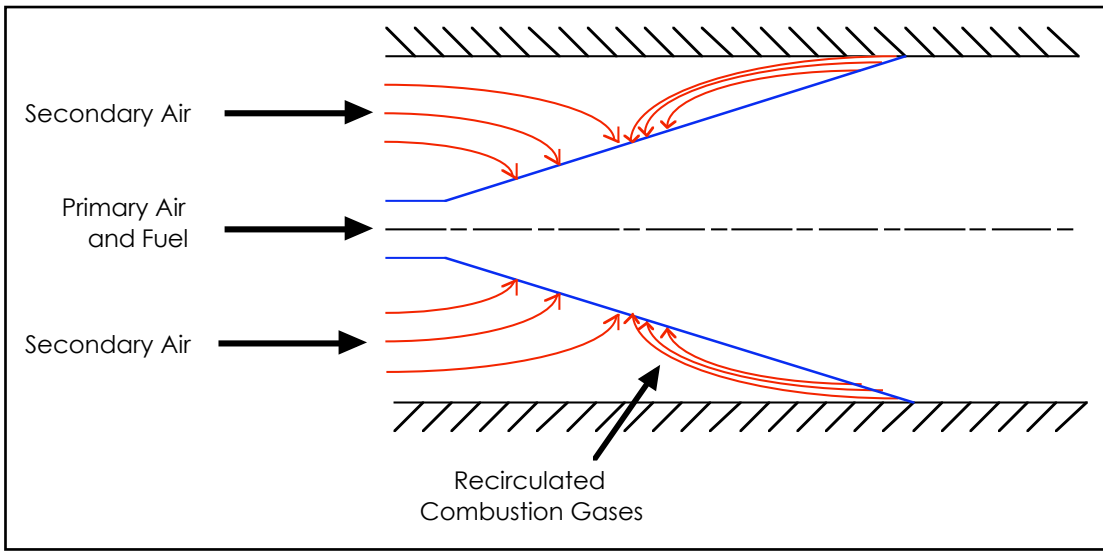

Figure 6: Recirculation in a confined jet.

Craya and Curtet (1955) defined the dimensionless parameter '*m*' to describe the onset of recirculation by simplifying the equations of motion for a constant density fluid and considering experimental observations. The parameter '*m*' is a function of the excess discharge ratio, *R*, which is the ratio of the excess volumetric flow rate of the primary discharge, *q*, to the total volumetric flow rate, *Q*. Their analysis relates *m* to *R* as follows:

$$m = R - 1.5R^2 + 0.579\frac{R^2}{\left(r_p / r_s\right)^2} \tag{3}$$

where : $$R = q/Q \tag{4}$$

$$q = \pi r_p^2\left(u_p - u_s\right) \tag{5}$$

$$Q = \pi\left(r_s - \delta^*\right)u_s + q \tag{6}$$

Here u_p and u_s are the average velocities for the primary and secondary flows. The boundary layer displacement thickness δ^* is usually negligible. Recirculation occurs for a Craya-Curtet parameter of approximately $m > 1.5$ (Georgallis, 2004).

3.2 Ash Rings

As has previously been mentioned, McDonald's Lime has issues with ring formation in Kiln Two. Rings are caused by a number of factors, including raw material composition and aerodynamic factors. In coal fired lime kilns the usual cause is a combination between the coal ash and newly calcined product. The aerodynamics of the kiln, the coal characteristics, coal fineness and the design of the burner all interact and, in unfavourable circumstances, can result in substantial ring problems.

In 1997 Fuel and Combustion Technologies were employed by McDonald's Lime to investigate their problems of ash ring formation (FCT, 1997a, 1997b). FCT concluded that the cause of the ash ring formation was a combination of coarse coal particles and flame impingement. At this time they described the probable mechanism of ring formation to be as follows:

- The coarse coal particles produced by the Atritor coal mill are too heavy to remain buoyant in the flame thus dropping out in the feed material in the flame impingement region.
- The high heat transfer to the feed prior to it entering this zone ensures that it is largely calcined. Hence the surface temperature will be high,

promoting a combination of the ash and lime to form, producing cement like material.

- This material sinters in the area of the flame impingement because reducing conditions lower the fusion temperature and a ring starts to form.
- As the ring reduces the effective kiln diameter, flame impingement increases, the area for particles to impact on increases and consequentially the ash ring grows rapidly.

FCT advised McDonald's Lime that resolution of the ash ring problem would require an upgrade of the coal firing system, based around a suitable coal mill and incorporating optimised primary air. Using a number of physical and mathematical models FCT found that a high momentum burner should be installed to overcome the poor kiln aerodynamics and prevent flame impingement. They recommended that the burner should be designed for a Craya-Curtet parameter of 2.46 at 31.5% Primary Air. FCT also suggested that the burner length should be such that the tip is level with the leading edge of the modified dam ring throat, in order to produce the most stable operating environment. Finally FCT suggested a number of suitable coal mills that would provide the desired coal grind. Polacsek (1992) also explains that a swirling air burner can reduce the chances of ash ring formation by promoting better mixing of fuel and air thus leading to less unburnt coal dropping into the bed.

As a result of the FCT reports McDonald's Lime replaced the Atritor coal mill with a Raymond mill and made some minor adjustments to the burner configuration. While these changes have meant that ash rings do not form as prominently as they did previously, they are still considered a problem and can cause down time every 10-12 days as the kiln burners use a modified shot gun to shoot the ash free from the refractory walls. As a result McDonald's Lime would like to further investigate the issue using numerical modelling, with the intention of understanding the characteristics of the heat transfer and flame aerodynamics that assist in the formation of an ash ring.

3.3 Coal Combustion

Coal is the most abundant fossil fuel accounting for 40% of the worlds overall energy use and 34% of the world's electricity generation, most of which uses the pulverised form. The effects of global warming and a concern for toxic atmospheric pollution have seen coal consumption decline in developed countries, especially those that agreed to reduce CO_2 emissions via the Kyoto protocol. There continues, however, to be vast growth of coal fired energy generation in developing countries.

The combustion of pulverised coal evolves in five partial processes. Convective and radiative heating first dries the particles; devolatilisation occurs as the particle temperature increases; the particle ignites; volatile matter combusts and finally the residual char combusts. A small portion of residual ash remains after the five steps are complete. The overall process is outlined in Figure 7.

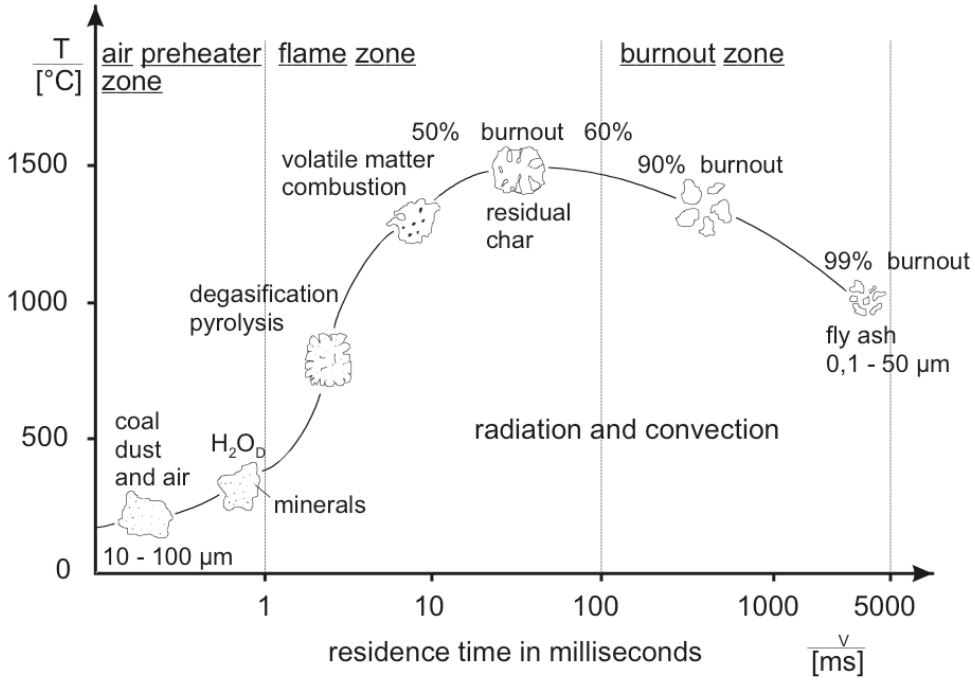

Figure 7: Schematic drawing of the combustion processes during pulverised coal firing *(Burgerscentrum, 2005)*.

The heating rate and final temperature of a coal particle holds great importance as it determines the characteristics of the evolved volatiles and the topography

of the remaining char. Consequently, this has a large effect on the flame properties, especially in the near burner region (Weber, Peters, Breithaupt, & Visser, 1995). While the convective and radiative heating of a coal particle during combustion would appear a relatively simple detail, there continues to be difficulties in quantitatively defining the heat transfer, as the outwards mass flow rate of volatiles is believed to have an effect on heat transfer to the particle. There are also difficulties that arise in predicting the specific heat of a coal particle given that it is a function of temperature and thus varies during the devolatilisation process (Williams, Pourkashanian, & Jones, 2001).

When injected into a flame such as that in a rotary lime kiln, coal particles are rapidly heated at rates higher than 10^4 K/s. Under such rapid heating conditions, substantially more volatiles are given off than under low heating conditions (1K/s) (Peters & Weber, 1996). For this reason, the proximate volatile matter content (ASTM) cannot be used during numerical modelling of devolatilisation rates. Instead, the so-called high-temperature volatile matter yield must be used. Peters and Weber undertook a number of Coal Characterization investigations and found most high-volatile coals exceeded the proximate volatile matter content by a factor of 1.6 to 1.7. This does not however apply for all coal ranks and thus the high-temperature volatile matter yield should ideally be obtained for each individual coal being modelled.

The Chemical Percolation Devolatilisation (CPD) model (Pugmire, Solum, & Grant, 1992) can be used to obtain the high-temperature volatile matter yield for a particular coal. The CPD model describes the devolatilisation behaviour of rapidly heated coal based on the chemical structure of the parent coal. The chemical structure of the parent coal is obtained using C NMR spectroscopy, a process which describes features such as the number of aromatic carbons per cluster and the number of attachments per aromatic cluster (Genetti & Fletcher, 1999). Analysing the structure of coal particles using C NMR spectroscopy is clearly a very complex procedure, not to mention expensive and time consuming. For these reasons Genetti and Fletcher developed a series of non-linear

correlations to estimate the structural parameters of coal when raw C NMR data is not available. Correlated C NMR data can then be used to find the required devolatilisation information.

During the coal devolatilisation process the volatiles undergo a mass transfer process from the solid coal particle to the surrounding gaseous phase. Here the volatiles oxidise with the surrounding combustion air following the commonly assumed reactions listed below:

$$Volatiles + O_2 \rightarrow CO + H_2O \quad (7)$$

$$CO + 0.5O_2 \rightarrow CO_2 \quad (8)$$

There are a number of different volatile gases that evolve into the gaseous phase. Figure 8 provides information on the composition of volatiles that evolve from a selection of coals.

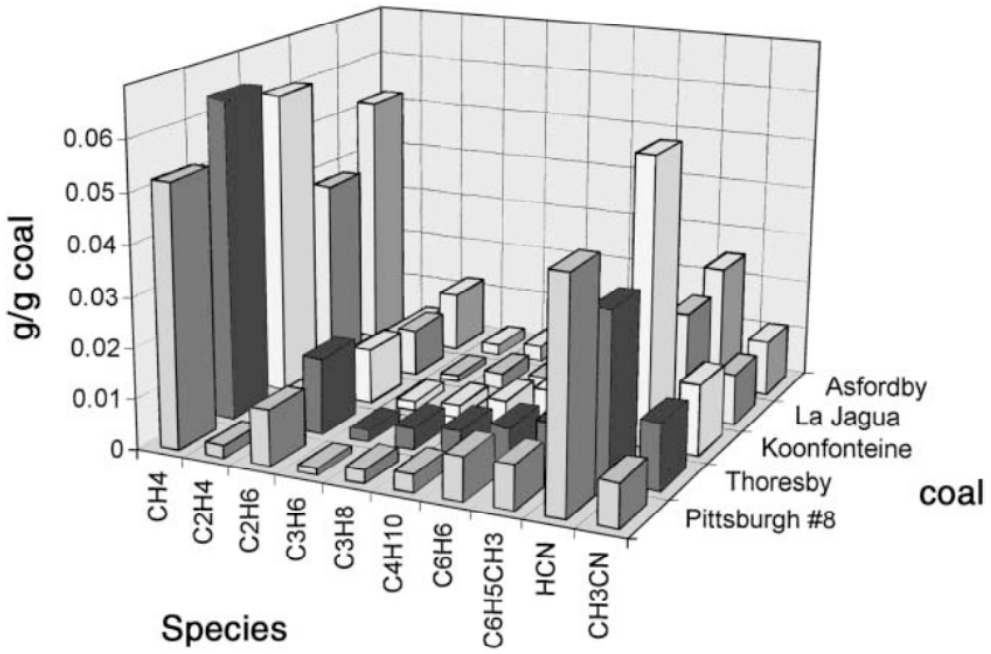

Figure 8: Composition of volatiles during pyrolysis for a selection of coals: Pittsburgh 8 (USA), Thoresby (UK), Koonfonteine (SA), La Jagua (Indonesia) ***(Williams et al., 2001).***

Once all of the volatile matter has evolved an oxidising reaction begins that consumes the combustible fraction of a coal particle. Despite extensive research into char combustion over the last forty years the mechanism of the oxidising

reaction is still not fully understood. However, factors that are known to affect the char combustion reaction include particle growth, mass transfer effects, particle size, char mineral content and fragmentation of the char particle. The limiting step however for the combustion process is commonly considered to be either the chemical reaction or gaseous diffusion to the particle, or a combination of both these (Williams et al., 2001).

Weber et al. (1995) does describe the generally assumed reaction mechanism of pulverised coal particles. On the surface and in the pores of the particle the char first reacts with oxygen to form CO and then inside a certain particle boundary layer this CO reacts further to give CO_2. The authors suggest that it is more likely that some of the char reacts directly to CO_2 in the very close vicinity of the coal particle, the amount being dependant on the gaseous phase temperature. The author proposes that as the boundary layer is probably much smaller than the surrounding turbulent eddy, it could be said that all char reacts directly to CO_2 given that the CO cannot be transported away from the particle before reacting to give CO_2.

3.4 Particle Size Distribution

A common method for defining the size of pulverised coal particles is by using a Rosin-Rammler distribution. The Rosin Rammler distribution function is based on the assumption that an exponential relationship exists between the particle diameter, d, and the mass fraction of the particles with diameter greater than d, Y_d:

$$Y_d = e^{-(d/\bar{d})^n} \tag{9}$$

Fluent refers to the quantity d in Equation 9 as the Mean Diameter and to n as the Spread Parameter. To solve for these parameters, the provided particle size data (ie. a sieve analysis) must be fitted to the Rosin-Rammler exponential equation. To achieve this the data must first be recast in the Rosin-Rammler format, as shown in Table 1.

Table 1: Example particle size data in Rosin-Rammler format

Diameter, d (μm)	Mass fraction with Diameter Greater than d, Y_d
70	0.95
100	0.85
120	0.50
150	0.20
180	0.05
200	(0.00)

A plot of Yd vs d for the example coal size data is shown in Figure 9.

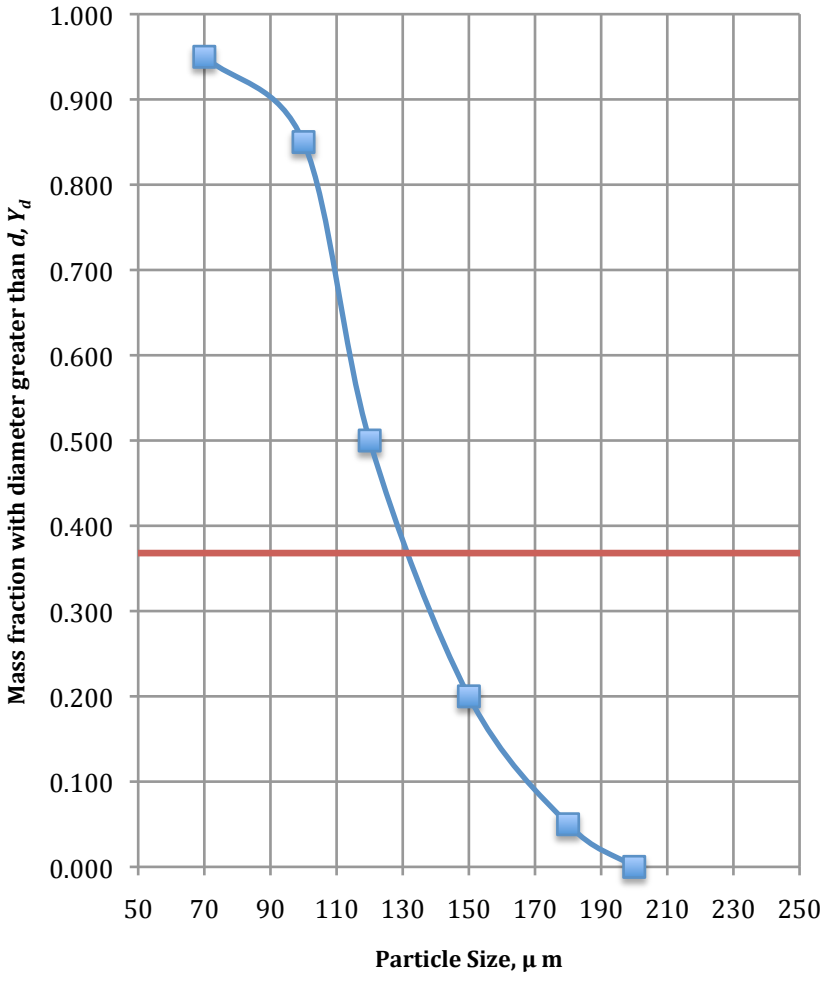

Figure 9: Cumulative size distribution of particles.

From here the values of $\bar{d}$ and n can be derived. The value for $\bar{d}$ is obtained by noting that this is the value of d at which $Y_d = e^{-1} \approx 0.368$. From Figure 9 it can be estimated that this occurs for $d \approx 131 \mu m$. The numerical value for n is given by

$$n = \frac{\ln(-\ln Y_d)}{\ln(d/\bar{d})} \tag{10}$$

By substituting the given data pairs for Y_d and $d/\bar{d}$ into Equation 10 it is possible to obtain values for n and then find an average. Doing so yields an average of $n = 4.52$ for the provided data. The resulting Rosin-Rammler curve fit is compared to the sieve analysis data in Figure 10.

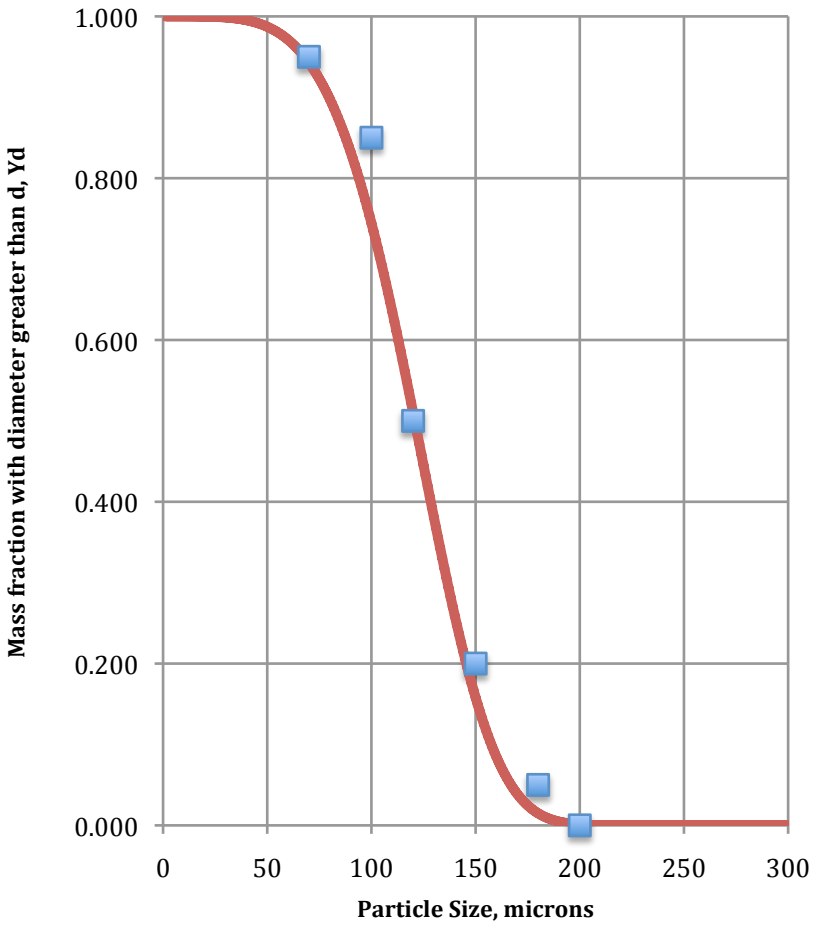

Figure 10: Rosin-Rammler curve fit for the provided sieve analysis data.

When using a Rosin–Rammler size distribution in Fluent the complete range of sizes is divided into an adequate number of discrete intervals, each of which is represented by a mean diameter for which trajectory calculations are performed.

3.5 Liquid Fuel Combustion

In numerous practical applications, the fuel supplied to an engine or burnt in a furnace is a liquid. Petrol for internal combustion engines, heavy oil for industrial burners and kerosene for turbo-jets are all liquid fuels. Even in the case of a candle it is actually the melted wax that is soaked up by the wick that burns. In all of these cases, however, it is not the liquid that burns, rather it is vaporised by the heat of the flame, usually decomposing to a certain extent in the process, and is then drawn towards the gaseous oxidant at which point combustion occurs (Borghi & Destriau, 1998).

To demonstrate the process of liquid fuel combustion further we consider the example of a small amount of alcohol heated in a spoon and then lit. Once combustion is established, a stable gaseous flame forms above the surface of the liquid. The heat produced by the flame acts in several ways. It heats up the surface of the liquid by conduction (and often by radiation) causing the liquid to vaporise, and then it heats these vapors as they approach the flame. In addition, the flame heats the air diffusing towards the flame, such that a reaction zone is sustained between the fuel and oxidant vapors in exactly the same way as a classical gas-phase diffusion flame. Figure 11 shows the situations schematically.

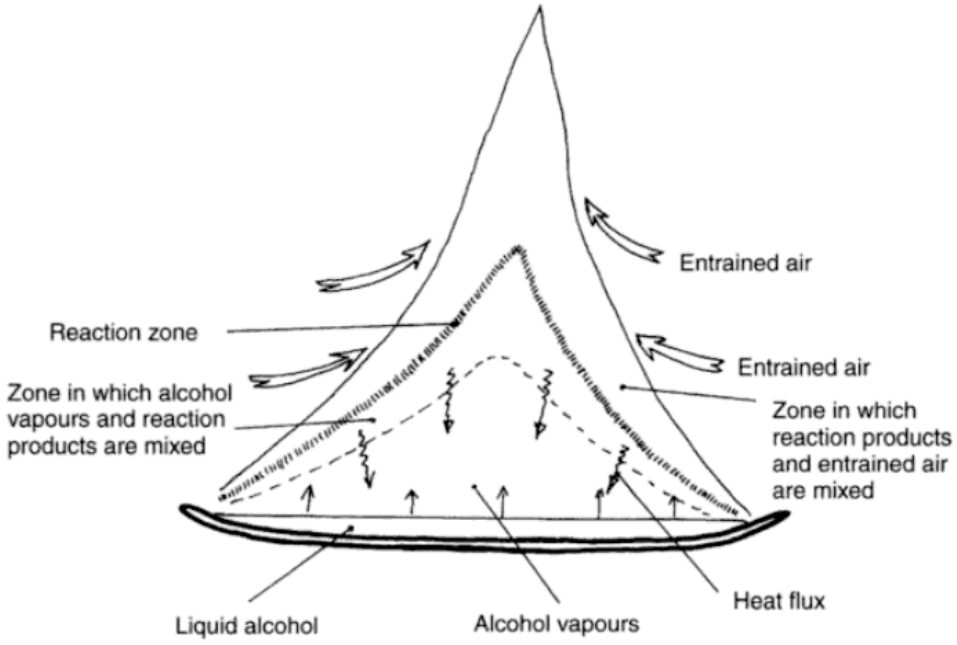

Figure 11: A simple experiment demonstrating liquid combustion *(Borghi & Destriau, 1998).*

Since the flame is self-sustaining close to the liquid surface, in practical applications, the best way to increase the amount of "combustion per unit volume" is to maximise the air-liquid contact area. This is the reason why all burners that operate with liquid fuel inject the fuel into the combustion area in the form of a spray of droplets. Obviously the degree of vaporisation will have an effect on the flame characteristics and this is one area that will be investigated for the McDonald's Lime waste oil firing system.

3.6 Rotary Kiln Burners

The burner in a rotary kiln has a significant influence on the fuel consumption, the final product quality, the surface life of refractory walls, the composition of exhaust gases and consequently, the environmental impact. Ultimately however, a burner must generate a flame that ensures suitable heat transfer to the charge. Although chemistry and fuel characteristics can play an important role in flame stability, it is the kiln aerodynamics, and consequently the burner, that almost solely dictate the flame shape and length. Combustion reactions are so fast at flame temperatures that the overall combustion of fuel, and subsequent heat release, proceed as fast as the fuel is brought in contact with the air (or more properly, with the oxygen in the air) (Gorog & Adams, 1987).

In the case of a long "lazy" flame the bed remains at a fairly constant temperature throughout the kiln, which may not be hot enough for the calcination reaction to take place. Conversely a flame that releases all of its heat in the first three metres of a kiln would merely overheat the front end of the kiln and the product would reach the hot zone at too low a temperature for any but the surface of the bed to react. What actually is required is a flame that is shaped and located so as to give the desired temperatures in the proper locations in the kiln, with the hot products of combustion performing the preheating, drying and heating functions (Garnick, 1963). Figure 12 displays the optimum heat transfer characteristics of a rotary kiln used for lime manufacture.

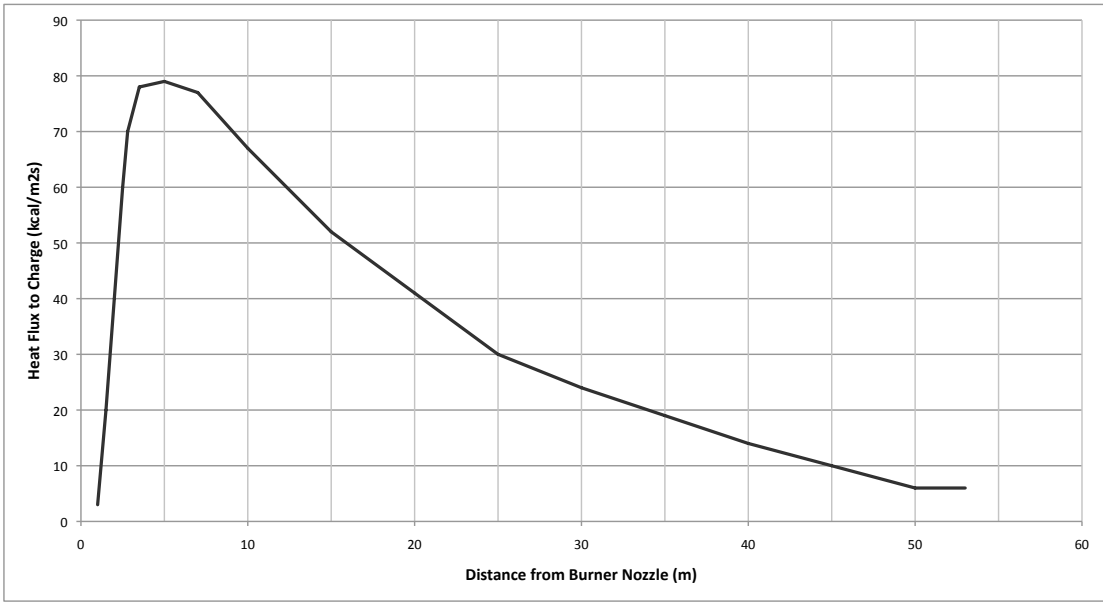

Figure 12: Optimum heat transfer characteristics for lime manufacture *(FCT, 1997a).*

Having recognised the need for control of the flame shape and location, the problem becomes how to achieve this optimum flame. In the case of modern multi channel burners there is often a number of variables that can be adjusted, such as axial and swirl air velocities; fuel type, rate and supply pressure; and lastly the burner configuration and setup. Single channel pulverised coal burners like those still used by McDonald's Lime are however long established technology and allow for little adjustment to the flame shape and location. Primary adjustments of the flame characteristics are made by adjustment of the primary air velocity with some additional adjustment possible through movement of the burner location.

The addition of a waste oil lance in the centre of the single channel burner pipe at McDonald's Lime will allow for greater adjustment of the flame shape and location. Garnick (1963) reports on the gas and oil firing of rotary kilns and describes how fuel oil supplied at 1000psig will have a high velocity leaving the burner and will tend to travel far down the kiln before it is all burned out. On the other hand feeding gas or oil at low pressures in general tends to create a shorter flame.

As most kilns use combustion air from a cooler there was a tendency in the 1960s to cut down on primary air because it is usually supplied at ambient, or close to ambient temperatures, and is therefore less efficient. Garnick, however, highlighted the importance of primary air in order to obtain the proper flame shape, increase productivity and have a higher quality product for each MJ of fuel inputted. Thus the use of 20 to 30 percent primary air is recommended by the author to give the desired flame shape that may well outweigh the loss in efficiency caused by the use of cold primary air.

The final method of controlling flame shape for an oil-fired system is through changes to the burner itself. The degree of atomization and the spray angle of the oil issuing from the atomizer will likely affect the flame pattern. This can often be adjusted simply by changing the oil nozzle socket. Many liquid fuel atomizers for rotary kilns are however designed to prevent fuel oil impingement on the kiln lining. This means that they invariably have a narrow spray angle which can only be obtained at the expense of atomizing efficiency (Cresswell, 1970). Primary air flow, spray angle, atomization and supply pressure are all aspects of the coal and hybrid coal/oil firing systems at McDonald's Lime that will be investigated using Computational Fluid Dynamics.

3.7 Buoyancy

There is often little mention of the effects of buoyancy when investigating the combustion characteristics of rotary cement or lime kilns. The following section presents a brief discussion using fundamental concepts to shed some light on the topic.

Consider a horizontal turbulent flame issuing from an orifice into still cold air within a confinement. Depending on the flame temperature, a vertical density gradient is experienced downstream of the orifice. As a result of this density gradient, a shearing motion, i.e. an increase of upwards velocity expressed as dU/dz, where z is the vertical axis, is created (Alyaser, 1998).

Using Prandtl's theory the Gradient Richardson Number can be developed, which describes the ratio of the rate at which energy is expended overcoming the buoyancy force, to the rate at which energy is produced by shear.

$$Ri = \frac{-g(d\rho/dz)}{\rho\left(\frac{dU}{dz}\right)^2} \tag{11}$$

Turbulence is completely suppressed when *Ri* reaches 0.45 or more. Broadly speaking, a large *Ri* indicates that important gravity forces are present.

Using the theory of Buckling Flows, Bejan derived an expression for the Richardson number of horizontal jets through a density-stratified reservoir (Alyaser, 1998):

$$Ri = \frac{-\frac{g}{\rho}\frac{d\rho}{dz}}{\left(\frac{U}{D}\right)^2} \tag{12}$$

where D is the diameter of the jet.

At the dimensional scale of the confinement, an expression of the characteristic measure of the relative effects of the gravity force to the inertial force of the flame can be suggested from the dimensional considerations, as follows:

$$Ri = \frac{r_c g \Delta\rho}{\rho_f U_f^2} \tag{13}$$

where r_c is the radius of the cylindrical confinement, U_f is the mean velocity at the orifice and the subscripts *f* and *a* (used later) refer to the flame and air, respectively. In terms of temperature, Equation 13 becomes:

$$Ri = \frac{r_c g \beta \Delta T}{U_f^2} \tag{14}$$

and

$$Ri = \frac{r_c g\left(T_f - T_a\right)}{T_f U_f^2} \tag{15}$$

where as this ratio increases, the flame becomes buoyant and less steady. In the case of a rotary lime the primary air velocity and secondary air temperatures replace kiln the flame velocity and air temperature respectively. In practice, many rotary kilns operate at a high primary jet momentum and with preheated secondary air, where the Richardson number is typically 1×10^{-3}. This typical practice is assumed to prevent buoyancy from having a significant effect on the flame dynamics.

3.8 Modelling of Rotary Kilns

There are two approaches taken to modelling the processes occurring in rotary kilns; physical and mathematical. Physical modelling most commonly involves acid/alkali plexiglass models, as was done by FCT for McDonalds Lime in the mid 1990's. In this case the primary jet was a solution of caustic soda, strongly diluted with water and mixed with thymolphthalein indicator. A dilute solution of hydrochloric acid was used for the surrounding secondary airflow. As the primary jet exits the burner nozzle and mixes with the surrounding hydrochloric acid, a neutralising reaction occurs changing the colour of the primary flow from blue to clear, and displaying the modelled flame length.

Early mathematical models were mostly one-dimensional where the dimension of interest was the kiln longitudinal axis. One of the greatest discrepancies in using one-dimensional models is the assumption that constant conditions are present over the cross section of the gas, wall and bed regions. The design of burners and flame characteristics proves to be extremely difficult when these assumptions are made, given that the flame is known to move considerably in the burner due to effects of the complex kiln aerodynmaics.

Appreciating the requirement for a mathematical model that could predict flame aerodynamics, Pai, Ritcher and Lowes (1975) created one of the first CFD models of the flow and mixing in a rotary cement kiln. While this early CFD model was encouraging for the development of CFD codes, the calculations of heat, mass and momentum transport did not simulate realistic conditions of the flame in a rotary kiln. Since this time however CFD has developed immensely and is now used for solving full three-dimensional systems involving heat transfer, fluid flow, combustion, turbulence and pollutant emissions. CFD is a common tool for the optimization of rotary kiln operations, gaining widespread recognition over the last decade as a useful tool for studying pulverised coal flames, especially for bitumous coals (Bosoaga et al., 2006).

Alyaser (1998) created an axisymmetric CFD model of the combustion aerodynamics and heat transfer in a natural gas fired rotary kiln, in the absence of a bed (but still accounting for the thermal load). Alyaser then validated his model with thermal measurements from the University of British Columbia's (UBC) pilot kiln. Alyaser's work focussed on the how a CFD model may be used to show the effects of changing inlet conditions, such as the primary air ratio and momentum, on the flame characteristics. He found the burner configuration to have a significant influence on the flame aerodynamics and heat transfer in the kiln. The combustion zone is also influenced by the burner configuration and the primary air ratio. Furthermore the effects of recirculation are found to be very influential.

Bui, Simard, Charette, Kocaefe and Perron (1995) were the first people to develop a full three-dimensional model for a rotary petroleum calciner. Although a coke calciner operates in a slightly different manner to lime kilns, evaluating the work of Bui et al. is worthwhile as, to the knowledge of the author, they were the first to employ a full 3D CFD model that considers all the physical phenomena of a rotary kiln under comparable plant conditions. The CFD code PHOENICS was used to solve the phenomena of interest such as the combustion of fuel, evolution and combustion of volatile species, evaporation of moisture, the

generation and combustion of coke dust, bed motion and thermal behaviour of the kiln walls. Due to the large size and complexity of the coke-calcining kiln model, the overall model was broken down into several sub models tied together by the heat fluxes flowing between and the temperatures at the boundaries. One model is built to denote each physical component of the kiln, those being the gas phase, refractories and the coke bed, each having their own grid domain.

Georgallis (2004) also developed a full three-dimensional model that considers all the phenomena of interest occuring in a natural gas fired lime kiln. The hot flow solution created by Georgallis was formulated using an existing in-house CFD code created at UBC by Nowak within the Department of Mechanical Engineering (He, Salcudean, Gartshore, & Nowak, 1996). The coupled results of the hot flow and wall models, which accounted for rotation and losses to the ambient, were used to investigate the effects of flame impingement on the refractory and how the secondary flow dynamics affect this phenomena. Details of the hood and kiln interactions are included along with the flame zone characteristics. The work of Georgallis also focussed on the calcination processes in the bed and the resulting CO_2 transfer that occurs between the bed and the hot gaseous phase.

Wang, Lu, Li, Li and Hu (2006) continued the work of Bui et al. (1995) and Georgallis (2004) to develop a full three-dimensional model for a cement rotary kiln. Of greatest importance is that Wang et al. considered all aspects of the pulverised coal combustion process used to fuel the kiln. The authors noted that while detailed coal combustion models had been considered in various fields, those models of rotary kilns failed to consider the effects of the clinker formation, which influences the gas phase temperature and furthermore, the coal combustion. Overall the work aimed to present a comprehensive mathematical model that included all phenomena of the gaseous phase, bed reactions and pulverised coal combustion, and the resulting interactions between them. While beyond the scope of work presented in this thesis, the zone heat flux model applied by Wang et al. to account for clinker formation is

worth mentioning. The bed of the kiln was divided into four zones (cooling, sintering, transition and decomposition). The heat flux was obtained for each zone by calculating the enthalpy changes that occur during the physical and chemical processes of each respective zone. The authors then used a user-defined function within the commercial CFD code FLUENT to implement the zone model as a wall thermal boundary condition.

Over time coal combustion has been modelled using a variety of different approaches. Recent research has focussed on using the mixture fraction/PDF approach, however the finite rate approach developed by Magnussen and Hjertager (1976) is also common, especially in early research codes developed specifically for combustion modelling. Sahajwalla, Eghlimi and Farrell (1997) performed a comparison between the finite rate and mixture fraction/PDF approaches and found the latter to predict more realistic results for oxygen concentration and char burnout. Also, since the PDF model does not require the solution of a large number of transport equations, it is more computationally efficient.

The previous work presented has shown that CFD will be a very useful tool for investigating the operation of a rotary lime kiln. CFD models can be created that account for the many different processes occurring in a rotary kiln and the interaction between the gaseous phase, bed and walls. The capabilities of CFD do in fact well exceed the scope of work that is to be presented in this thesis.

4 CFD Methodology

Investigations into the combustion characteristics of the McDonalds Lime kiln have primarily been conducted using Computational Fluid Dynamics and therefore it is necessary to provide some background on the subject. This chapter introduces the basic concepts and terminologies of numerical modelling with FLUENT, as well as some of the more complex sub-models required when modelling combustion.

Computational Fluid Dynamics, or CFD as it is commonly known, is the analysis of systems involving fluid flow, heat transfer and associated phenomena such as chemical reactions by means of a computer based simulation (Malalasekera & Versteeg, 1995). CFD methods were developed as early as the 1920s but it was not until the 1960s that it became an integrated research and design tool, particularly within the aerospace industry. With the advent of high-powered workstations over the last few decades, CFD has become an established tool for a variety of industries. Applications range from the design of internal combustion engines, boat hulls, electronics and chemical plants, to the modelling of human blood flow and weather prediction.

4.1 Solution Process

Modelling a flow field with a CFD package generally consists of three steps; pre-processing, solving and post-processing. Pre-processing consists of the input of a flow problem to a CFD program by means of an operator-friendly interface and the subsequent transformation of this input into a form suitable for use by the solver. The user-activities during the pre-processing stage include:

- Definition of geometry of the region of interest: the computational domain.
- Sub-dividing the geometrical domain into a number of smaller, non overlapping sub domains: a grid (or mesh) of cells (or control volumes).

- Selection of the physical and chemical phenomena to be modelled
- Definition of fluid and particle properties.
- Specification of appropriate boundary conditions at the bounding faces of the computational domain.

For the work presented in this thesis four pieces of software were used during the pre-processing stage. Solidworks 2008 was used to create the initial geometries. The definition of solution domains and creation of meshes was undertaken using a combination of Gambit v2.2 (ANSYS) and Harpoon v2.5 (SHARC). All boundary conditions and fluid properties were then defined in FLUENT.

Both FLUENT v6.3 and v12 were used for solving the fluid flow problem. This solution process requires no user interaction and is therefore usually carried out as a batch process. Background into the computations performed during the solution process is explained in subsequent sections of this chapter.

Post-processing involves taking the numerically generated data and presenting it in a visual manner. Modern CFD codes are equipped with a wealth of post-processing tools ranging from obtaining point values and x-y plots to tracking discrete phase trajectories and creating animations.

4.2 Governing Equations

CFD is a branch of fluid mechanics that utilises numerical methods and algorithms to solve the governing equations of fluid flow in order to predict the flow fields in and around objects of engineering interest. The governing equations of fluid flow represent mathematical statements of the conservation laws of physics. The conservation laws of physics known as 'Continuity', 'Newtons Second Law', and the 'First Law of Thermodynamics' state that mass, momentum and energy are conserved respectively.

By applying the three conservation laws to a small fluid volume the governing equations of fluid flow can be derived. The governing equations of the flow of a compressible Newtonian fluid are presented in Table 2.

Table 2: Governing Equations of a Compressible Newtonian Fluid *(Malalasekera & Versteeg, 1995)*

Continuity	$\frac{\partial \rho}{\partial t} + \nabla \cdot (\rho U) = 0$	Eq. 16
x-momentum	$\rho \frac{Du}{Dt} = -\frac{\partial p}{\partial x} + \nabla \cdot (\mu \cdot \nabla u) + S_{Mx}$	Eq. 17
y-momentum	$\rho \frac{Dv}{Dt} = -\frac{\partial p}{\partial y} + \nabla \cdot (\mu \cdot \nabla v) + S_{My}$	Eq. 18
z-momentum	$\rho \frac{Dw}{Dt} = -\frac{\partial p}{\partial z} + \nabla \cdot (\mu \cdot \nabla w) + S_{Mz}$	Eq. 19
Energy	$\frac{\partial (\rho i)}{\partial t} + \nabla \cdot (\rho i U) = -p \cdot \nabla U + \nabla (k \cdot \nabla T) + \Phi + S_i$	Eq. 20
Equations of State	$p = p(\rho, T)$ and $i = i(\rho, T)$	Eq. 21

where ρ = fluid density; t = time; U = velocity vector; u = x-component velocity; v = y-component velocity; w = z-component velocity; μ = dynamic viscosity; S_M = momentum source term in x, y, z directions; i = internal (thermal) energy; p = pressure; k = thermal conductivity; T = temperature; Φ = dissipation function; and S_i = internal energy source term.

The equations shown in Table 2 are all seen to have a similar form. For a general variable ϕ, the conservative form of all fluid flow equations is.

$$\rho \frac{\partial \phi}{\partial t} + \nabla (\rho \phi \mathrm{u}) = \nabla \cdot (\Gamma \cdot \nabla \phi) + S_\phi \qquad (22)$$

This equation is the transport equation for property ϕ, the meaning of which can be more clearly expressed in the words below.

Rate of increase of ϕ of fluid element + Net rate of flow of ϕ out of fluid element = Rate of increase of ϕ due to diffusion + Rate of increase of ϕ due to sources

By substituting ϕ for various transport properties, Equation 22 can be used to obtain special forms of each of the five partial differential equations in Table 2. The aim of any predictive study is to solve these special form transport equations for pressure, density, velocities and temperature throughout a flow

domain. Computational Fluid Dynamics involves solving these equations numerically using, in the case of FLUENT, a Finite Volume Method. To achieve this the transport equations are approximated by algebraic expressions at a number of discrete points in the flow domain, a process known as discretisation.

4.3 Pressure-Velocity Coupling

The momentum transport equations solved by a CFD code yield values for each velocity component. The continuity equation also includes all three velocity components meaning that it is coupled with all three momentum equations. A pressure gradient term is also present in the momentum equations, however there is no transport equation for pressure. In most engineering problems the pressure field is a desired output of the final solution and therefore is not normally known prior to solving.

If the flow is compressible the continuity equation may be considered as a transport equation for density and the energy equation as a transport equation for temperature. The pressure may then be obtained from the density and pressure using the equation of state, $p = p(\rho,T)$.

If the flow is incompressible however the density is constant and is thus no longer linked to the pressure. In this case an iterative procedure is introduced. If the correct pressure field is applied in the momentum equations the resulting velocity field should satisfy continuity. There are several iterative pressure-velocity coupling algorithms that have been developed, the most suitable depending on the flow type. FLUENT includes the SIMPLE, SIMPLEC and PISO algorithms. The SIMPLE algorithm uses a relationship between velocity and pressure corrections to enforce mass conservation and obtain the pressure field. SIMPLEC is very similar however there is a difference in the expression used for the face flux correction. One of the limitations of the SIMPLE and SIMPLEC algorithms is that new velocities, and corresponding fluxes, do not satisfy the momentum balance after the pressure-correction equation is solved. As a result,

the calculation must be repeated until the balance is satisfied. To improve the efficiency of this calculation, the PISO algorithm performs two additional corrections: neighbour correction and skewness correction. Each of these algorithms can also be used in the case of compressible flow instead of using a coupled system, with advantages and disadvantages of both approaches. All the modelling presented in this thesis uses the SIMPLE algorithm.

4.4 Turbulence Models

The vast majority of fluid flows experienced in engineering practice, including rotary kiln flames, are turbulent in nature. Turbulent flow exists when the Reynolds number is above a critical value causing the flow structure to become random and chaotic. At low Reynolds numbers a flow is laminar.

The basic form of the continuity, momentum and energy equations can correctly describe flows in the laminar regime. Greater consideration must however be given to turbulent regimes as flow properties such as velocity and pressure are uncorrelated over distances greater than the eddy size. The equations describing the mean velocity and pressure of a turbulent flow are obtained by decomposing the instantaneous fields into mean and fluctuating components and then time averaging the Navier-Stokes equations. This process results in an extra term known as the Reynolds Stresses, which is the product of the fluctuating velocities. These equations are known as the Reynolds Averaged Navier-Stokes (RANS) equations and are the equations governing the mean velocity and pressure fields in a turbulent flow. With the addition of the Reynolds Stress term there are insufficient equations to solve for all the unknowns. A turbulence model is introduced to model the Reynolds stress and consequently close the RANS equations.

The turbulence model used for the research presented in this thesis was the standard k-epsilon model (Launder & Sharma, 1974), one of the most widely used turbulence models. The two-equation k-epsilon model solves transport equations for the turbulent kinetic energy (k) and its rate of dissipation (ε). The

eddy viscosity can be derived from k and ε using the mixing length model introduced by Prandtl in 1925.

$$\mu_t = \rho C_\mu \frac{k^2}{\varepsilon} \tag{23}$$

where C_μ is a dimensionless coefficient. The eddy viscosity is related to the Reynolds stresses in the RANS equations using Boussinesq's eddy viscosity concept, the basis of many turbulence models. Boussinesq proposed that the Reynolds Stresses should be proportional to the local mean strain rate in the fluid (Malalasekera & Versteeg, 1995).

The standard model uses the following transport equations to calculate k and ε.

$$\frac{\partial}{\partial t}(\rho k) + \frac{\partial}{\partial x_i}(\rho k u_i) = \frac{\partial}{\partial x_j}\left[\left(\mu + \frac{\mu_t}{\sigma_k}\right)\frac{\partial k}{\partial x_j}\right] + G_k + G_b - \rho\varepsilon - Y_M + S_k \tag{24}$$

$$\frac{\partial}{\partial t}(\rho \varepsilon) + \frac{\partial}{\partial x_i}(\rho \varepsilon u_i) = \frac{\partial}{\partial x_j}\left[\left(\mu + \frac{\mu_t}{\sigma_\varepsilon}\right)\frac{\partial \varepsilon}{\partial x_j}\right] + C_{1\varepsilon}\frac{\varepsilon}{k}(G_k + C_{3\varepsilon}G_b) - C_{2\varepsilon}\rho\frac{\varepsilon^2}{k} \tag{25}$$

In these equations, G_k represents the generation of turbulence kinetic energy due to the mean velocity gradients, G_b is the generation of turbulence kinetic energy due to buoyancy, and Y_M represents the contribution of the fluctuating dilatation in compressible turbulence to the overall dissipation rate. $C_{1\varepsilon}$, $C_{2\varepsilon}$, and $C_{3\varepsilon}$, are constants. σ_k and σ_ε are the turbulent Prandtl numbers for k and ε, respectively. S_k and S_ε are user-defined source terms.

The equations contain five adjustable constants $C_{1\varepsilon}$, $C_{2\varepsilon}$, $C_{3\varepsilon}$, σ_k and σ_ε. The standard k-ε model employs values for the constants that are arrived at by comprehensive data fitting for a wide range of turbulent flows.

$$C_{1\varepsilon} = 1.44 \quad C_{2\varepsilon} = 1.92 \quad C_\mu = 0.09 \quad \sigma_k = 1.0 \quad \sigma_\varepsilon = 1.3$$

It is possible to modify these constants to suit a particular application however this would require significant validation testing using known experimental data. For this reason all modelling presented in this thesis used the default values.

As with any turbulence model there are a number of strengths and weaknesses making each one better suited to different applications. The advantages and disadvantages of the *k*-*ε* turbulence model are listed below.

Advantages

- Simplest model.
- Excellent performance for many industrially relevant flows, compared to other two-equation RANS models.
- Well established and validated.

Disadvantages

- More expensive to implement than mixing length model (two extra PDE's).
- Poor performance in unconfined, rotating and swirling flows.

Application of the *k*-epsilon for modelling the swirling pulverised coal flame presented in the validation case of Chapter Five is likely to be questioned. As mentioned above the *k*-epsilon model is commonly considered to perform poorly when modelling isothermal swirling flows. In the swirling pulverised coal flame considered, the volatile matter entering the gaseous phase is rapidly mixed with the combustion air and the ignition front is located in the close vicinity of the fuel injector. The inlet swirling flow is combustion accelerated in the vicinity of the fuel injector and the importance of centrifugal forces, when compared to inertial forces, is reduced, as the latter increase significantly. It has been demonstrated that for these type-2 flames little can be gained by applying a higher order turbulence model and that *k*-epsilon is adequate (Peters & Weber, 1996). Meanwhile Georgallis (2004) reports the standard *k*-epsilon does a reasonable job in predicting the mean and turbulent profiles along the length of a rotary lime kiln that is fired in a similar manner to the one at McDonalds Lime.

4.5 Discrete Phase Modelling

In addition to solving transport equations for the continuous phase, FLUENT allows the simulation of a discrete second phase in a Lagrangian frame of

reference. This second phase consists of spherical particles (which may also be taken to represent droplets or bubbles) dispersed in the continuous phase. FLUENT computes the trajectories of these discrete phase entities, as well as the heat and mass transfer to/from them. The coupling between phases and the resulting impact on both the discrete phase trajectories and the continuous phase gas flow can be included.

The discrete phase formulation used by FLUENT contains the assumption that the second phase is sufficiently dilute that particle-particle interactions and the effects of the particle volume fraction on the gas phase are negligible. In practice these issues imply that the discrete phase must be present at a fairly low volume fraction, perhaps less than 10-12% (FLUENT, 2006), a value which is justified for the modelling work presented in this thesis.

4.5.1 Calculation of discrete phase trajectory

Fluent predicts the trajectory of a discrete phase particle by integrating the force balance on the particle, which is written in a Lagrangian reference frame. This force balance equates the particle inertia with the forces acting on the particle. The force balance includes the effects of gravity, however it is important to note that in FLUENT the default gravitational acceleration is zero.

The dispersion of particles due to turbulence in the fluid phase is calculated using the stochastic tracking model. This model includes the effects of instantaneous turbulent velocity fluctuations on the particle trajectories through the use of stochastic methods.

4.5.2 Heat/Mass Transfer Calculations

Several heat and mass transfer relationships, termed “laws”, are available in FLUENT for modelling reacting discrete phase particles and their impact on the continuous phase. Which laws are active depends on the particle type that is selected. The sequence of laws used for droplets and combusting particles are listed below.

Table 3: Active particle laws for different particle types.

Step	Process	Corresponding Law
Droplet		
1	Inert Heating	1
2	Droplet Vapourisation	2
3	Droplet Boiling	3
4	Inert Cooling	6
Combusting Particle		
1	Inert Heating	1
2	Devolatilisation	4
3	Surface Combustion	5
4	Inert Cooling	6

"Law 1/Law 6": Inert Heating or Cooling

The inert heating law is applied when the temperature of a particle is less than the user defined vaporisation temperature, T_{vap}. Above this temperature a non-inert particle or droplet may proceed to obey one of the mass-transfer laws (2, 3, 4, and/or 5). The inert cooling law is applied towards the end of the reaction process when the volatile portion, $f_{v,0}$, of a particle/droplet has been consumed. These conditions may be written as:

$$\text{Law 1:} \qquad T_p < T_{vap} \tag{26}$$

$$\text{Law 6:} \qquad m_p \leq (1 - f_{v,0}) m_{p,0} \tag{27}$$

where T_p is the particle temperature, $m_{p,0}$ is the initial mass of the particle and m_p is its current mass.

When using the inert heating or cooling laws FLUENT uses a simple heat balance to relate the particle temperature to the convective heat transfer and the absorption/emission of radiation at the particle surface. This process assumes that there is negligible internal resistance to heat transfer (particles are assumed to behave as a thermally thin material). The heat lost or gained by the particle as it traverses each computational cell appears as a source or sink of heat in subsequent calculations of the continuous phase energy equation.

"Law 2": Droplet Vaporisation

Law 2 is applied to predict the vaporisation from a discrete phase droplet. Law 2 is initiated when the temperature of the droplet reaches the vaporisation temperature, T_{vap}, and continues until the droplet reaches the boiling point, T_{bp}, or until the droplet's volatile fraction is completely consumed.

$$T_p < T_{bp} \tag{28}$$

$$m_p > (1 - f_{v,0}) m_{p0} \tag{29}$$

The onset of the vaporisation law is determined by the setting of T_{vap}, a temperature that has no other physical significance.

During Law 2 the rate of vaporisation is governed by gradient diffusion, with the flux of droplet vapour into the gas phase related to the gradient of the vapour concentration between the droplet surface and the bulk gas. Finally, the droplet temperature is updated according to a heat balance that relates the sensible heat change in the droplet to the convective and latent heat transfer between the droplet and the continuous phase. The heat transferred to or from the gas phase becomes a source/sink of energy during subsequent calculations of the continuous phase energy equation.

"Law 3": Droplet Boiling

Law 3 is applied to predict the convective boiling of a discrete phase droplet when the temperature of the droplet has reached the boiling temperature, T_{bp}, and while the mass of the droplet exceeds the non-volatile fraction, $(1\text{-}f_{v,0})$:

$$T_p \geq T_{bp} \tag{30}$$

and

$$m_p > (1 - f_{v,0}) m_{p,0} \tag{31}$$

When the droplet temperature reaches the boiling point, a boiling rate equation is applied. The droplet is assumed to stay at constant temperature while the boiling rate is applied. Once the boiling law is entered is it applied for the

duration of the particle trajectory. The energy required for vaporisation appears as a negative source term in the energy equation for the gas phase. The evaporated liquid enters the gaseous phase as species *i,* as defined by the user.

"Law 4": Devolatilisation

The devolatilisation law is applied to a combusting particle when the temperature of the particle reaches the vaporisation temperature, T_{vap}, and remains in effect while the mass of the particle, m_p, exceeds the mass of the non-volatiles in the particle:

$$T_p \geq T_{vap} \tag{32}$$

and

$$m_p > (1 - f_{v,0}) m_{p,0} \tag{33}$$

Fluent provides a choice of three devolatilisation models:

- The constant rate model.
- The single kinetic rate model.
- The two competing rates model (not considered in the present work).

The constant rate devolatilisation law dictates that the volatiles are released at a constant rate:

$$-\frac{1}{f_{v,0}(1 - f_{w,0}) m_{p,0}} \frac{dm_p}{dt} = A_0 \tag{34}$$

where A_0 is the rate constant in s^{-1} *and* $f_{w,0}$ is the mass fraction of the evaporating/boiling material if Wet Combustion is selected (otherwise $f_{w,0} = 0$).

The single rate model (Badzioch & Hawksley, 1970) assumes that the rate of devolatilisation is first-order dependent on the amount of volatiles remaining in the particle:

$$-\frac{dm_p}{dt} = k(m_p - (1 - f_{v,0}) m_{p,0}) \tag{35}$$

where k is the kinetic rate (s^{-1}). This equation has the approximate analytical solution:

$$m_p(t+\Delta t) = (1-f_{v0})m_{p0} + \left[m_p(t) - (1-f_{v0})m_{p0}\right]e^{-k\Delta t} \tag{36}$$

which is obtained by assuming that the particle temperature varies only slightly between discrete time integration steps. The kinetic rate, k, is defined by input of an Arrhenius type pre-exponential factor and an activation energy.

$$k = A_1 \exp(-E/RT) \tag{37}$$

During devolatilisation the diameter of a combusting particle changes according to the swelling coefficient, C_{sw}, which is user defined. Heat transfer to the particle during the devolatilisation process includes contributions from convection, radiation and the heat consumed during devolatilisation.

"Law 4": Surface Combustion

After the volatile component of the particle is completely evolved, a surface reaction begins, which consumes the combustible fraction, f_{comb}, of the particle. Law 5 is thus active (for a combusting particle) after the volatiles are evolved:

$$m_p > (1-f_{v0})m_{p0} \tag{38}$$

and until the combustible fraction is consumed:

$$m_p > (1-f_{v0}-f_{comb})m_{p0} \tag{39}$$

When the combustible fraction, f_{comb}, has been consumed in Law 5, the combusting particle may contain some residual ash that reverts to the inert heating law, Law 6.

The surface combustion law consumes the reactive content of the particle as governed by the stoichiometric requirement, S_b, of the surface burnout reaction:

$$char(s) + S_b O(g) \rightarrow Products(g) \tag{40}$$

where S_b is defined in terms of mass of oxidant per mass of char.

Fluent provides a choice of three heterogeneous surface reaction rate models for combusting particles:

- The diffusion-limited rate model.
- The kinetic/diffusion-limited rate model (used for the presented work).
- The intrinsic model.

The kinetic/diffusion-limited reaction rate model assumes that the surface reaction rate is determined either by kinetics or a diffusion rate. FLUENT uses the models of Baum and Street (1971) and Field (1969) in which the diffusion rate

$$R_1 = C_1 \frac{\left[\left(T_p + T_\infty\right)/2\right]^{0.75}}{D_p} \tag{41}$$

and a kinetic rate

$$R_2 = C_2 \exp(-E/RT_p) \tag{42}$$

are weighted to yield a char combustion rate of

$$\frac{dm_p}{dt} = -\pi D_p^2 P_0 \frac{R_1 R_2}{R_1 + R_2} \tag{43}$$

where P_O is the partial pressure of oxidant species in the gas surrounding the combusting particle, and the kinetic rate R_2 incorporates the effects of chemical reaction on the internal surface of the char particle and pore diffusion. FLUENT recasts Equation 43 in terms of the oxidant mass fraction, m_O, as

$$\frac{dm_p}{dt} = -\pi D_p^2 \frac{\rho R T m_O}{M_O} \frac{R_1 R_2}{R_1 + R_2} \tag{44}$$

The particle size is assumed to remain constant in this model while the density is allowed to decrease.

During char combustion the surface reaction consumes the oxidant species in the gas phase and consequently supplies a negative source term during the

computation of the transport equation of that species. Similarly, the surface reaction is a source species in the gas phase: the product of the heterogeneous surface reaction appears in the gas phase as a user selected chemical species. The surface reaction also consumes or produces energy in an amount determined by the heat of reaction of the combusting particle.

4.5.3 Coupling Between the Discrete and Continuous Phases

As the trajectory of a particle is computed, FLUENT keeps track of the heat, mass and momentum gained or lost by the particle stream that follows that trajectory. These quantities can be incorporated in the subsequent continuous phase calculations. Thus, while the continuous phase always impacts on the discrete phase, the effects of the discrete phase trajectories on the continuum can also be included. This two way coupling is accomplished by alternately solving the discrete and continuous phase until the equations in both phases have stopped changing. This interchange of heat, mass and momentum from the particle to the continuous phase is depicted qualitatively in Figure 13.

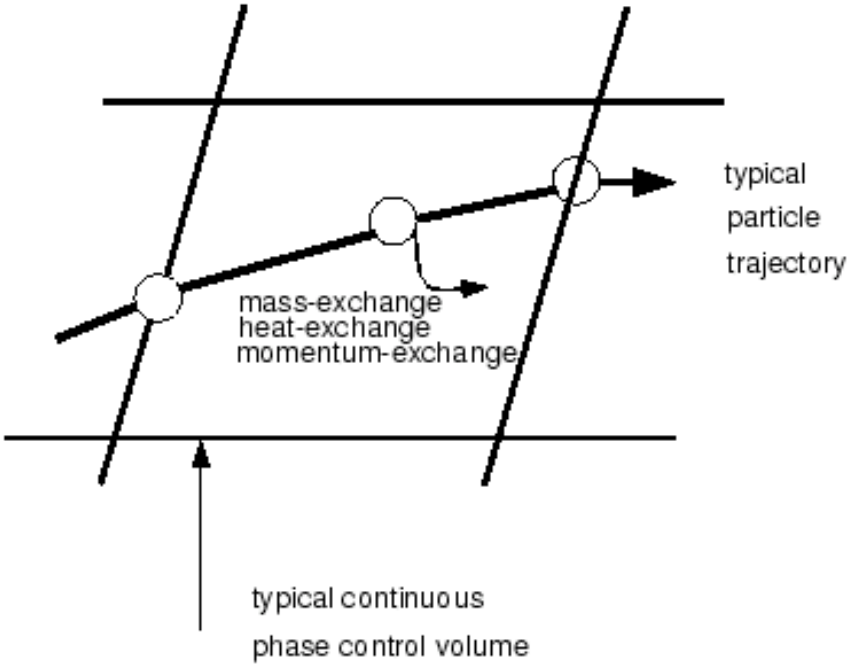

Figure 13: Heat, mass and momentum transfer between the discrete and continuous phases *(FLUENT, 2006).*

4.5.4 Initial Conditions

The initial conditions of a discrete phase particle or droplet are defined by creating a particle injection and assigning a number of properties to it. FLUENT provides five types of injections.

- Single
- Group
- Cone
- Surface
- Read from a file

The following initial conditions provide the starting values for all of the dependant discrete phase variables that describe the instantaneous conditions of an individual particle.

- Position of the particle: This can either be expressed as an *x, y, z* location or from a particular surface.
- Velocities (*u, v, w*) of the particles: Velocity magnitudes and spray cone angle can also be used (in 3D) to define the initial velocities.
- Diameter of the particle: This can either be defined as a uniform value or as a range of diameters using either a Rosin-Rammler or logarithmic Rosin-Rammler diameter distribution.
- Particle Temperature
- Mass flow rate of the particle stream that will follow the trajectory of the individual particle/droplet.

These dependant variables are updated according to the equations of motion and according to the heat/mass transfer relations applied as the particle/droplet moves along its trajectory.

4.6 Combustion Chemistry

During any combustion process there are a number of chemical reactions occurring. Gaseous phase reactions exist that may involve NO_x and other

pollutant formation. There may also be particle surface reactions in the case of coal char combustion, for example where a reaction occurs at the surface of a discrete-phase particle. FLUENT is able to model both of these reaction types and provides several approaches to do so. For the work presented in this thesis both the Generalized Finite-Rate Model and Non-Premixed Combustion Model were used.

4.6.1 Generalized Finite-Rate Model

The generalised finite-rate model solves the species transport equations for reactants and product concentrations, in which the chemical reaction mechanism is explicitly defined. Fluent predicts the local mass fraction of species, Y_i, through the solution of a convection-diffusion equation for the *i*th species. This conservation equation takes the following general form:

$$\frac{\partial}{\partial t}(\rho Y_i) + \nabla \cdot (\rho \vec{v} Y_i) = \nabla \cdot \vec{J}_i + R_i + S_i \tag{45}$$

where R_i is the net rate of production of species *i* by chemical reaction and S_i is the rate of creation by addition from the dispersed phase. An equation of this form is solved for *N-1* species where *N* is the total number of fluid phase chemical species present in the system.

Turbulent mixing for most fuels controls the overall rate of burning. Fluent provides a turbulence-chemistry interaction model based on the work of Masnussen and Hjertager (1976), called the eddy-dissipation model. The net rate of production of species *i* due to reaction *r*, $R_{i,r}$, is given by the smaller of the two expressions below:

$$R_{i,r} = \nu'_{i,r} M_{w,i} A \rho \frac{\varepsilon}{k} \min_H \left(\frac{Y_H}{\nu'_{H,r} M_{w,H}} \right) \tag{46}$$

$$R_{i,r} = \nu'_{i,r} M_{w,i} A B \rho \frac{\varepsilon}{k} \frac{\sum_P Y_P}{\sum_j^N \nu''_{j,r} M_{w,j}} \tag{47}$$

where ν' is the stoichiometric coefficient for reactants, ν'' is the stoichiometric coefficient for products and M is the molecular weight. Y_p is the mass fraction of any product species, P, and Y_H is the mass fraction of a particular reactant, H. A and B are empirical constants equal to 4.0 and 0.5 respectively. This model relates the rate of reaction to the rate of dissipation of the reactant and product containing eddies.

4.6.2 Non-Premixed Combustion Model

The non-premixed combustion model, commonly referred to as the mixture fraction/PDF approach, was specifically developed for the simulation of turbulent diffusion flames and simplifies the combustion process into a mixing problem. In this approach individual species transport equations are not solved. Instead, transport equations for one or two conserved scalars (the mixture fractions) are solved and the thermo-chemical properties of the fluid are derived from the predicted mixture fraction distribution. Since the non-premixed combustion model does not require the solution of multiple species transport equations it is more computationally efficient than the generalised finite rate approach. For all modelling presented in this thesis the equilibrium chemistry model was used, which assumes that combustion chemistry is rapid enough for chemical equilibrium to exist at a molecular level. The mixture fraction can be written in terms of the atomic mass fraction as:

$$f = \frac{Z_i - Z_{i,ox}}{Z_{i,fuel} - Z_{i,ox}} \tag{48}$$

where Z_i is the elemental mass fraction for element i. The subscripts *ox* and *fuel* denote the values at the oxidiser and fuel stream inlets respectively. The mixture fraction is a conserved scalar and its value at each control volume is calculated via the solution of the following transport equation for the Favre mean (density-averaged) value of f.

$$\nabla \cdot \left(\rho \vec{v} \overline{f} \right) = \nabla \cdot \left(\frac{\mu_t}{\sigma_t} \nabla \overline{f} \right) + S_m \tag{49}$$

The source term, S_m is due to the transfer of mass into the gas phase from reacting coal particles. In addition to solving for the Favre mean mixture fractions, Fluent solves a conservation equation for the mixture fraction variance $\overline{f^{'2}}$.

$$\nabla \cdot \left(\rho \vec{v} \overline{f^{'2}}\right) = \nabla \cdot \left(\frac{\mu_t}{\sigma_t} \nabla \overline{f^{'2}}\right) + C_g \mu_t \left(\nabla \cdot \overline{f}\right)^2 - C_d \rho \frac{\varepsilon}{k} \overline{f^{'2}} \tag{50}$$

where $f^{'} = f - \overline{f}$. The default values for the constants σ_t, C_g and C_d are 0.85, 2.86 and 2.0 respectively. Under the assumption of chemical equilibrium all thermo-chemical scalars (species fractions, temperature and density) are uniquely related to the instantaneous fuel mixture fraction.

$$\phi_i = \phi_i(f) \tag{51}$$

where ϕ_i represents the instantaneous species concentration, temperature or density. In a non-adiabatic systems such as the two cases presented in this thesis the effect of heat loss/gain is parameterised as

$$\phi_i = \phi_i(f, H) \tag{52}$$

for a single mixture fraction system where H is the instantaneous enthalpy.

The effects of turbulence on combustion chemistry are accounted for using an assumed shape probability density function (PDF) approach. The probability density function, *p(f),* which describes the temporal fluctuations of the mixture fraction, *f*, in the turbulent flow is used to compute the averaged values of variables that depend on *f*.

FLUENT also allows for a secondary stream to be included. This may consist of another fuel or oxidant or a non-reacting stream. If a secondary stream is included the fuel and secondary mixture fractions are simply the elemental mass fractions of the fuel and secondary streams, respectively. The sum of all three mixture fractions in the system (fuel, secondary stream, and oxidiser) is always equal to One:

$$f_{fuel} + f_{sec} + f_{ox} = 1 \tag{53}$$

Modelling a secondary stream and the associated transport equations is described in full in the FLUENT User Guide.

4.7 Domain

Modelling a fluid flow problem with a three-dimensional domain provides the most accurate solution, however there are times when a two-dimensional domain may be more appropriate due to the simpler mesh setup and smaller computational times. Within Fluent there are several approaches to modelling a two-dimensional (2D) domain as is explained below.

4.7.1 Two Dimensional

The simplest form of the two-dimensional domain involves solving the 2D Carteisan form of the governing equations. The modelled domain assumes plane flow with a unit width of one metre.

4.7.2 Two Dimensional Axisymmetric

Axisymmetric indicates that the domain is axisymmetric about the *x* axis. When axisymmetric is enabled the 2D axisymmetric form of the governing equations is solved instead of the 2D Cartesian form.

4.7.3 Two Dimensional Axisymmetric with Swirl

This situation applies when the problem is axisymmetric with respect to geometry and flow conditions but still includes swirl or rotation. In this case the flow can be modelled in 2D (i.e., by solving the axisymmetric problem) but also include the prediction of the circumferential (or swirl) velocity. It is important to note that while the assumption of axisymmetry implies that there are no circumferential gradients in the flow, there may still be non-zero swirl velocities.

The tangential momentum equation for 2D swirling flows may be written as

$$\frac{\partial}{\partial t}(\rho w)+\frac{1}{r}\frac{\partial}{\partial x}(r\rho uw)+\frac{1}{r}\frac{\partial}{\partial r}(r\rho vw)=\frac{1}{r}\frac{\partial}{\partial x}\left[r\mu\frac{\partial w}{\partial x}\right]+\frac{1}{r^2}\frac{\partial}{\partial r}\left[r^3\mu\frac{\partial}{\partial r}\left(\frac{w}{r}\right)\right]-\rho\frac{vw}{r} \quad (54)$$

where *x* is the axial coordinate, *r* is the radial coordinate, *u* is the axial velocity, *v* is the radial velocity and *w* is the swirl velocity.

4.8 Mesh

In order to simulate the fluid characteristics in a given flow domain, the domain must be broken down into smaller sub-domains, or cells, to create a mesh. The transport equations are then solved for each of these cells. Care must be taken during mesh generation to ensure that no gaps are present between the cell faces so that the discrete solutions can be concatenated together to present a complete picture of the flow in the entire domain.

There are three different types of mesh that can be generated and used in CFD codes, namely structured, unstructured and hybrid meshes. Hybrid meshes are a combination of structured and unstructured meshes and are intended to incorporate the advantages of both types and exclude the disadvantages.

Structured meshes are computationally more efficient during solving, use less memory and often provide greater accuracy, however they can take a long time to set up especially for complex geometry. Unstructured meshes, however, are much simpler to set up and offer greater flexibility in representing complex geometries, which often leads to more accurate solver results. The disadvantages of unstructured meshes are that there is a lack of user control and they need more memory due to the storage of connectivity information.

As with many parameters within a CFD simulation, the ideal mesh is not known prior to solving beginning. While experienced CFD engineers are likely to be well informed on suitable mesh sizes, it is a common exercise to perform a mesh convergence study. A mesh convergence study involves refining the mesh, either throughout the entire domain or in specific areas, until the perceived accuracy of

the solution converges to an acceptable error level. As a mesh is refined the computational cost increases and therefore a CFD engineer must find a mesh that has a feasible solve time while maintaining an acceptable level of accuracy.

4.9 Convergence Criterion

After reviewing FLUENT documentation and previous combustion modelling problems, a series of steps were chosen that would be used to determine whether a coal combustion simulation had reached a converged solution. This set of convergence criterion, listed below, was applied to both the validation case and McDonald's Lime kiln simulations.

- Incoming and outgoing mass fluxes should have an imbalance of less than 1%.
- Incoming and outgoing enthalpy fluxes should have an imbalance of less than 5%.
- Values of temperature and velocity monitored at discrete points in the flow domain have converged to a constant value. Small fluctuations will be neglected.
- The exit gas temperature has converged to a constant value. Small fluctuations will again be neglected.
- Transport equation residuals are of acceptable values and are not divergent.
- A minimum of 70 Discrete Phase Model iterations is performed to obtain converged particle trajectory calculations.
- There is less than 5% incomplete particle tracking.

A decision is made as to whether a model is converged after taking into account all of the above considerations.

5 Validation Case

Computational Fluid Dynamics (CFD) has become an incredibly popular tool throughout the engineering community as it is an easy and convenient way of investigating fluid flow characteristics, without having to carry out cumbersome, and often impractical, experimental tests. However, it is crucial that the accuracy of any CFD code is determined before being implemented as a research and design tool. The following chapter focuses on validating the accuracy of FLUENT for modelling combustion applications such as the operation of a rotary lime kiln. This is achieved by comparing published experimental measurements to the results of numerical simulations performed by FLUENT. Furthermore, the validation study investigates the effects of different combustion sub models, and methods for defining the particle size distribution of pulverised coal. The best procedure for solving a combustion model with FLUENT is also explored.

The validation study is based on a 2.5MW aerodynamically air staged burner (AASB), firing a type two, pulverised coal flame into the International Flame Research Foundations (IFRF) No. 1 Furnace (Figure 14 & Figure 15). Experimental measurements are obtained from a paper by Peters and Weber (1996), during which the authors compare the measurements to the results of their own combustion modelling code. The paper provides measured in-flame temperatures, chemical species concentrations, and coal burnout at seven traverses within the furnace. Velocity and turbulence measurements are given at four traverses; radiative heat fluxes near the furnace refractory are provided, as well as the heat extraction of the seven cooling loops inside the furnace.

Further assistance was gained from Eastwick, Pickeing and Aroussi (1999) who used the same experimental measurements to compare the validity and accuracy of an earlier version of FLUENT with another commercial CFD code, FLOW3D (now CFX). A FLUENT tutorial, which uses the IFRF furnace to demonstrate coal combustion modelling using the Finite Rate chemistry model, was also consulted.

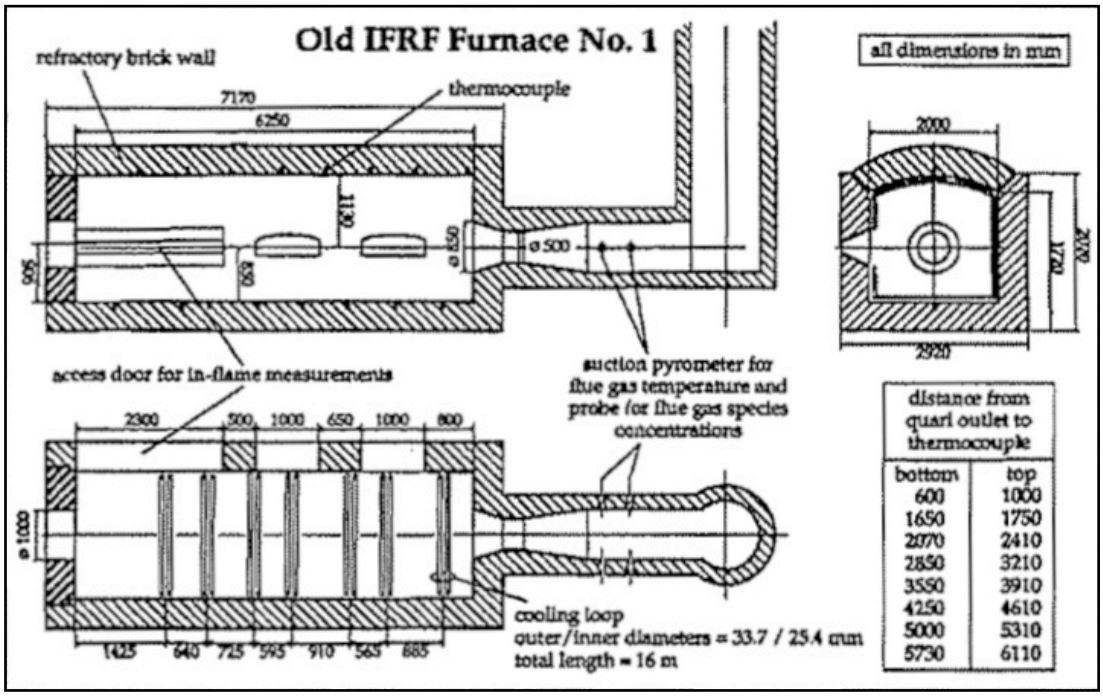

Figure 14: Schematic of IFRF Furnace *(Peters & Weber, 1996).*

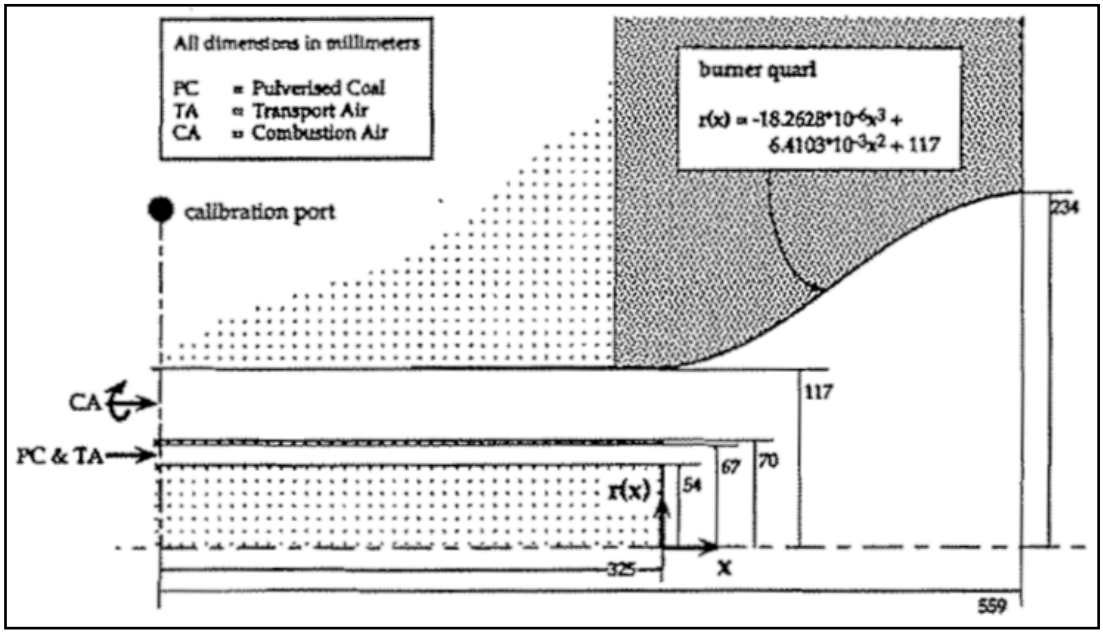

Figure 15: Burner Configuration *(Peters & Weber, 1996).*

5.1 Operating Conditions

The operating conditions of the IFRF Furnace were primarily extracted from the paper written by Peters and Weber (1996), with additional reference made to the coal combustion tutorial from FLUENT.

5.1.1 Coal Properties

The IFRF Furnace was fired using a pulverised Saar Coal: Gottelborn hvBb. Table 4 details the chemical properties of the Saar coal while Table 5 contains information about the coal particle size.

Table 4: Chemical Properties of the Saar coal *(Peter & Weber, 1996).*

Proximate Analysis	**Weight %, Dry**
Volatile matter	37.4
Fixed Carbon	54.3
Ash	8.3
Ultimate Analysis	**Weight %, DAF**
Carbon	80.36
Hydrogen	5.08
Nitrogen	1.45
Sulphur	0.94
Oxygen	12.17
Other Properties	
LCV (MJ/kg DAF)	32.32
Density (kg/m^3, dry)	1000
Specific Heat (J/kg.K, dry)	1100

Table 5: Size distribution of pulverised Saar coal *(ANSYS, 2008)*.

Sieve Analysis	**Diameter**	**Mass %**
1	1 µm	1
2	5 µm	4
3	10 µm	7
4	25 µm	24
5	50 µm	32
6	75 µm	19
7	100 µm	8
8	200 µm	4
9	300 µm	1
Rosin- Rammler Parameters		
Minimuim Diameter		1 µm
Maximum Diameter		300 µm
Mean Diameter		45 µm
Spread Parameter		1.29

Note: There is a slight discrepancy between the spread parameter provided in the paper by Peters and Weber and that calculated from the sieve-type analysis provided in the FLUENT tutorial. All other variables listed in the two documents are the same, however, and there is negligible difference between results obtained using the two different spread parameters.

5.1.2 Material Properties

Table 6 on the following page lists the material property settings in FLUENT for the gaseous mixture and the combusting coal particle, all of which are based on the settings of the FLUENT tutorial used as a guide.

Table 6: Validation case material properties

Fluid Mixture	
Specific Heat	mixing-law
Thermal Conductivity	0.025 W/m.K
Viscosity	2e-05 kg/m.s
Absorption Coefficient	Weighted Sum of Grey Gases Model - cell based
Scattering Coefficient	0.5 m^{-1}
Scattering Phase Function	Isotropic
Refractive Index	1
Combusting Particle	
Density	1300 kg/m^3
Cp	1000 J/kg.K
Thermal Conductivity	0.0454 kg/m.s
Latent Heat	0 J/kg
Vaporisation Temp	500 K
Binary Diffusivity	0.0005
Particle Emissivity	0.9
Swelling Coefficient	1
Devolatilisation Model	Single A = 100000 E = 7.4 x 10^7 j/kgmol
Combustion Model	Kinetics/Diffusion-Limited Rate Constant = 5 x 10^{-12} Pre-Exponential Factor = 0.002 Activation Energy = 7.9 x10^7 j/kgmol

5.1.3 Inlet Conditions

The inlet conditions of the burner are listed in Table 7. The combustion air flow rate of 2684 kg/h, transport air flow rate of 421 kg/h and the coal flow rate of 263 kg/h provide the burner with a theoretical fuel thermal input of 2.165 MW and an excess air level of 22%. When the sensible heat flow rates of the combustion air, transport air and coal are also considered the overall thermal input to the furnace becomes 2.386 MW.

Table 7: Burner Input Conditions *(Peter & Weber, 1996).*

Combustion Air Inlet	
Mass flow rate (Dry)	0.7456 kg/hour
Inlet area	$2.7611 \times 10^{-2} m^2$
Temperature	573.15 K
Density	$0.616\ kg/m^3$
Mean axial velocity	43.83 m/s
Mean swirl velocity	49.42 m/s
Turbulence intensity	20%
Characteristic length	23.5 mm
Transport Air and Coal Inlet	
Coal mass flow rate (Dry)	0.0731 kg/hour (Surface Injection)
Air mass flow rate (Dry)	0.1169 kg/hour
Inlet area	$4.9417 \times 10^{-3} m^2$
Temperature	343.15 K
Density	$1.028\ kg/m^3$
Mean Axial Velocity	23.02 m/s
Turbulent Intensity	10%
Characteristic length	6.5 mm

5.1.4 Wall Boundary Conditions

The seven cooling loops were each modelled as a 240mm wide section around the furnace wall. While not truly representative of the real cooling loop geometry this method simplifies mesh generation and provides the same surface area in order to replicate the heat extraction of the loops. Further thermal boundary conditions are listed in Table 8.

Table 8: Model thermal boundary conditions *(Peter & Weber, 1996).*

Boundary	Temperature (K)	Emissivity
Inlet duct walls	343/573	0.6
Coal gun front wall	800	0.6
Burner quarl wall	1273	0.6
Furnace front wall	1400	0.5
Furnace cylinder wall	1400	0.5
Cooling loops	1000	0.4
Furnace back wall	1300	0.5
Chimney wall	1300	0.5

5.1.5 Buoyancy

The Richardson number for the turbulent flame inside the IFRF Furnace was calculated to be approximately 0.005 and therefore any effects of buoyancy are considered negligible based on the explanation provided in the Literature Review.

5.1.6 Solution Procedure

Using the validation case, a study was undertaken to find the best combustion modelling procedure that would lead to the fastest convergence. The same method also proved very effective when solving the McDonald's Lime kiln simulations. The solution procedure used throughout the CFD modelling presented in this thesis is detailed in Table 9, while Table 10 lists the under-relaxation factors for each step.

During the initial setup the coal devolatilisation temperature should be set to ~200K below the secondary air temperature, both in the materials panel and when creating the PDF table. The devolatilisation temperature is lowered to begin with and then once the flame is established it should be increased to the correct value.

Table 9: CFD Solution Procedure

STEP 1: Unreactive Flow	**Iterations**
• Turn off PDF equations and discrete phase interaction.	**300**
STEP 2: Ignite Flame	
• Turn on PDF equations and discrete phase interaction. • Patch a high temperature to the flame region.	**1**
STEP 3: Reactive Flow	
• Set the number of continuous phase iterations per discrete phase iteration to 50.	**300**
STEP 4: Radiation Model	
• Turn on Discrete Ordinates radiation model (including particle radiation ineraction).	**500**
STEP 5: Discretization Scheme	
• Change discretization scheme to Second Order Upwind for all equations, except Discrete Ordinates which is left as First Order	**300**
STEP 6: Converged Model	
• Set the coal devolatilisation temperature to the correct value. This requires a new PDF table.	**Until Converged**

Table 10: Under-relaxation Settings

URF	**1**	**2**	**3**	**4**	**5**	**6**
Pressure	0.3	0.3	0.3	0.3	0.3	0.3
Density	0.5	0.5	0.5	0.5	0.5	0.5
Body Forces	1	1	1	1	1	1
Momentum	0.7	0.7	0.7	0.7	0.7	0.7
Turbulent Kinetic Energy	0.7	0.7	0.7	0.7	0.6	0.6
Turbulent Dissipation Rate	0.7	0.7	0.7	0.7	0.6	0.6
Turbulent Viscosity	1	1	1	1	1	1
Energy	1	0.95	0.95	0.95	0.8	0.8
Temperature	1	1	1	1	0.8	0.8
Discrete Ordinates	1	1	1	1	1	1
Mean Mixture Fraction	1	1	1	1	0.8	0.8
Secondary Mean Mixture Fraction	0.9	0.9	0.9	0.9	0.7	0.7
Mixture Fraction Variance	1	1	1	1	0.8	0.8
Secondary Mixture Fraction Variance	0.9	0.9	0.9	0.9	0.7	0.7
Discrete Phase Sources	-	1	0.1	0.1	0.1	0.1

5.2 Mesh

A three-dimensional, quarter-geometry mesh containing 52,000 tetrahedral cells was initially constructed using Gambit. As with any CFD simulation, it is important to undertake a grid-independence study to ascertain the accuracy of a mesh. Therefore, after running a basic coal combustion simulation with the initial mesh, three further meshes were generated using the gradient adaption tool in FLUENT. Mesh refinements were made in areas of high velocity and temperature gradients to produce meshes with 114,000, 220,000 and 440,000 cells respectively.

To check the mesh independence two lines were created on the four respective meshes at consistent arbitrary points. Both lines were situated on one side of the quarter-domain geometry (ie, on the mid plane). The two lines were 0.25 metres and 1.25 metres respectively from the burner quarl outlet. Axial velocity and temperature profiles were obtained at each line for the four meshes and combined in Microsoft Excel to allow for investigation of the mesh independence.

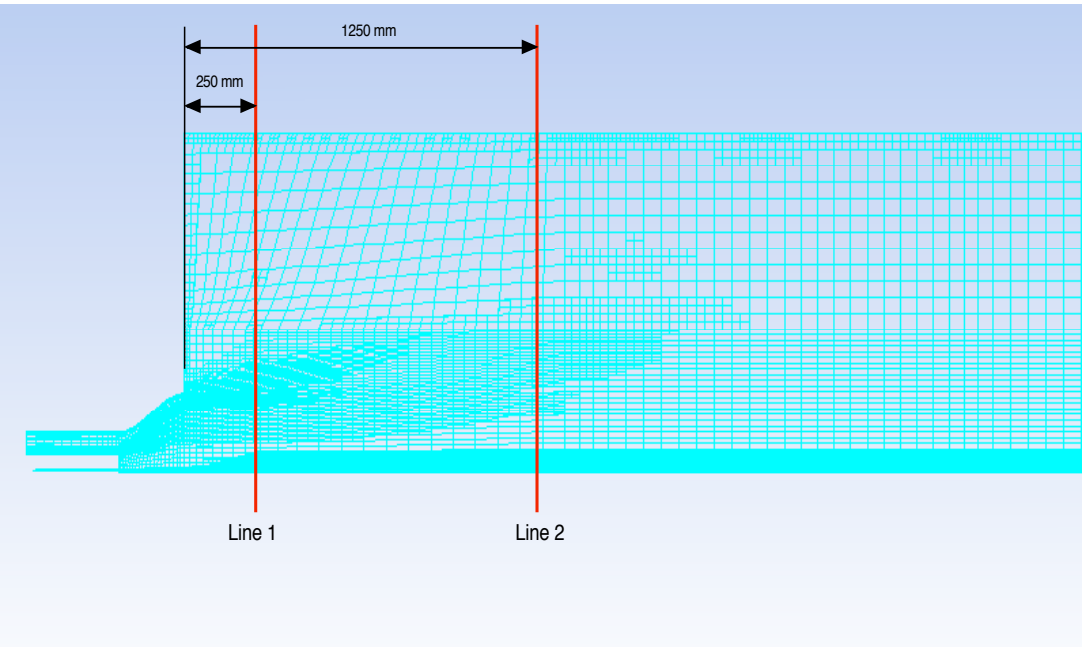

Figure 16: Shows location of the two lines used for investigating mesh independence.

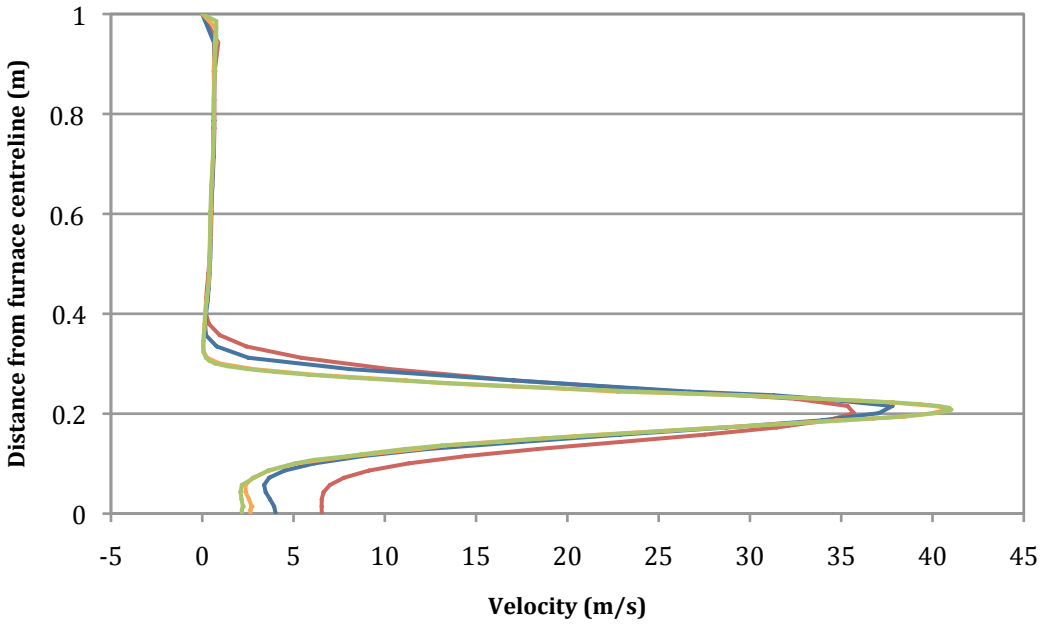

Figure 17: Axial velocity profiles at Line 1 for the 58,000 cell (■), 114,00 cell (■), 220,000 cell (■) and 440,000 cell (■) meshes.

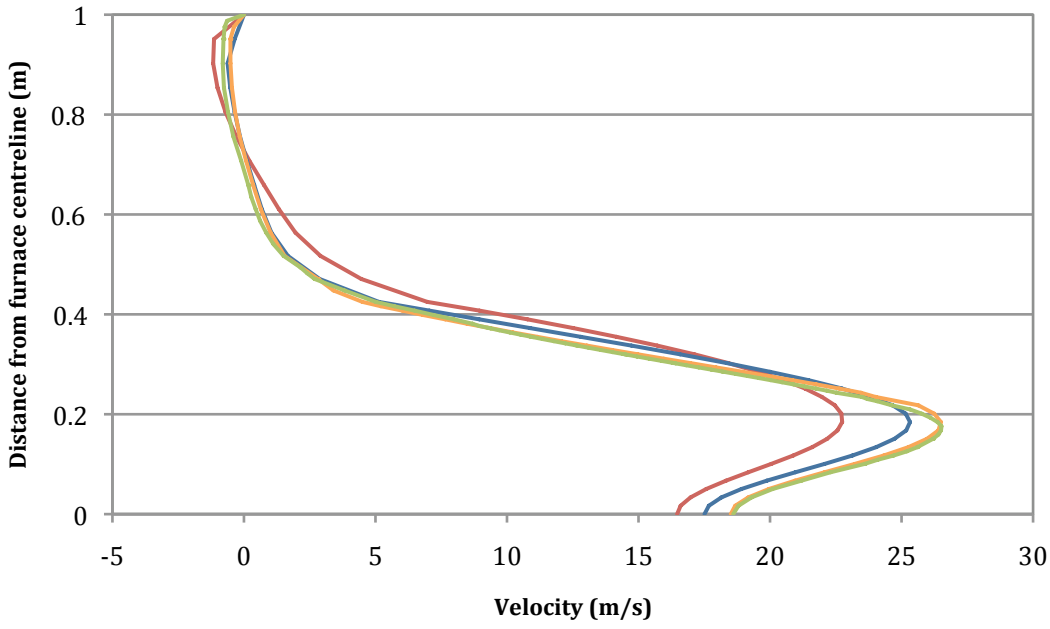

Figure 18: Axial velocity profiles at Line 2 for the 58,000 cell (■), 114,00 cell (■), 220,000 cell (■) and 440,000 cell (■) meshes.

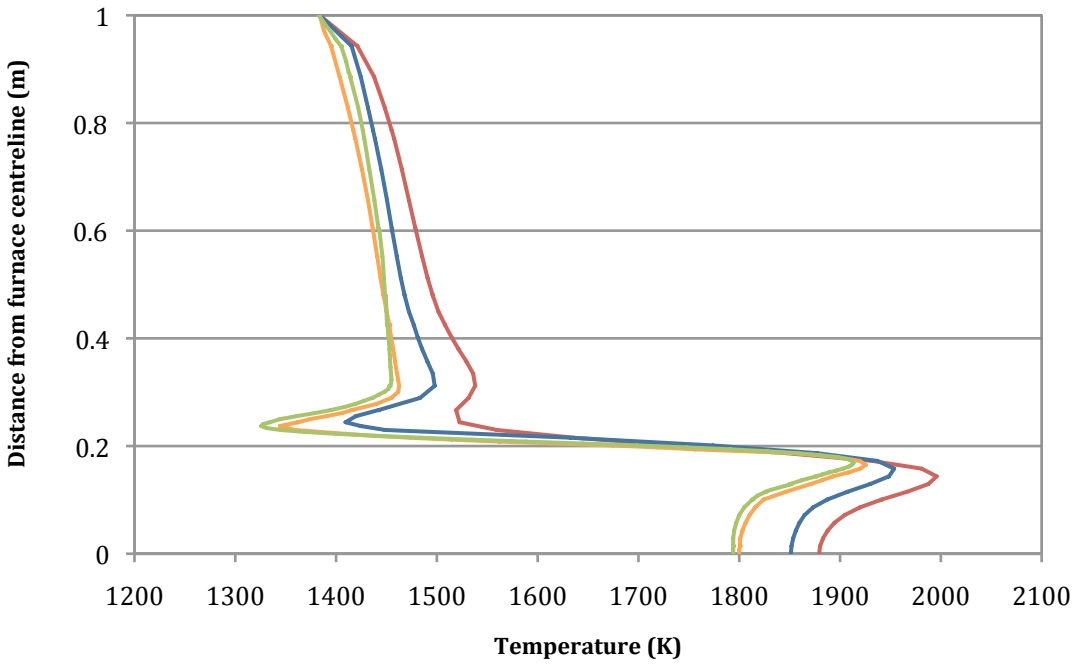

Figure 19: Temperature profiles at Line 1 for the 58,000 cell (■), 114,00 cell (■), 220,000 cell (■) and 440,000 cell (■) meshes.

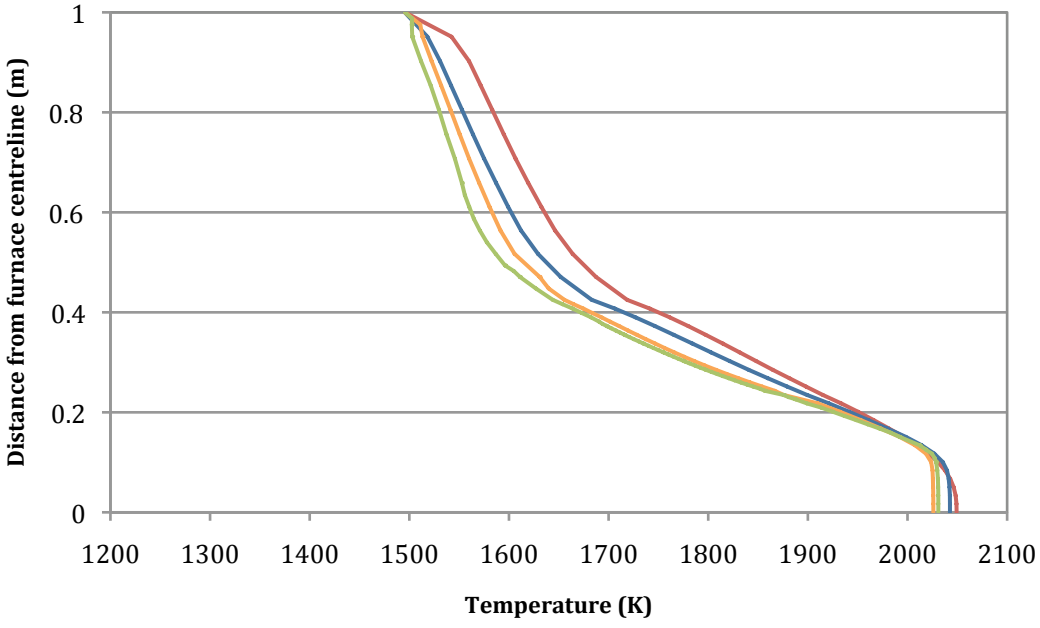

Figure 20: Temperature profiles at Line 2 for the 58,000 cell (■), 114,00 cell (■), 220,000 cell (■) and 440,000 cell (■) meshes.

Figure 17 and Figure 18 show velocity profiles of each mesh at Lines 1 and 2. Refinements of the original mesh in areas of high velocity gradient are seen to have a notable effect on the velocity profiles; however there is little difference between the two larger meshes. The same situation is seen in the temperature profiles of Figure 19 and Figure 20, especially close to the burner outlet. The mesh independence study has shown that the 220,000 cell mesh is the most suitable for investigating the IFRF furnace providing an accurate result while using minimal computational resources.

5.3 Preliminary Studies

The first stage of the validation case involved investigating the sensitivity of different parameters and sub models used for coal combustion simulations in FLUENT. Variations in the chemistry and devolatilisation sub models and the way in which the coal particle size is defined all returned interesting results, as explained in the following sections

.

5.3.1 Coal Size Distribution

Simulations of the validation case were run with the size distribution of the pulverised coal injections defined in two different ways, albeit for the same coal sample. In the first case multiple injections were used, with each injection having a different uniform particle size. This essentially meant taking the sieve analysis data from Table 5 and setting an injection for each sieve size, with the corresponding diameter and mass flow rate. In the second case a single injection was used with a Rosin Rammler distribution based on the same sieve analysis data. The centreline temperature profile for each case is shown in Figure 21, plotted against the experimental measurements. The species transport approach to combustion chemistry was used in this comparison.

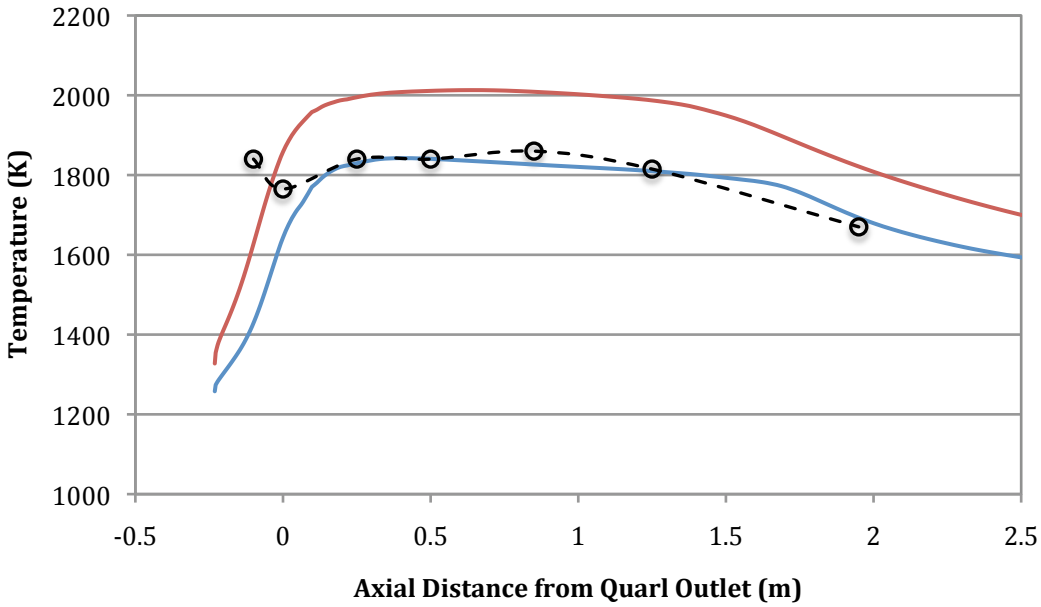

Figure 21: Centre line temperature profile of the IFRF Furnace for; experimental results (○), multiple injections with a uniform size distribution (■), and single injection with a Rosin-Rammler distribution (■)

Inside the burner region neither of the two simulations presented in Figure 21 produces an accurate representation of the real furnace. Further downstream however the multiple injection case simulates the real furnace very well. Meanwhile the single Rosin-Rammler injection case returns a centreline temperature profile that is 100-200K hotter than the experimental measurements.

These findings suggest that for future work it would be best to use multiple uniformed sized injections when modelling pulverised coal combustion as they return the most accurate result. However, for the case of the McDonald's Lime rotary kiln, the sieve analysis data is of rather poor quality with nearly 57% of the average sample's mass passing through the smallest 53 μm sieve. Therefore the author felt it would be best to use a Rosin Rammler distribution to ensure adequate representation of the range of small particles. Future work will look at obtaining a more accurate sieve analysis of the pulverised coal produced at McDonald's Lime.

Suggestions have however been made that the inaccuracies seen when using a Rosin Rammler particle size distribution may have arisen due to an inadequate amount of representative particle diameters being used for the coal particle injection. Time constraints meant that this issue was not further investigated and therefore it is recommended that if work continues on the current project the setup of particle injections with a Rosin Rammler size distribution be investigated.

5.3.2 Devolatilisation Sub-Models

Comparisons were made between the single kinetic rate and constant rate devolatilisation models. Parameters for the single rate model were taken directly from the paper of Peters and Weber (1996). For the constant rate model a constant of 50 s^{-1} was used which was the setting used in the FLUENT tutorial that has been referred to. The centreline temperature profile for each case is shown in Figure 22, plotted against the experimental measurements. The species transport approach was again used in this comparison.

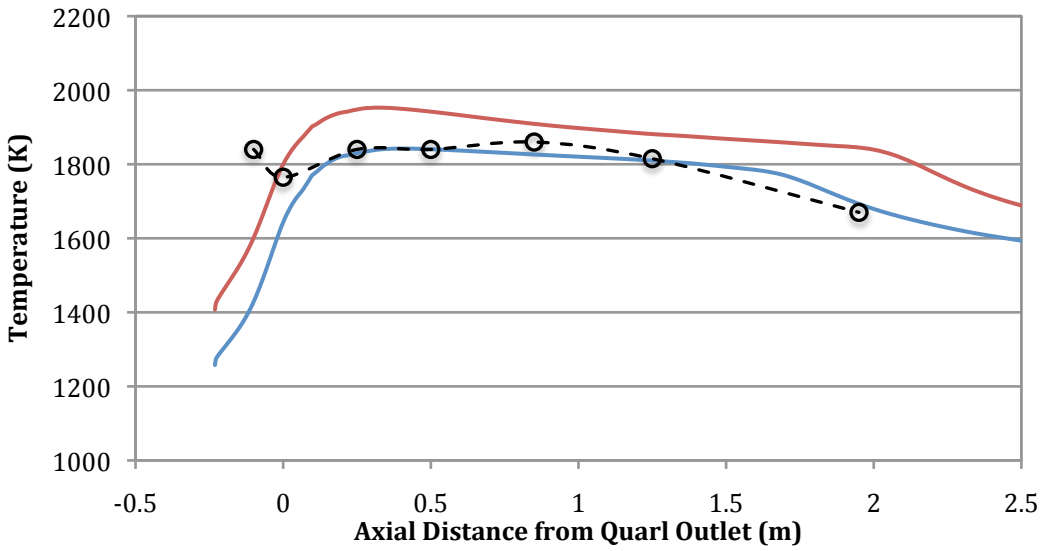

Figure 22: Centre line temperature profile of the IFRF Furnace for; experimental results (○), single-rate devolatilisation model (■), and constant rate (A_0=50) devolatilisation model (■).

Figure 22 shows that the constant rate model returns the most accurate representation of the real furnace and thus all future modelling used this devolatilisation model.

5.3.3 Combustion Sub-Models

At the very beginning of the current project a significant amount of time was spent resolving which would be the best combustion chemistry approach to use; species transport or mixture fraction/PDF. As a result a study was undertaken to compare the differences between the two approaches. The study primarily focused on the validation case, however models were also run on the 3D Kiln Two mesh, at which point problems such as slow convergence and even divergence were encountered when using the species transport approach. This problem was put down to the high computational expense needed to solve the many transport equations of the species transport model. In comparison, the mixture fraction/PDF approach worked very well on the 3D Kiln Two mesh and therefore this model was used for all future modelling.

In spite of the need to use the mixture fraction/PDF approach for modelling the McDonald's Lime kiln, a comparison of the two combustion chemistry models has been performed using the IFRF furnace. The centreline temperature profile for each case is shown in Figure 23, plotted against the experimental measurements. Both models use the constant rate devolatilisation model and multiples uniform sized injections.

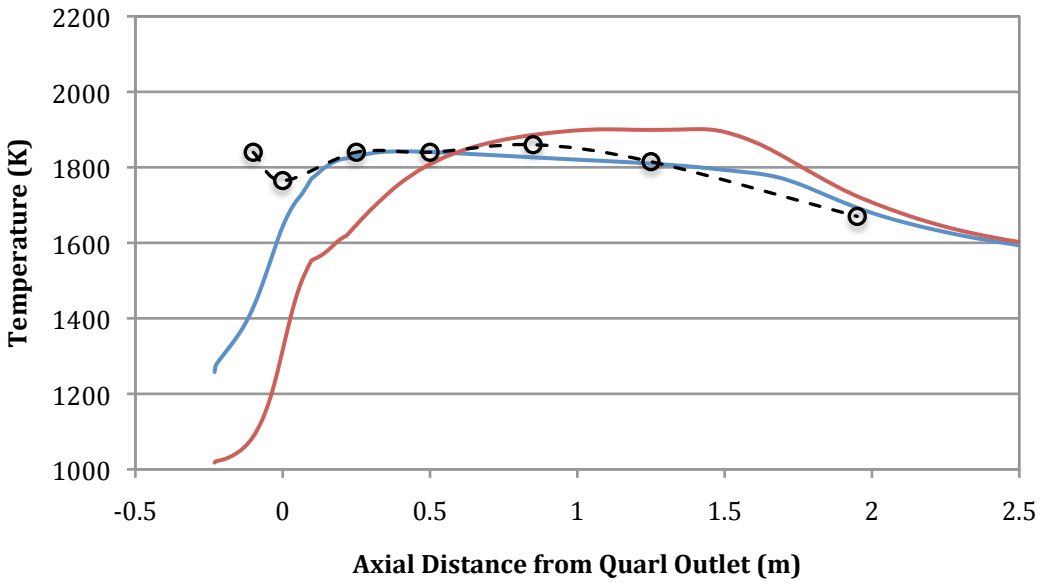

Figure 23: Centre line temperature profile of the IFRF Furnace for; experimental results (O), the mixture fraction/PDF approach (■), and the species transport approach (■).

As shown previously, the species transport model accurately duplicates the experimental measurements, except in the near burner region. The mixture fraction/PDF model is less accurate in the portion of the kiln that has experimental measurements recorded; however well downstream there appears to be reasonable agreement between the two models.

The author suggests that the mixture fraction/PDF approach may not cope with swirling flow as well as the species transport approach. As will be seen later in the velocity contour plots, the intensity of the swirling flow diminishes downstream of the burner and this may be a reason for the accuracy of the mixture fraction/PDF approach improving. There is little evidence to support this theory however and therefore it is a suggestion that future work may investigate the performance of the two combustion chemistry approaches for both swirl and non-swirl burners.

5.3.4 McDonalds Lime kiln modelling approach

As a result of the preliminary validation case investigations it was decided that future modelling of the McDonald's Lime rotary kiln would be conducted using the mixture fraction/PDF approach to combustion chemistry, the constant rate devolatilisation model and a single particle injection with a Rosin Rammler size distribution. Figure 24 shows a plot of the centre line temperature profile using these submodels, plotted against the experimental results. Subsequent sections of this chapter will continue to investigate the validity of replicating pulverised coal combustion using FLUENT and the chosen sub models.

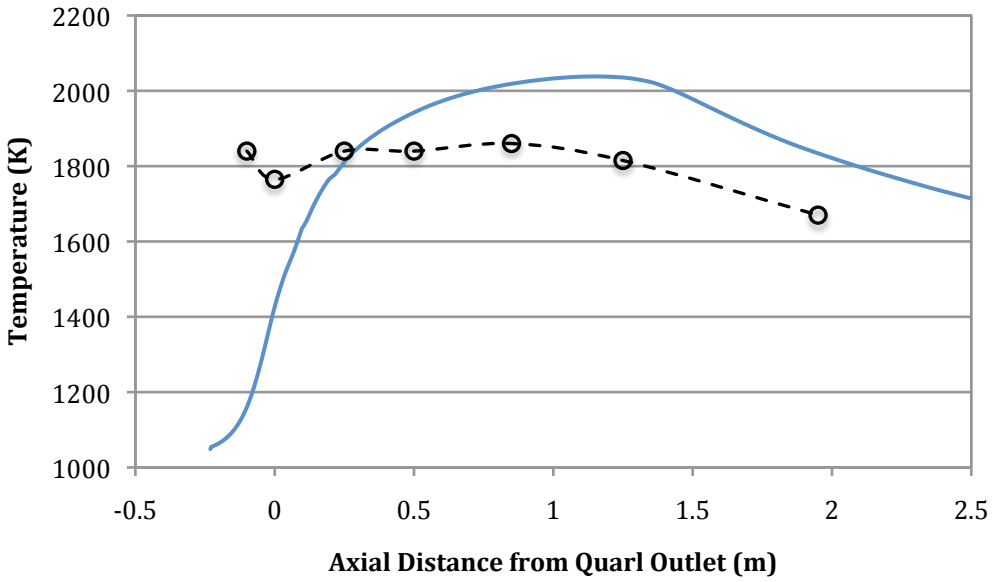

Figure 24: Centre line temperature profile of the IFRF Furnace for the experimental results (O), and mixture fraction/PDF approach with Rosin Rammler particle size distribution and constant rate devolatilisation model (■).

5.4 Calculated Results Versus Measurements

This section fully investigates the accuracy of FLUENT for modelling pulverised coal combustion, using the sub models detailed in the previous section. Temperatures, velocities and species concentrations of the validation case are investigated before a conclusion is made about the validity of further modelling.

5.4.1 Model Reliability

The first path towards providing an accurate model is for FLUENT to have acceptable mass and energy balances. The thermal input for the overall energy balance consists of the sensible heat flow rates of the transport air, combustion air and coal and the overall heat release rates of the combusting coal. The thermal output of the energy balance consists of the convective and radiative heat transfer rates to the walls and cooling loops, and the sensible heat flow rate of the flue gas at the outlet. Figure 25 presents a diagram highlighting each of the components of heat and mass transfer, while Table 11 provides an overall summary.

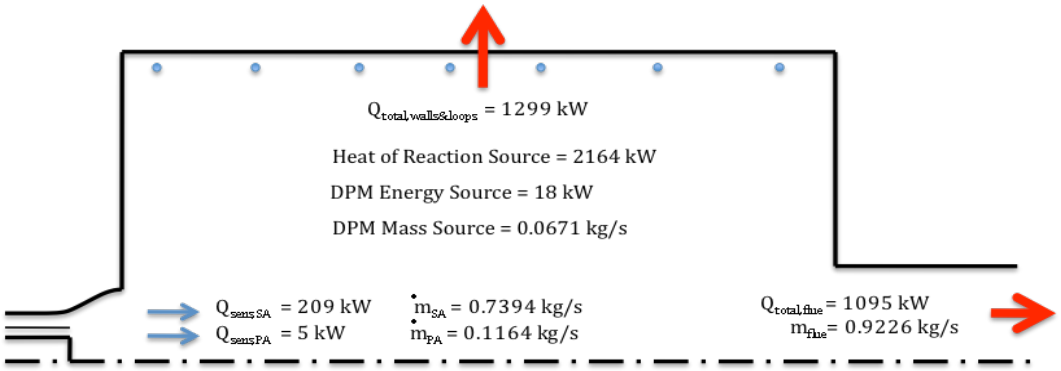

Figure 25: IFRF furnace mass and energy flows. Mass flow rates are in kg/s and energy flow rates are in kW.

Table 11: Furnace Modelling Results

Mass Balance	
In	0.9229 kg/s
Out	0.9226 kg/s
Energy Balance	
In	2378 kW
Out	2411 kW
DPM Enthalpy Source	-17.7 kW
Continuous Phase Imbalance	-18.7 kW

The incoming and outgoing mass and energy flows are seen to balance very well with imbalances of only 0.03% and 1.4%, respectively. The thermal input from the coal in the FLUENT simulation is 2164 kW, which compares well to the theoretical input of 2165 kW. Overall, it is considered that the current model returns an accurate and balanced solution and therefore will be used for validation of FLUENT for combustion modelling.

There is a commonly recognised way to check the energy balance of a simulation that is much simpler than analysing the total energy in and out of a system, as has been done above. This method involves comparing the DPM Enthalpy Source and the total imbalance of the continuous phase. If the difference between the two values is small (<5%), as is the case above, then the system is considered balanced. This is the process used to check the energy imbalance of all future models.

5.4.2 Temperature Profiles

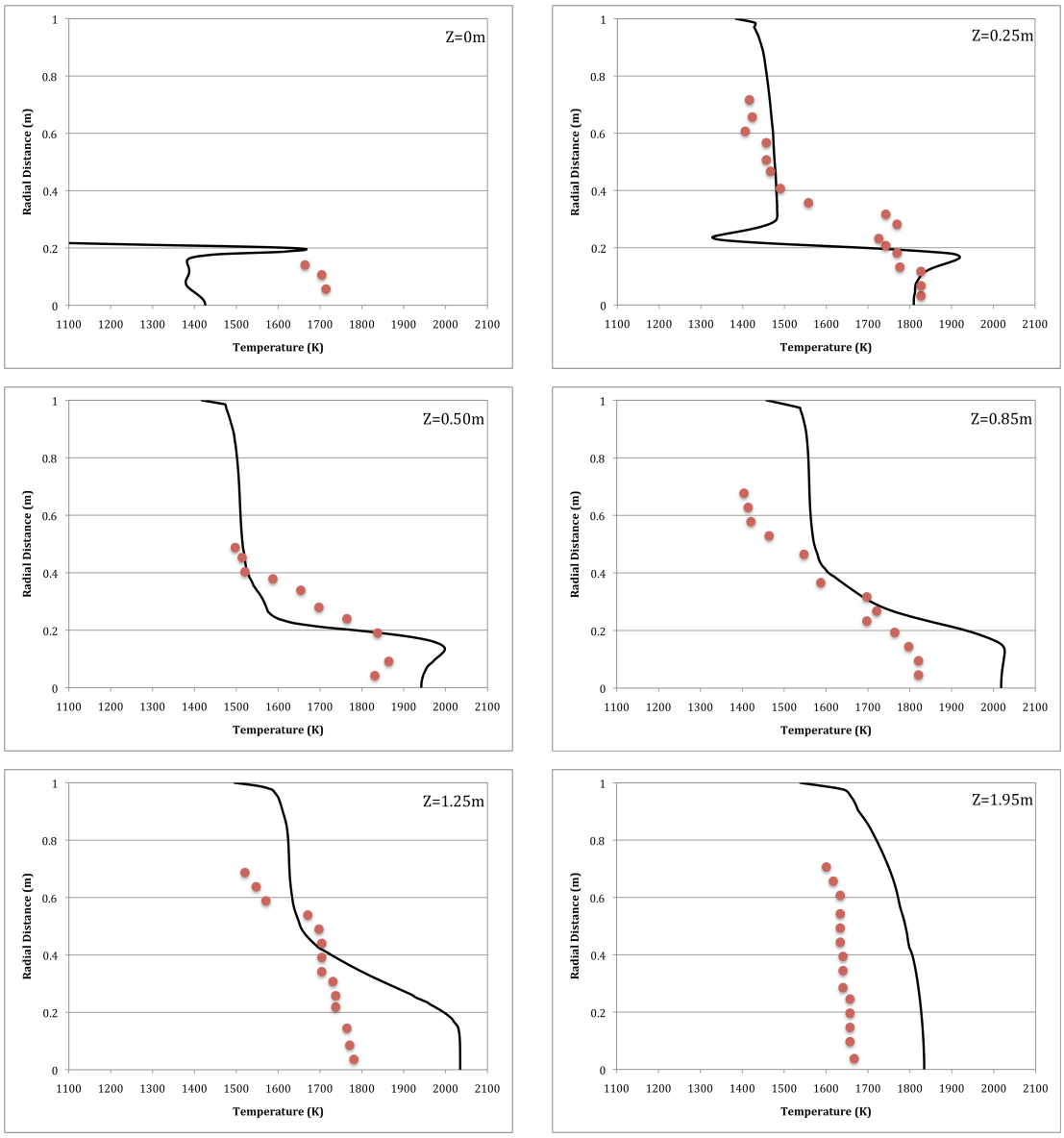

Figure 26 (a) – (f): Measured and calculated temperature profiles at six traverses in the IFRF furnace.

The vertical temperature profiles highlight the same trends seen earlier in the centreline profile comparisons. Close to the burner there is little agreement between experimental and numerical results. Downstream the numerical results demonstrate a similar trend to the experimental results however they are consistently 100-200K hotter. The numerical results also appear to have larger temperature gradients when moving radially outwars in comparison to the measured data.

5.4.3 Velocity Profiles

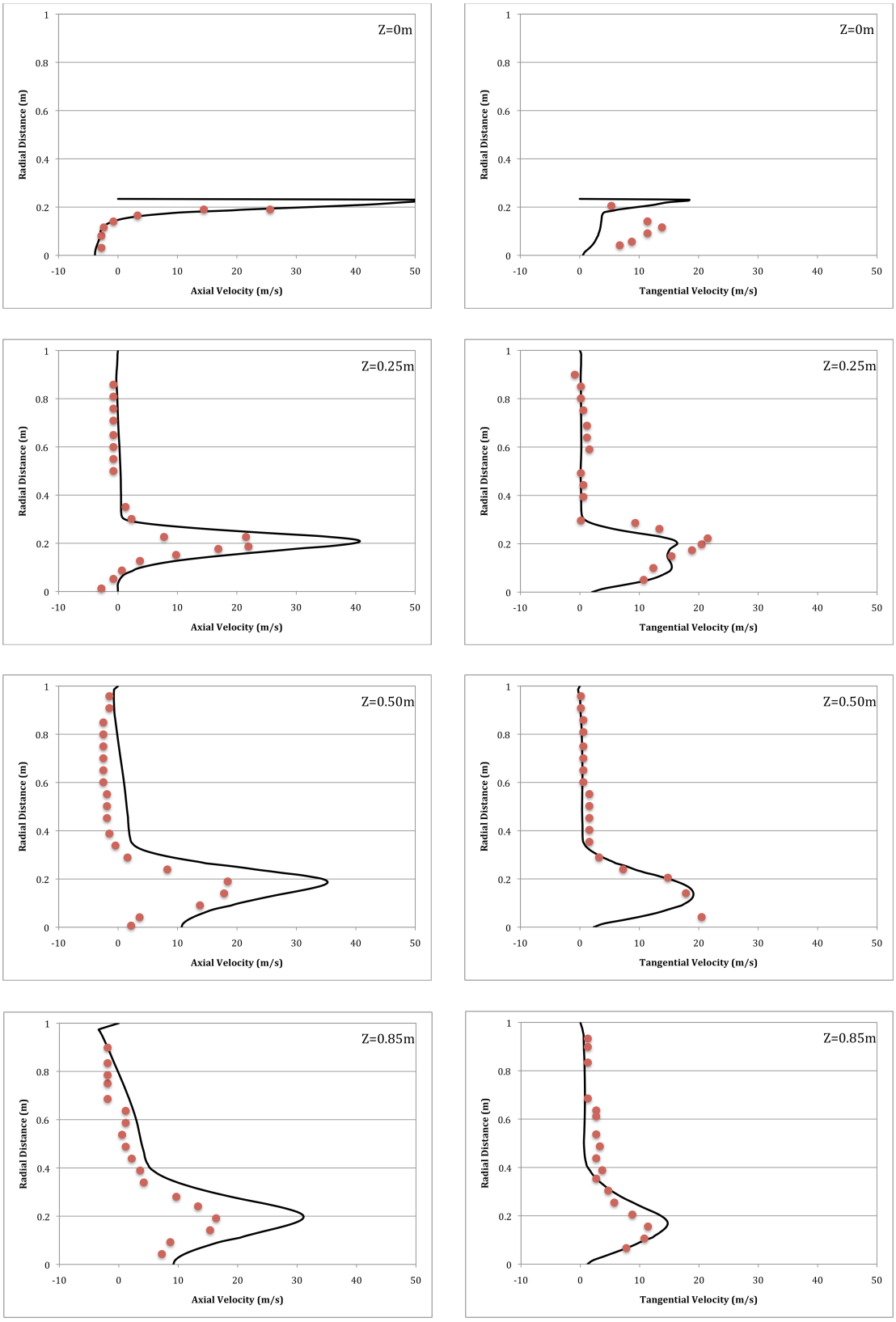

Figure 27 (a) – (h): Measured and calculated velocity profiles at eight traverses in the IFRF furnace.

When comparing the predicted and experimental velocity profiles it can be concluded that FLUENT predicts the axial velocity field with respectable accuracy in the near burner region. Further downstream however the results differ slightly more with FLUENT over predicting the axial velocity in the region close to the kiln centre line and thus under predicting the size of the internal recirculation zone (IRZ). A sensitivity study of the devolatilisation model and its rate constants found that the flow field is affected by the rate of volatile release and that by slowing the release rate of volatiles the IRZ increases in size and the axial velocity field can be matched more accurately to the experimental results. This is, however, at the expense of creating a temperature profile that is incredibly inaccurate.

While the swirl velocity is modelled with acceptable accuracy, it is slightly under predicted in the near burner region. Further downstream there is better agreement between the two sets of results, with the exception of the measurement closest to the furnace centreline at z = 0.50m. This single point does not appear to follow the trend in tangential velocity shown by all the other measurements and therefore little notice is taken of it. Overall it is thought that FLUENT provides a good representation of the flow field in the test case furnace.

The inaccuracy in the swirl velocity estimations close to the burner may be due to the LDV technique used for velocity measurement. Weber, Dugue, Sayre and Visser (1992) argued that the high viscosity of the hot flue gas and a large number of small particles (<5μm) result in a very high probability that the detected LDV signals do represent the gas velocity, with the exception of the close vicinity of the coal injector.

5.4.4 Species Profiles

Oxygen and Carbon Dioxide concentrations are compared at seven traverses in the IFRF Furnace.

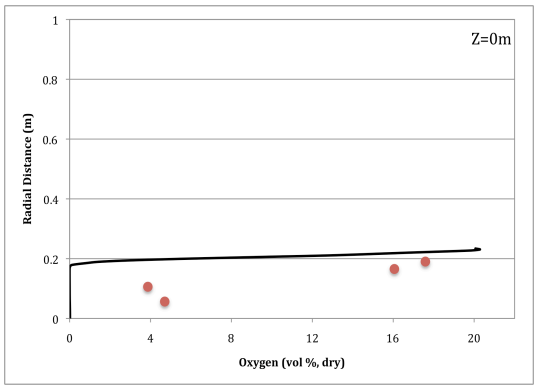

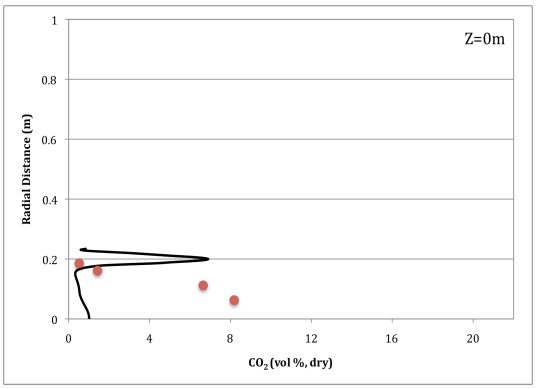

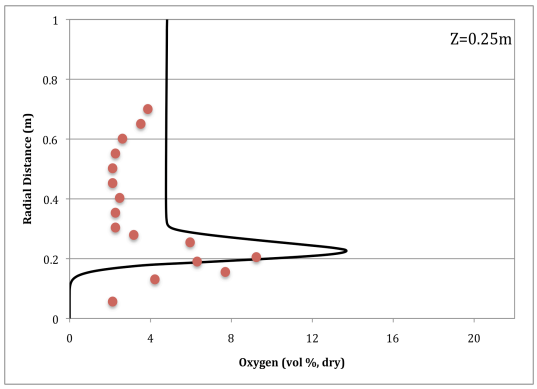

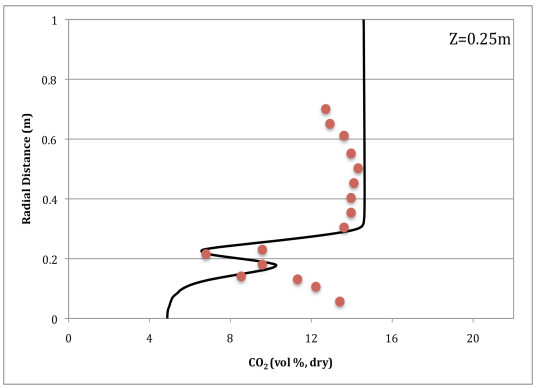

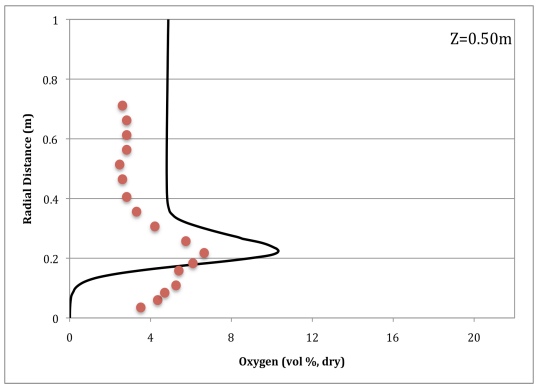

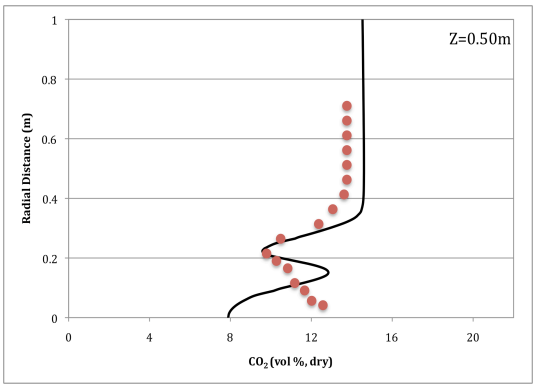

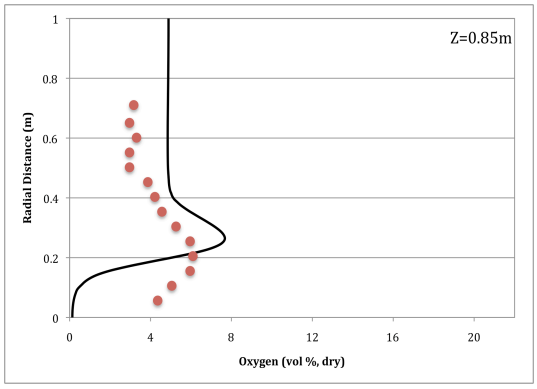

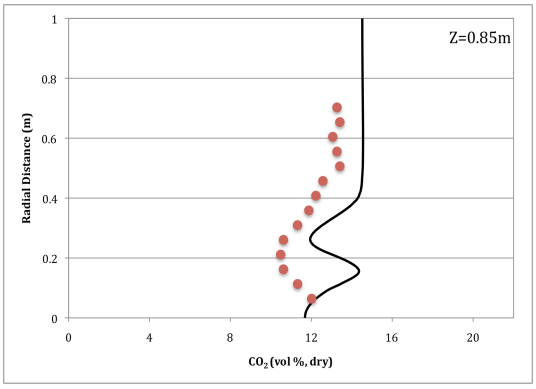

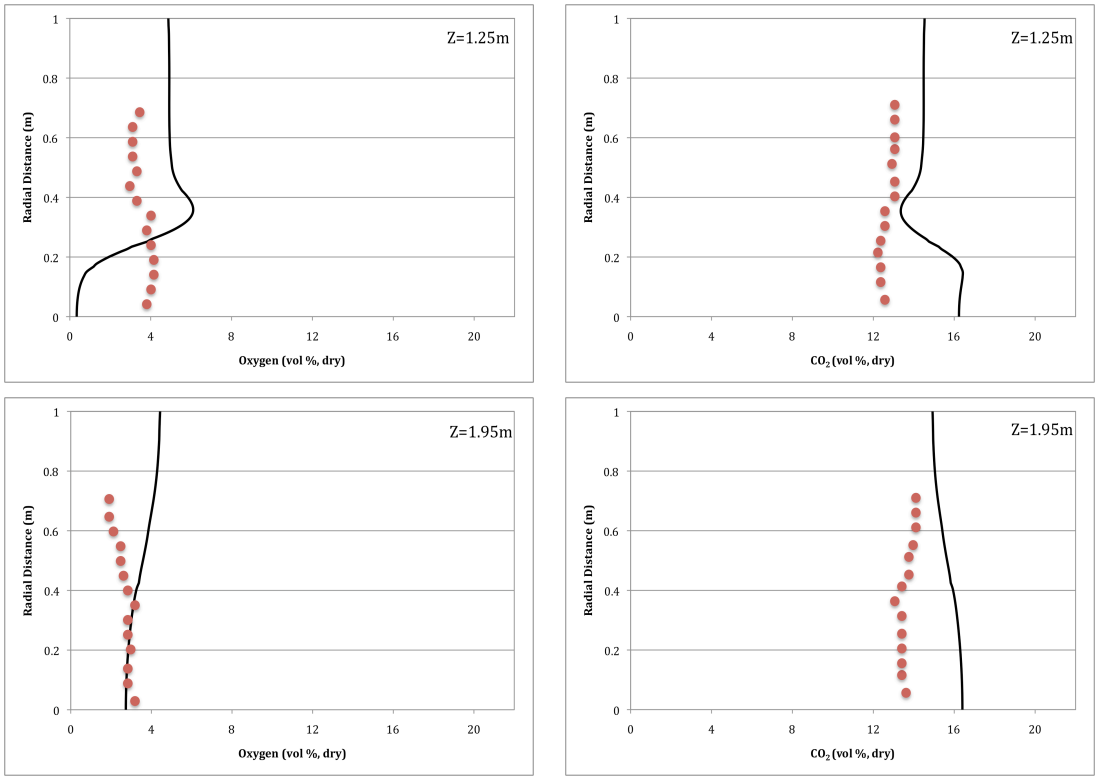

Figure 28: (a) – (h): Measured and calculated Oxygen and Carbon Dioxide concentration contours at eight traverses in the IFRF furnace.

The species profiles show the oxygen to be consistently under predicted in the flame region close to the kiln centreline. Meanwhile the Carbon Dioxide is under predicted up to z = 0.85m before being over predicted further downstream. There are a number of reasons as to why the O_2 could be under predicted near the furnace centreline. One possibility is that the volatiles are being released too fast. As the volatiles are released the oxygen being drawn inwards by the swirling flow is quickly consumed as the volatiles oxidise and produce heat. In contrast this theory would suggest that an over prediction of oxygen would be seen near the central axis when the volatile release rate is too slow, and oxygen diffuses inwards faster than the rate at which it is consumed. Having a greater oxygen concentration in the central region may also lead to greater char combustion in the same area. If this was to occur it may even out the spike in temperature that occurs in the shear region as can be seen in the temperature profiles. The default devolatilisation rate of 50 s^{-1} was however used for the validation case, and consequently further modelling, as it provided the best representation of measured data and conformed to Peters and Webers (1996) and Weber et al's (1995) explanation of devolatilisation characteristics. These

authors propose that a high volatile bitumous coal does not release any volatile matter into the gaseous phase until the particle has reached 500°C and then at a temperature of 1000°C all remaining volatiles are released. It was for this reason that the devolatilisation temperature is set at 500°C. Inside the quarl zone of the IFRF Furnace, temperatures in excess of 1200°C are seen suggesting that the temperature at the exit of the burner annulus is close to 1000°C. Therefore it is most likely that the volatile matter is released inside the quarl region, close to the burner annulus.

Another factor that could lead to discrepancies in the oxygen and carbon dioxide predictions is that the reaction

$$CO + OH \rightarrow CO_2 + H \tag{55}$$

is not considered by FLUENT in the combustion process. The reaction shown is considered to be of great significance in the reaction of hydrocarbon fuels and even to be preferred over the reaction of CO and O_2, especially over temperatures of 1000K (Peters & Weber, 1996). If the reaction was considered by FLUENT then immediately there would be less CO present and a greater CO_2 concentration in the region where combustion is taking place. At the same time more there would be a greater concentration of O_2 present with OH being the favoured reactant. The inclusion of this reaction may help bring the species concentration predictions in line with the experimental results.

5.5 Conclusion

Overall it is concluded that FLUENT is a suitable program for CFD modelling of combustion in the McDonald's Lime rotary kiln. The species transport approach to combustion chemistry was seen to return the most accurate numerical results, however the mixture fraction/PDF approach will be used for future modelling of Kiln Two due to its computational efficiency.

Comparisons were made at several traverses in the IFRF Furnace between experimental measurements and numerical results obtained using the mixture fraction/PDF approach to combustion chemistry. Temperature profiles highlighted the same trends, however they were up to 200K different in some areas. Both the axial and tangential velocity profiles correlated well with the experimental measurements however the numerical model was seen to underestimate the internal recirculation zone. There were some discrepancies seen in the species concentration comparisons, however these are likely due to the way FLUENT handles the species reaction processes.

In future it is felt that it would be beneficial to find a validation case without a swirl burner and investigate the way in which the two combustion chemistry models handle both swirling and non-swirling flow. It is also thought that the current case could be enhanced with further investigation and adjustment of the many combustion-modelling parameters.

6 Operating Conditions

In order to develop a numerical model of Kiln Two at Mcdonald's Lime it was necessary to capture the operating conditions such as flow rates, temperatures and fuel composition. The operating conditions obtained were based on average values and were thus used to develop a 'control' numerical simulation. The subsequent research into the performance of Kiln Two involved making small changes to the control case to investigate how different parameters affect the combustion characteristics.

Where possible the operating conditions have been obtained from existing production logs, and in this case averages were taken for a three-month period. There were instances, however, where to obtain a suitably accurate model, new equipment was installed to capture previously unknown operating conditions. In these situations, multiple samples/measurements were taken to ensure an accurate representation of the required parameter was obtained.

6.1 Modelling Bounds

To fully model the expansive Kiln Two system from the product cooler to smoke stack would require a very complex CAD model, an enormous mesh and the incorporation of many moving parts such as fans, conveyors and cyclones. Consequently the modelled flow domain focuses on the cylindrical kiln section where combustion is taking place. The modelling bounds, as shown in Figure 29, are also extended to include the transfer chute and firing hood, regions that are though likely to influence the flow field through the kiln.

The modelled domain consists of two velocity inlets and two pressure outlets. Primary air enters the domain through the single tube burner pipe while secondary, preheated, combustion air enters through the boundary at the top of the product cooler. A small portion of secondary air, extracted for use in the coal

mill, exits the flow domain at the top of the firing hood. All the combustion gases and any excess air exit the modelled domain at the transfer chute boundary.

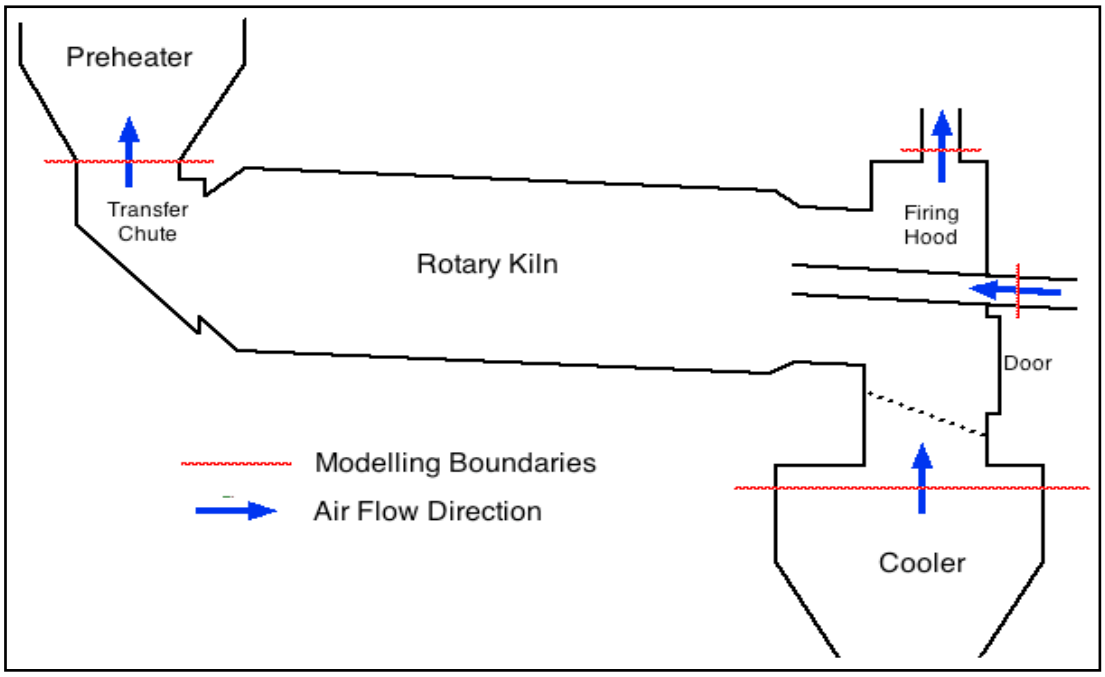

Figure 29: Schematic of Kiln Two highlighting boundaries of the CFD modelling.

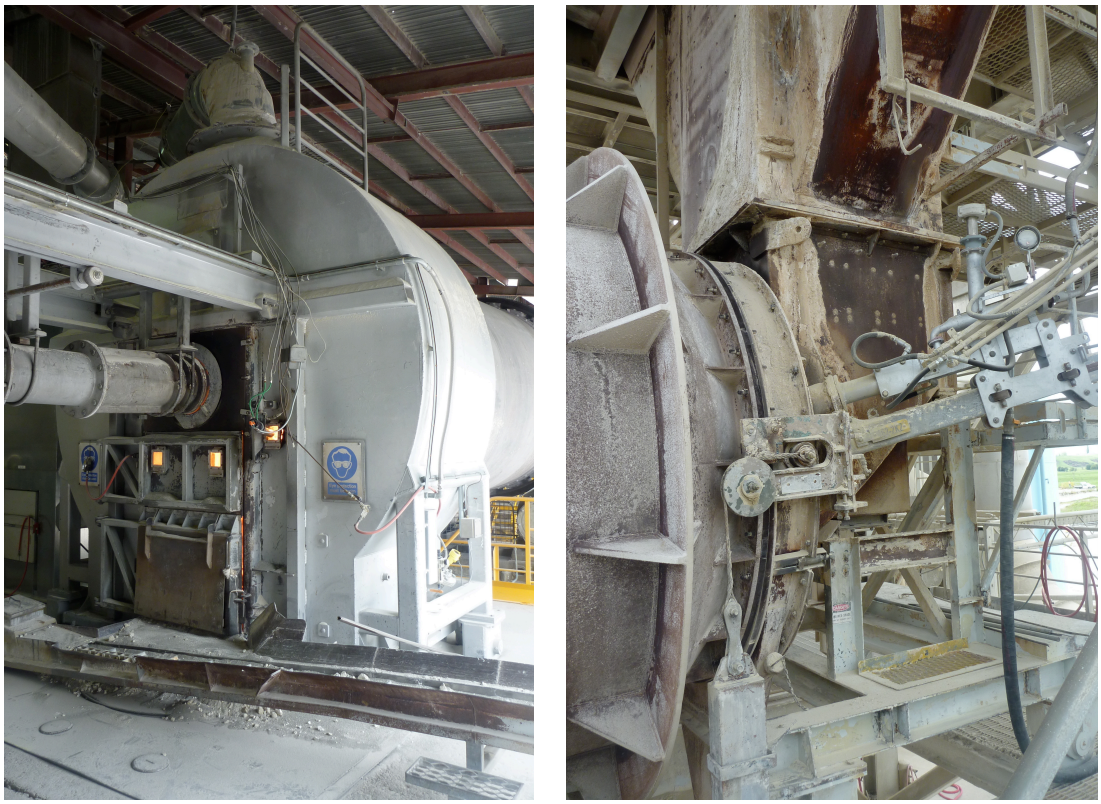

Figure 30: Photos of the Firing Hood (left) and Transfer Chute (right) at either end of the cylindrical kiln section.

6.2 Wall Boundary Conditions

CFD modelling of Kiln Two is limited to the internal flow domain and therefore appropriate boundary conditions must be applied to account for the actual conditions at the bounding walls. As the thickness and material type of the walls varies significantly throughout the kiln system, the walls of the modelled domain have primarily been split into three distinct areas, as listed below, in order to simplify the mesh building process, setup time and solve time. Furthermore, the work presented in this thesis is focussed on comparing the flame characteristics for different fuels and air flow rates. There is little focus on heat transfer to the walls and therefore it is not deemed necessary to implement highly accurate wall boundary conditions, especially in the firing hood and transfer chute areas.

1. Firing Hood/Cooler
2. Cylindrical Kiln
3. Transfer Chute

The Firing Hood/Cooler region has a temperature boundary condition that is the same temperature as the secondary combustion air that flows through it (712K). The Cylindrical Kiln section has a convective boundary condition applied that is modified from the true wall properties in order to account for the energy that is absorbed by the calcinating lime bed in the real kiln. The application of this boundary condition is explained in more depth in the next section of this chapter. The Transfer Chute area again has a temperature boundary condition, set as the average temperature of the exit gas (1281K) and the incoming limestone (1023K). Addtionally the grating and bullnose have a zero heat flux boundary condition, while the burner pipe wall is set to the temperature of the fluid flowing through it.

In addition to applying a convective coefficient to the wall boundary, an emissivity has been chosen based on the wall material. The three different emissivities used during the current modelling work are listed in Table 12.

Table 12: Wall Emissivity's.

Wall Surface	Emissivity
Firebricks / Lime Dust	0.85
Covered in Coal Dust	0.95
Bare Steel	0.5

6.3 Modelling the Thermal Load

Chapter Five presented a validation case to highlight FLUENT's predictability of combustion and heat transfer in a furnace. Validation of the model was limited to the case of an empty kiln with a large fraction of the heat being lost through the kiln walls, most significantly in the hot (flame) end. However in the presence of a bed, such as in a rotary lime kiln, further energy is absorbed as the limestone heats up and then chemically decomposes to calcium oxide. Although predicting the bed behaviour is not within the scope of this project, the energy it absorbs must be accounted for otherwise the temperature inside the kiln becomes overestimated. The thermal load due to the presence of a bed can be addressed for the limiting case of an inert bed, where the heat consumption is assumed constant throughout the length of the kiln.

It is assumed that the mean axial temperature profile of the bed is very close to that of the inside wall. Previous studies by Barr, Watkinson and Brimacombe (1989) on a pilot kiln at the University of British Columbia found that the bed is almost at the same temperature as the inside wall, while past numerical simulations involving calcination of petroleum coke show that the temperature of the internal core of the bed is about 125°C lower than the inside wall temperature (Kocaefe et al., 1992). Hence the thermal load of the bed may be lumped with that of the refractory wall by adjusting the thermal conductivity of the refractory wall by a certain amount (Alyaser, 1998). Ignoring the thermal resistances across the steel shell, the equivalent steady-state heat transfer rate through the refractory wall, q_w, is described as follows:

$$q_w = \frac{2\pi k_{equiv}(T_b - T_a)}{\ln(r_s / r_w)} \tag{56}$$

where, k_{equiv} is the equivalent thermal conductivity accounting for the thermal load, T_b is the mean temperature of the bed, T_a is the shell temperature and r_w and r_s are the inner and outer radii of the kiln respectively. The rate of heat absorption by the bed over the entire length of the kiln (cylindrical section only) is calculated using the flow rate and reaction enthalpy of limestone.

$$\frac{\dot{m}\Delta H_r(1-x)}{L} = \frac{2\pi k_{bed}(T_b - T_a)}{\ln(r_s/r_w)} \tag{57}$$

from which an expression for the replicated bed thermal conductivity is derived as follows:

$$k_{bed} = \frac{\dot{m}\Delta H_r(1-x)\ln(r_s/r_w)}{2\pi L(T_b - T_a)} \tag{58}$$

and

$$k_{equiv} = k_{wall} + k_{bed} \tag{59}$$

where $\dot{m}$ and ΔH_r are the mass flow rate and reaction enthalpy of the limestone bed, respectively. x is the portion of the decomposition reaction that occurs in the preheater. The above calculations return a modified thermal conductivity of 5.974 W/m.K which translates to a convective coefficient of 33.9 W/m^2.K for a wall thickness of 176 mm. The freestream temperature is set as the average shell temperature of 563 K.

6.4 Primary Air

Primary air enters the kiln through a single tube burner pipe. To develop a CFD model it is necessary to know the flow rate and temperature of the air as it enters the flow domain.

6.4.1 Temperature

The primary air temperature of 337.72K was obtained from an existing thermocouple situated in the firing pipe, which runs between the firing fans and the burner pipe.

6.4.2 Flow Rate

McDonald's Lime has an existing venturi flow meter used for monitoring the primary airflow of Kiln Two. This flow meter outputs a pressure difference (mm of H_2O), which must be ultimately converted to a velocity at the point the primary air enters the flow domain. The computer readout for the venturi flow meter was checked using a conventional water manometer and found to be suitably accurate.

The air travelling through the venturi flow meter includes water vapour that has been driven from coal in the mill. This is accounted for when calculating the airflow, however the effects of any residual coal dust travelling through the venturi have been neglected. To find the primary air inlet velocity, the velocity through the wide portion of the venturi, V_1, is first calculated:

$$V_1 = \sqrt{\frac{2\rho_w g h}{\rho_{all}\left[\left(A_1/A_2\right)^2 - 1\right]}} \tag{60}$$

where ρ_w and h are the density and height of water in the manometer respectively, A_1 and A_2 are the areas in the wide and narrow portions of the venturi respectively and ρ_{all} is the combined density of the air and water vapour travelling through the venturi.

$$\rho_{all} = \rho_{air} + \frac{\dot{m}_{vap}}{A_1 V_1} \tag{61}$$

V_1 reappears in the calculation for ρ_{all} and thus an iterative procedure must be taken during the above calculations. When a value for V_1 is obtained the air flow rate through the venturi can be found.

$$\dot{m}_{air} = \rho_{air} A_1 V_1 \tag{62}$$

where ρ_{air} is the density of air travelling through the venturi. This is based on the air temperature measured by the thermocouple in the firing pipe. It is assumed that the air remains at a constant temperature between the coal mill

outlet and firing pipe inlet. Finally, the mass flow rate can be used to find the velocity of primary air as it enters the flow domain.

$$V_{inlet} = \frac{\dot{m}_{air}}{\rho_{air} A} \tag{63}$$

where A is the cross-sectional area of the burner pipe at the flow domain entry. The calculations explained above provide a control primary air flow rate of 3.006kg/s which is then used to find the corresponding flow velocity at the entrance to the flow domain.

6.5 Secondary Air

Secondary combustion air is preheated as it travels up through the product cooler and into the rotary kiln. As with the primary air, the temperature and flow rate of the secondary air must be known in order to develop a CFD model.

6.5.1 Flow Rate

Secondary combustion air enters the kiln system below the product cooler where it is drawn in by a large fan and forced up through the cooler into the rotating kiln. The ID fan situated on the downstream side of the preheater is also instrumental in moving secondary combustion air through the kiln system.

Initial work to quantify the flow of secondary air focussed on measuring the air velocity (and thus flow rate) through the cooler fan inlet duct. The measured flowrate was much less than expected based on the stoichiometric requirement, suggesting that air is leaking into the kiln system. This leakage is most likely through the firing hood door given the poor seal the door often makes with the hood itself, as is seen in Figure 31.

Figure 31: Firing hood door.

Because air is leaking into the kiln system it is impossible to quantify a specific flow rate for the secondary combustion air. Therefore, it was decided through discussion with the McDonald's Lime Engineers and consultation of reports by FCT (FCT, 1997b) that the overall excess air for the system would be 10%. This allowed the required flowrate of secondary combustion air to be calculated, and consequently the velocity at the inlet to the modelled flow domain.

6.5.2 Temperature

The temperature of the secondary combustion air was taken as 712K, the average temperature measured by the existing thermocouple in the hot air duct at the top of the firing hood. The air at this point is considered to best represent the air entering the cylindrical kiln, as it will consist of the preheated air that has travelled through the cooler, mixed with any cooler air that has leaked into the system through the firing hood.

6.6 Outlet Boundary Conditions

The two regions where fluid leaves the flow domain are defined using a pressure outlet boundary condition. Air is drawn away through the hot air outlet and the transfer chute by various fans. Therefore it was necessary to ascertain the pressure at each outlet so the correct flow characteristics would be reproduced in the simulation. To achieve this two static pressure probes were placed in the respective locations (Figure 32) and measurements were taken hourly over a number of days to obtain an average pressure for each outlet (Table 13). Also listed in Table 13 is the backflow temperature at each outlet, which is taken from existing thermocouple measurements.

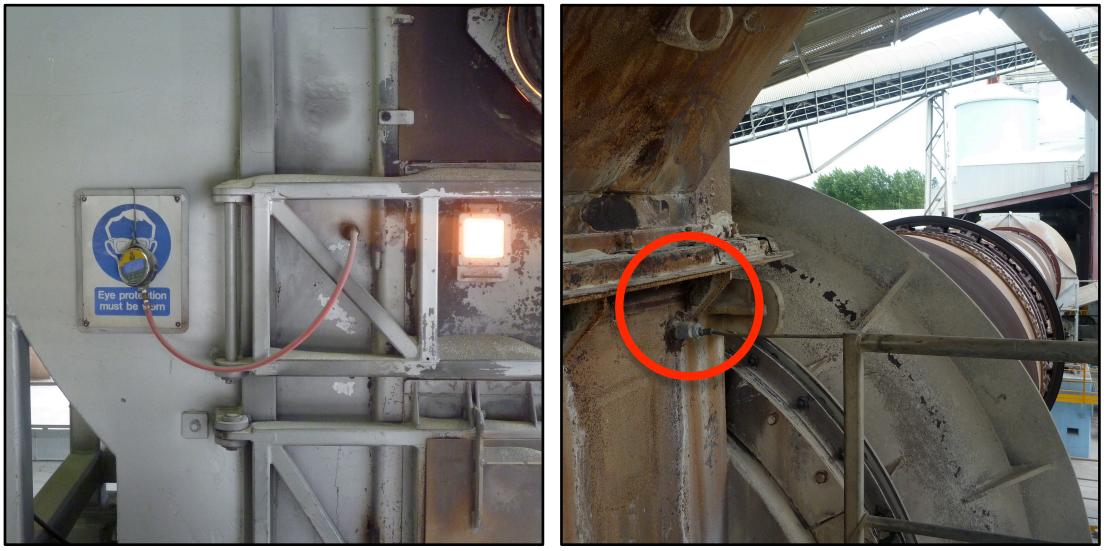

Figure 32: Static pressure probe locations on the firing hood (left) and transfer chute (right).

Table 13: Pressure outlet characteristics.

Outlet	Pressure	Backflow Temperature
Hot Air Duct	-12.5 Pa	712 K
Transfer Chute	-310 Pa	1281 K

6.7 Buoyancy

The Richardson number for the turbulent flame inside Kiln Two at McDonald's Lime was calculated to be approximately 0.005 and therefore it was felt acceptable to ignore the effects of buoyancy during the presented CFD modelling.

6.8 Coal Properties

The coal used in Kiln Two is primarily Environ Coal from Huntly, New Zealand. This section details the various different properties of Environ Coal that are necessary for developing a CFD model.

6.8.1 Chemical Properties

Five samples of the raw Environ Coal were taken from the McDonald's Lime stockpile and sent to CRL in Wellington for analysis. CRL returned a report for each sample listing the proximate analysis, ultimate analysis and gross heating value. An average value was then derived for each variable based on the five samples.

Table 14: Average Chemical Properties of Stockton Coal

Proximate Analysis	
Volatiles	33.3 %
Char	39.3 %
Ash	7.2 %
Moisture	20.2 %
Ultimate Analysis	
C	74.91 %
H	5.18 %
O	18.31 %
N	1.27 %
S	0.32 %
Gross Heating Value	
21.62 MJ/kg	

To simulate coal combustion FLUENT requires the Lower Calorific Value (LCV) of the coal, which can be obtained using the chemical properties listed above. The Gross Heating Value accounts for water in the exhaust leaving as vapour and includes any liquid water in the fuel prior to combustion. The LCV is determined by subtracting the heat of vaporisation of the water vapour produced during combustion and any initial liquid water.

Calculating the heat of vaporisation of any initial water is a relatively easy step as the mass fraction of H_2O in a sample is given by the proximate analysis. The same step is much more complicated however for the moisture produced during combustion, as the quantity of H_2O is not readily available. To determine the amount of H_2O produced it is necessary to obtain the composition of volatile gases and the resulting stoichiometric equation for the oxidation reaction of these volatiles (Eq. 64). This allows the quantity of water produced per kilogram of coal burnt to be determined and as a result the heat of vaporisation value can be calculated. The total energy required for vaporisation of all H_2O is then subtracted from the Gross Heating Value to give the LCV of Environ Coal as 20.42 MJ/kg.

$$C_{4.63}H_{9.18}O_{2.03}N_{0.16}S_{0.018} + 6.43O_2 \rightarrow 4.63CO_2 + 5.59H_2O + 0.08N_2 + 0.018SO_2 \qquad (64)$$

6.8.2 High Temperature Volatile Yield

As explained in the literature review the high temperature volatile yield can be calculated using the CPD model, with the assistance of non-linear correlations for defining the required C NMR parameters. The required C NMR parameters are M_δ (the average side-chain molecular weight), M_{cl} (the average molecular weight per aromatic cluster), $\sigma+1$ (the average number of attachments per cluster) and c_0 (the initial char bridge population). A quadratic correlation is used to obtain values for M_δ, M_{cl} and $\sigma+1$.

$$y = c_1 + c_2X_C + c_3X_C^2 + c_4X_H + c_5X_H^2 + c_6X_O + c_7X_O^2 + c_8X_{VM} + c_9X_{VM}^2 \qquad (65)$$

where $y = M_\delta$, M_{cl} and $\sigma+1$. X_C, X_H, X_O and X_{VM} are the mass fractions of Carbon, Hydrogen, Oxygen and Volatile Matter respectively, obtained from the proximate and ultimate analyses,all on a dry-ash-free basis. The coefficients c_1 through to c_9 are listed in Table 15.

Table 15: List of coefficients used for C NMR correlations.

	M_δ	M_{cl}	σ+1
c_1	4.220E+02	1.301E+03	-5.211E+01
c_2	-8.647E+00	1.639E+01	1.639E+00
c_3	4.639E-02	-1.875E-01	-1.076E-02
c_4	-8.473E+00	-4.548E+02	-1.237E+00
c_5	1.182E+00	5.171E+01	9.319E-02
c_6	1.154E+00	-1.007E+01	-1.657E-01
c_7	-4.340E-02	7.608E-02	4.096E-03
c_8	5.568E-01	1.360E+00	9.261E-03
c_9	-6.546E-03	-3.136E-02	-8.267E-05

The correlation used for c_0 for high heating rates is:

$$c_0 = \min[0.36,\max\{(0.118X_C - 10.1),0.0\}] + \min[0.15,\max\{(0.014X_O - 0.175),0.0\}] \quad (66)$$

It is now possible to calculate the hypothetical ultimate gas yield, $f_{gas,\infty}$ (dry-ash-free), using the C NMR parameters calculated with the above correlations.

$$f_{gas,\infty} = \frac{m_b(\sigma+1)(1-c_0)}{[2m_a + m_b(\sigma+1)(1-c0)]} \quad (67)$$

where m_b (the average molecular weight of a liable bridge) is twice the molecular weight of a side chain ($m_b = 2M_\delta$). m_a (the average molecular weight of the aromatic part of the cluster) is found using Equation 68.

$$m_a = M_{cl} - M_\delta(\sigma+1) \quad (68)$$

6.8.3 Particle Size

The validation case presented in Chapter Five concluded that to obtain the most accurate results for a pulverised coal combustion simulation, the particle size distribution is best described directly using the results of a sieve analysis, whereby a series of uniform sized injections are specified. However, the sieve analysis of coal from the Raymond Mill at McDonald's Lime provides a poor representation of the size distribution, with over half the pulverised coal

particles passing through the smallest sieve (53μm). Therefore it was felt that a Rosin-Rammler distribution, based on the provided sieve analysis, would provide a better representation of the actual size distribution by ensuring that the smallest particles are taken into consideration.

Table 16: Sieve analysis data

Size Range (μm)	Mass %
0-53	56.9
53-75	19.3
75-90	7.3
90-212	15.8
212+	0.7

Before proceeding further it is necessary to obtain values for the maximum and minimum size of the particles. This was achieved with the assistance of a Scanning Electron Microscope (SEM). After analysing a range of samples it appeared that 300μm and 1μm would be a good approximations for the maximum and minimum particle sizes respectively. Given that only 0.7% of the total mass is present in particles greater than 212μm it is unlikely that adjustment of the maximum particle size would affect the results anyway. Similarly particles less than 1μm contain such little mass that the adjustment of the minimum size is unlikely to affect the results.

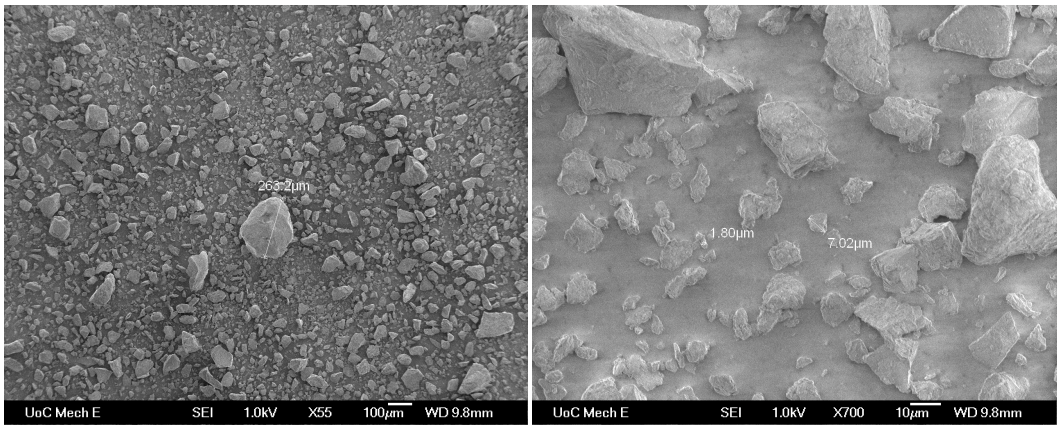

Figure 33: SEM images of pulverised coal particles at 55x magnification (left) and 700x magnification (right).

Using the theory explained in the literature review section, the Rosin Rammler properties of Environ coal were calculated and are listed in Table 17 below.

Table 17: Rosin-Rammler Parameters for Stockton Coal.

Maximum Particle Diameter	300µm
Minimum Particle Diameter	1µm
Mean Particle Diameter	58µm
Spread Parameter	1.56

6.8.4 Flow Rate

The daily flow rate of raw coal into the coal mill was available from the Kiln Two production logs. The average daily rate for a three-month period was obtained and then converted to provide a flow rate of 1.077kg/s.

6.8.5 Moisture

Moisture enters the kiln system through the burner pipe in both the liquid and vapour phase. As raw coal passes through the mill, the hot transport air evaporates moisture within the coal. This vapour is then carried through the firing pipe and into the kiln. Any remaining moisture in the coal particle enters the system as liquid water. To ascertain the level of residual water in the pulverised coal three samples of the as-fired coal were extracted from the firing pipe and sent to CRL for analysis. The average moisture content in the as fired coal was found to be 5.2%.

Moisture passing through the kiln system absorbs energy as it undergoes a temperature increase between the inlet and outlet. As a result the overall energy output of the kiln reduces. The energy absorbed by any moisture is calculated as follows:

$$\Delta E_v = \dot{m}_v Cp_v (T_{outlet} - T_{inlet}) \tag{69}$$

$$\Delta E_l = \dot{m}_l Cp_l (T_{outlet} - T_{inlet}) \tag{70}$$

$$\Delta E_{H_2O} = \Delta E_v + \Delta E_l \tag{71}$$

where $\dot{m}$ is the mass flow rate, *Cp* is the specific heat and *T* is the temperature. The subscripts *l* and *v* represent the liquid and vapour phases respectively. The *inlet* corresponds to the burner inlet temperature and *outlet* to the kiln back end temperature.

The combined energy absorption by liquid and vapour phase H_2O within Kiln Two at McDonald's Lime was found to be 2.54% of the total energy output. Because of the small impact moisture has on the overall system energy, all effects of moisture were neglected during the CFD modelling work presented in this thesis. The pulverised coal was assumed to contain no residual water and any vapour entering through the burner pipe was ignored.

6.8.6 Additional Properties

Table 18 lists additional material properties of the environ coal that are required when setting up a numerical model in FLUENT. The properties are a combination of measured or researched values and default parameters set by FLUENT.

Table 18: Addtional Environ coal properties

Parameter	Value
Density	1346 kg/m^3
Specific Heat	1200 J/kg.K
Thermal Conductivity	0.0454 W/m.K
Latent Heat	0 J/kg
Vaporisation Temperature	773 K
Volatile Component Fraction	51.5 %
Binary Diffusivity	3 e^{-5} m^2/s
Particle Emissivity	0.9
Particle Scattering Factor	0.15
Swelling Coefficient	2
Burnout Stoichiometric Ratio	2.67
Combustible Fraction	39.5 %
Devolatilisation Model	Constant Rate (A_0 = 50)
Combustion Model	Kinetics/Diffusion Limited Rate Constant = 5 e^{-12} Pre-Exponential Factor = 0.002 Activation Energy = 7.9 e^7

6.9 Oil Properties

6.9.1 Chemical Composition

Throughout the work presented in this thesis, the chemical properties of waste oil are based on the properties of a "generic" crude oil (Helton, 1996).

Table 19: Chemical Properties of Heavy Crude Oil

Ultimate Analysis	
C	85.0%
H	11.5 %
O	0.2 %
N	0.3 %
S	3.0 %
Lower Calorific Value	
42.69 MJ/kg	
Density	
870 kg/m^3	

6.9.2 Oil Inlet Properties

The control flow rate of waste oil is based on a 25% thermal energy substitution, with an assumed inlet temperature of 298K. The energy input of each fuel source can be calculated using Equations 72 and 73.

$$\Delta E_c = \dot{m} \times LCV_c \tag{72}$$

$$\Delta E_o = Q \times \rho \times LCV_o \tag{73}$$

where m is the mass flow rate of coal (DAF), Q is the volumetric flow rate of oil (ash free) and ρ is the density of oil. The subscripts c and o refer to coal and oil respectively.

6.10 Oil Nozzle

The nozzle used to inject vaporised oil into Kiln Two is a 'Laval' pneumatic nozzle from Lechler which operates on the ultrasonic principal. The liquid is fed in axially, while the atomizing air is fed radially through multiple openings to a

conical mixing chamber where gas and liquid are combined in an intensive, two-stage, mixing process. Downstream of the mixing chamber is a 15° divergent section that reduces the pressure and accelerates the mixture to ultrasonic speed in a manner similar to the Laval principle. As a result the droplets are atomized to an extremely fine degree.

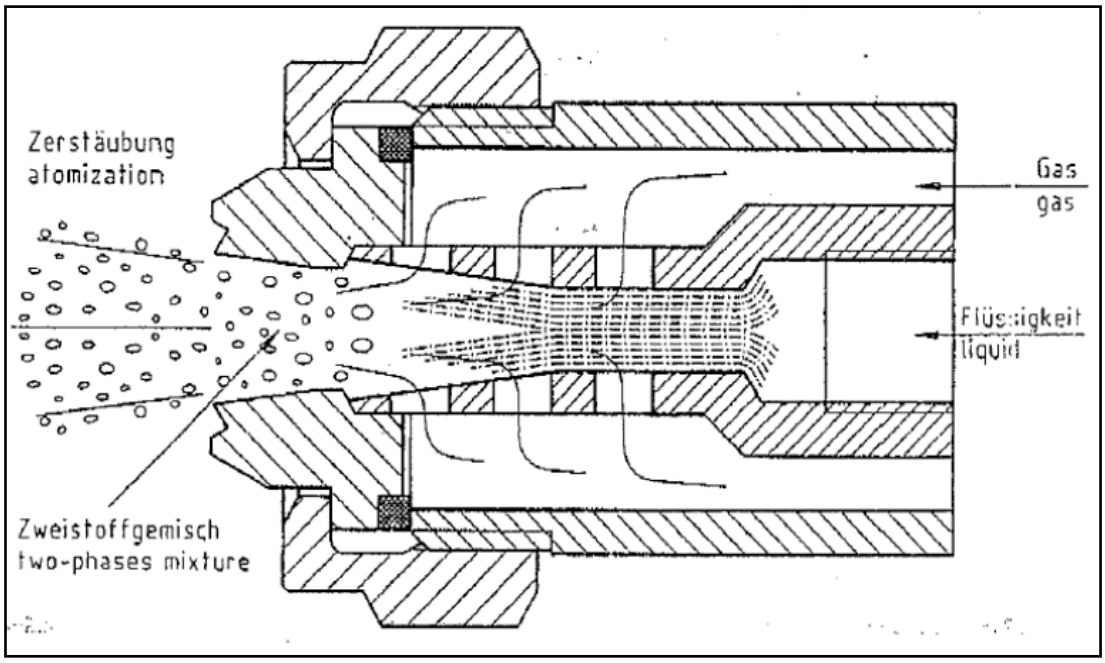

Figure 34: Lecheler Pneumatic Laval Nozzle Schematic.

The fineness of the droplet spectrum is critically dependant on the air/liquid ratio and the pressurization of the two elements. Thus the higher the air/liquid ratio, and the higher the pressures to which the air and liquid are subjected, the finer the droplet spectrum will be. It is known that air will enter the proposed Laval nozzle at 3 bar, while the oil flow rate is calculated according to the desired thermal substitution of coal. Thus using Figure 35 it is possible to calculate the corresponding droplet size and air flow rate, from which the velocity of air entering the flow domain can be calculated.

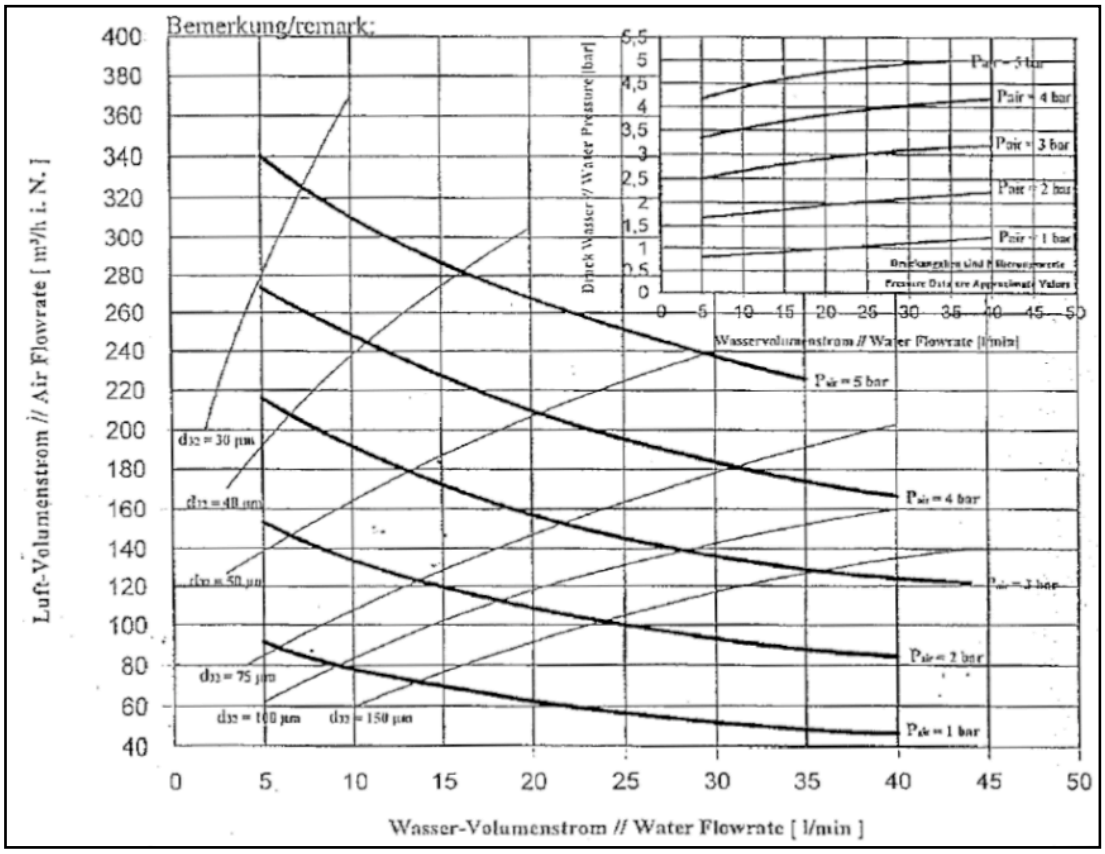

Figure 35: Information sheet used to find the nozzle outlet characteristics.

The chart in Figure 35 is based on the liquid stream being water, and not oil as is the case in the current work. Consequently, any differences in the droplet size stemming from water and oil having different physical properties have been neglected. Furthermore, the mesh used when modelling oil combustion does not completely replicate the internal geometry of the nozzle. Instead of being released through the divergent nozzle, the streams of oil and air are simply released from a surface with appropriate axial and radial velocity components in order to replicate the relevant spray angle. This allows for a simpler mesh to begin with and for the spray angle to be adjusted without having to modify the geometry and create a new mesh.

6.10.1 Additional Properties

Table 20 lists additional material properties of the waste oil that are required when setting up a numerical model in FLUENT. The properties are a combination of measured or researched values and default parameters set by FLUENT.

Table 20: Generic crude oil material properties.

Parameter	Value
Density	870 kg/m^3
Specific Heat	1880 J/kg.K
Thermal Conductivity	0.12 W/m.K
Latent Heat	124000 J/kg
Vaporisation Temperature	400 K
Boiling Point	589 K
Volatile Component Fraction	99.6 %
Binary Diffusivity	3.79 e^{-6} m^2/s
Particle Emissivity	1
Particle Scattering Factor	1
Heat of Pyrolysis	0 J/kg

6.11 PDF Properties

As explained in previous chapters of this thesis the mixture fraction/PDF approach to combustion chemistry is being used for modelling of Kiln Two. Table 21 lists the fluid properties of the PDF mixture that must be set in FLUENT, all of which are either default values or are based upon FLUENT's own coal combustion tutorials.

Table 21: PDF mixture properties.

Property	Setting
Specific Heat	mixing-law
Thermal Conductivity	0.0454 W/m.K
Viscosity	2 e^{-5}
Absorption Coefficient	wsggm-cell-based
Scattering Coefficient	0.5 m^{-1}
Scattering Phase Function	Isotropic
Refractive Index	1

7 Modelling Approach

At the inception of this project it was intended that all modelling would be undertaken using a three-dimensional flow domain. Three-dimensional modelling however proved to be overly complex and computationally demanding with jobs taking in excess of five days to solve on the University of Canterbury's IBM p575 HPC. Consequently, two-dimensional axisymmetric modelling was investigated and proved to be a much better alternative, providing suitably accurate results and reasonable solve times. The following chapter presents the meshes used for both the two-dimensional and three-dimensional modelling, as well as a comparison of the results obtained using the two different approaches. All investigations have been conducted using the control coal combustion case.

For both dimensional approaches to modelling Kiln Two, a number of simplifications and assumptions were made to reduce overall complexity. Firstly the scope of the CFD modelling work presented in this thesis does not include modelling the heat transfer through solid objects such as the bounding walls. Therefore appropriate boundary conditions are applied to the walls to account for any heat transfer through them.

The current work also ignores the effects of the bed and rotating walls. Investigations by Moles, Watson and Lain (1973) and Ruhland (1967) have shown that ignoring the physical presence of the bed in a rotary kiln is a reasonable simplifying practice. Since in most kilns the cross-sectional percent fill is about 15% or less, the physical presence of the bed is assumed to have no effect on the internal geometry of the kiln, and more importantly, no effect on the flame aerodynamics. For a high primary-jet momentum flame such as that in a typical rotary kiln, the degree of recirculation, which is important for the combustion aerodynamics, is largely determined by the magnitude of the primary-jet momentum, and to a much lesser extent, by the diameter of the kiln, which may be altered by the percent fill. At a 15% fill, the extent of alteration in

the kiln diameter is less than 8% and therefore unlikely to significantly affect any recirculation.

Finally, since typical rotation is about 1 RPM, the axial velocities are orders of magnitude higher than the tangential velocities. Therefore, rotation has no significant effect on the aerodynamic behaviour of the flame and consequently, for the current modelling work, the cylindrical kiln is modelled as being stationary.

7.1 Three-Dimensional Mesh

A three-dimensional CAD model of Kiln Two was generated using Solidworks (2008). The dimensions required for generating the model were obtained from a number of old technical drawings with additional measurements taken from the kiln itself. Care was taken to accurately recreate the real kiln, however some simplifications were made in areas that were considered unlikely to drastically affect the flow field, in order to reduce setup and solve time. When the CAD model was complete an inverse solid representing the internal flow domain was generated and imported into Harpoon where a hex-dominant mesh was generated.

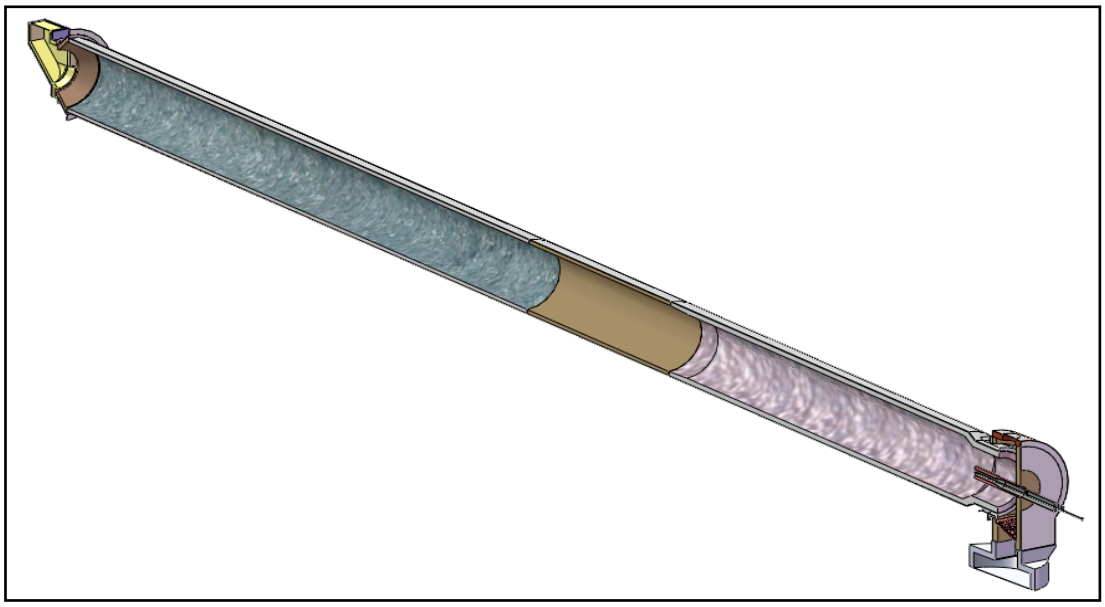

Figure 36: Section view of the Kiln Two CAD model generated using Solidworks.

7.1.1 Grid Independence Study

As was done for the validation case, a grid-independence study was undertaken to ascertain the mesh size needed to return an accurate result. Harpoon was initially used to create a hex-dominant mesh with 2,620,992 cells. Within this mesh, refinements were made where the flame burns and in regions of complex geometry. After running a coal combustion simulation using the initial Harpoon mesh, two further meshes', containing 3,817,082 cells and 4,577,859 cells respectively, were generated using the gradient adaption tool within FLUENT. Adaption's were made in areas of high temperature and velocity gradients.

To check the mesh independence two lines were created on the three respective meshes at consistent arbitrary points. Both lines were in the vertical direction and located on the mid plane of the cylindrical kiln section. The two lines were one metre and 7.5 metres respectively from the burner pipe outlet. Axial velocity and temperature profiles were obtained at each line for the three meshes and combined in Microsoft Excel to allow for investigation of the mesh independence. Mass and energy imbalances of the two meshes were also investigated and are listed in Table 22.

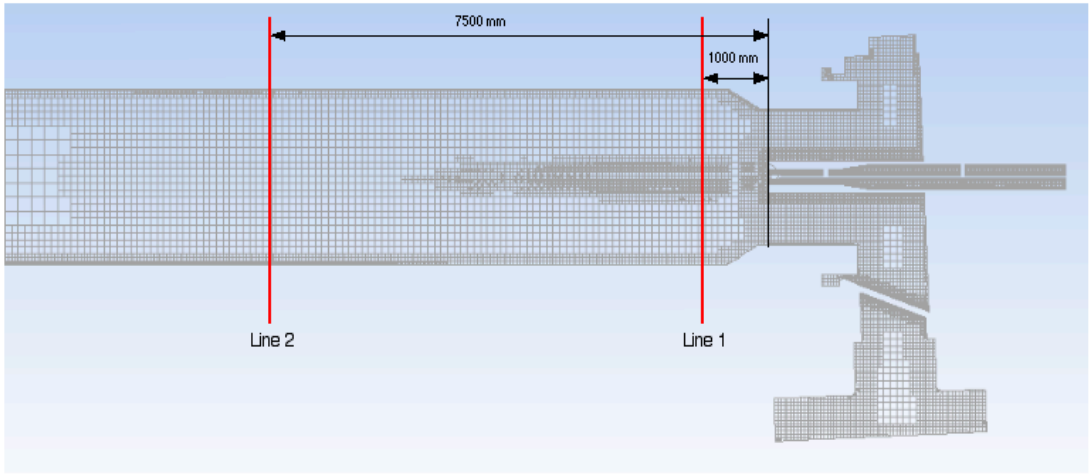

Figure 37: Shows location of the two lines used for investigating mesh independence.

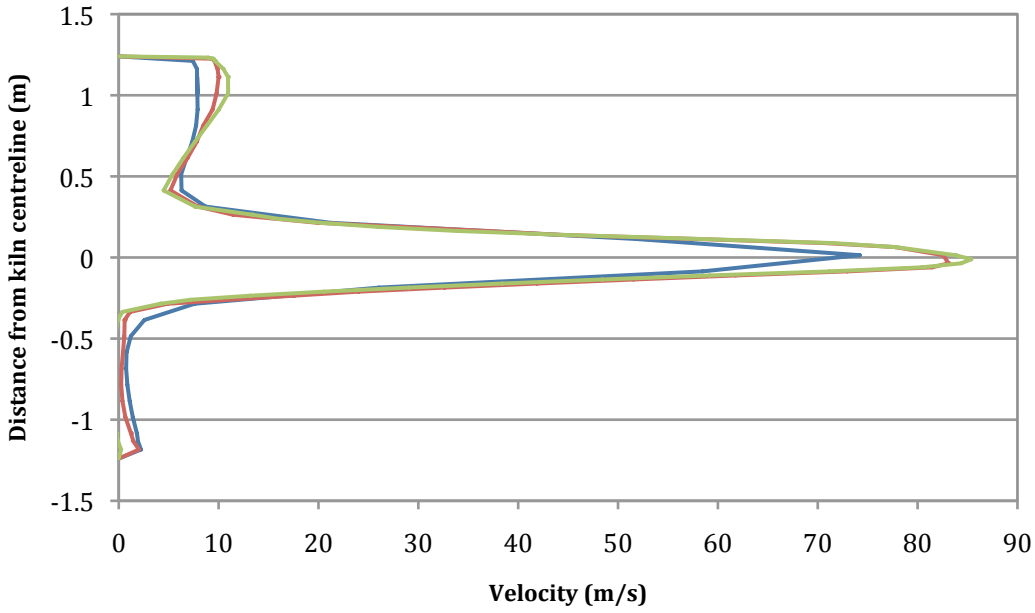

Figure 38: Axial velocity profiles at Line 1 for the 2.6 million cell (■), 3.8 million cell (■), and 4.6 million cell (■) meshes.

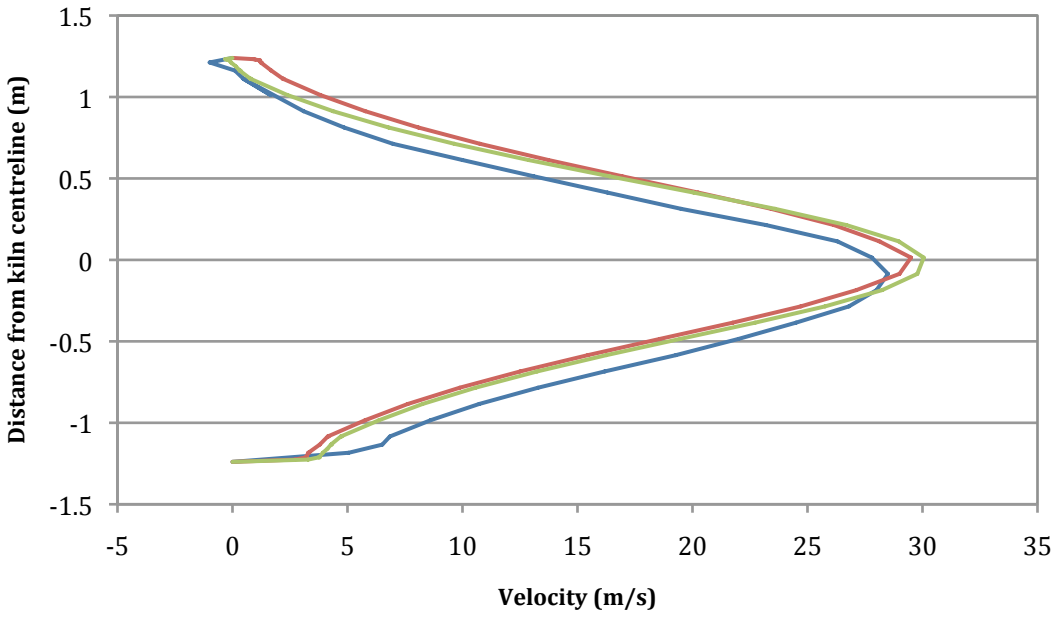

Figure 39: Axial velocity profiles at Line 2 for the 2.6 million cell (■), 3.8 million cell (■), and 4.6 million cell (■) meshes.

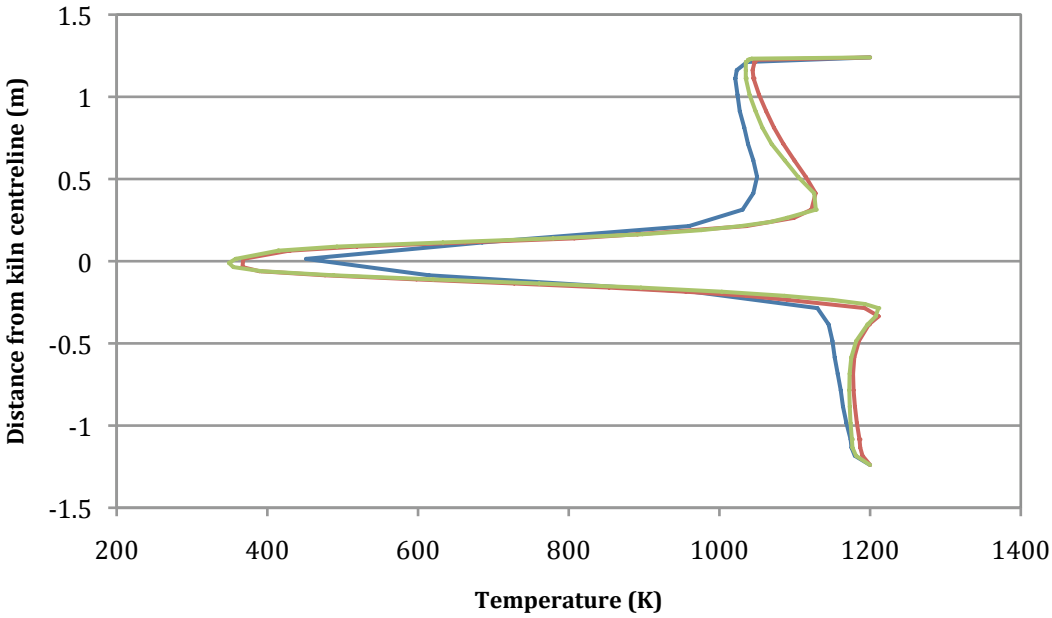

Figure 40: Temperature profiles at Line 1 for the 2.6 million cell (■), 3.8 million cell (■), and 4.6 million cell (■) meshes.

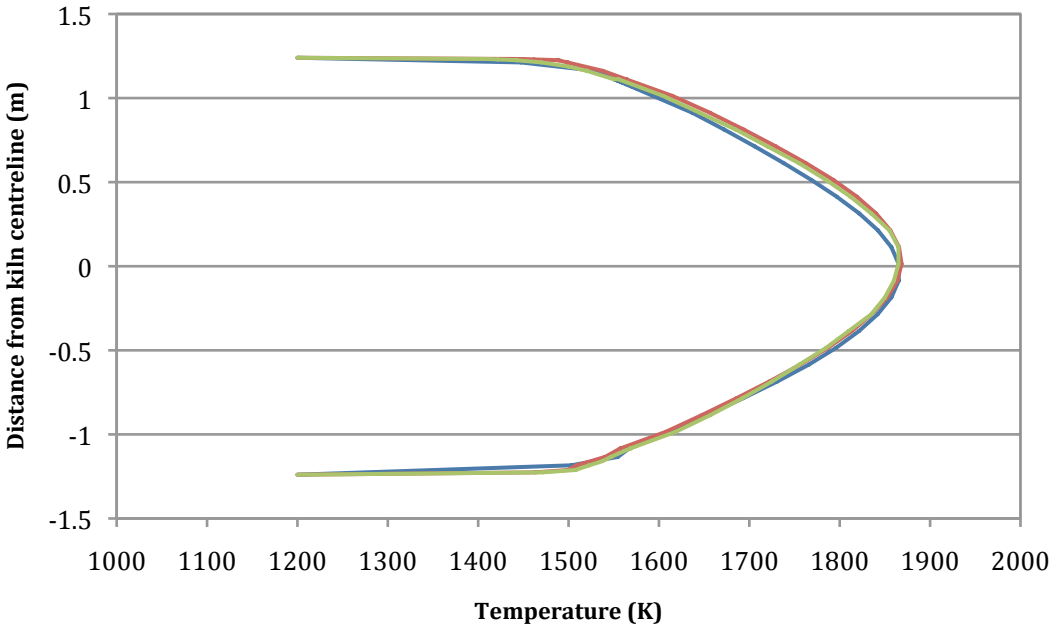

Figure 41: Temperature profiles at Line 2 for the 2.6 million cell (■), 3.8 million cell (■), and 4.6 million cell (■) meshes.

Table 22: Mass imbalance of three different sized 3D meshs.

Mesh Size	Mass Imbalance	Energy Imbalance
2.6 million cells	0.032%	3.9%
3.8 million cells	0.008%	2.4%
4.6 million cells	0.016%	2.6%

Figure 38 and Figure 39 show velocity profiles of each mesh at Lines 1 and 2. Refinements of the original mesh in areas of high velocity gradient are seen to have notably changed the velocity profiles; however there is little difference between the two larger refined meshes. The same situation arises for the temperature profiles in Figure 40 and Figure 41 where the profiles for the larger meshes are noticeably different to the original mesh, especially closest to the burner outlet. Both the mass and energy imbalances are similar and of acceptable values for the three meshes. The mesh independence study has shown that the 3.8 million cell mesh is the most suitable for future modelling of Kiln Two. This mesh will provide an accurate result while using the least computational resources possible.

7.1.2 Performance of chosen 3D Mesh

The three three-dimensional meshes were solved on the University of Canterburys IBM p575 HPC using 16 processors. Simulations using the chosen 3.8 million cell and the control coal case took approximately five days to solve using the HPC, with 6500 iterations needed to ensure convergence.

7.2 Two Dimensional Mesh

Using a two-dimensional axisymmetric approach to modelling Kiln Two eliminates modelling the flow phenomena in the firing hood and transfer chute as their geometry is not axisymmetric. Consequently, with so many simplifications to the overall kiln system the two dimensional model of Kiln Two is represented purely as a 52m long cylinder of 1.225 m radius. The inlet is split into three sections to represent the compressed, primary and secondary air

inlets. Gambit was first used to create the two-dimensional geometry and from there a structured quad mesh was generated.

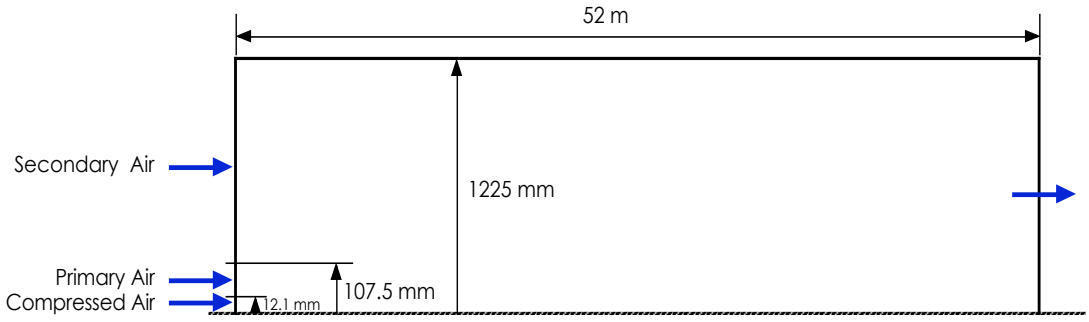

Figure 42: Simple schematic of 2D modelled domain(not to scale). Grid Independence Study

Once again a grid-independence study was conducted to determine the size of the two-dimensional, axisymmetric mesh that is needed to obtain an accurate result. Gambit was initially used to create a mesh with 64,000 cells. Within this mesh, refinements were made close to the burner inlets region. After running a coal combustion simulation using the initial Gambit mesh, two further meshes, containing 98,000 cells and 124,000 cells respectively, were generated using the gradient adaption tool within FLUENT. Adaption's were made in areas of high temperature and velocity gradients.

To check the mesh independence two vertical lines were created on the three respective meshes at consistent arbitrary points. The two lines were one metre and 7.5 metres respectively from the burner pipe inlet. Axial velocity and temperature profiles were obtained at each line for the three meshes and combined in Microsoft Excel to allow for investigation of the mesh independence. Mass and energy imbalances of the two meshes were also investigated and are listed in Table 23.

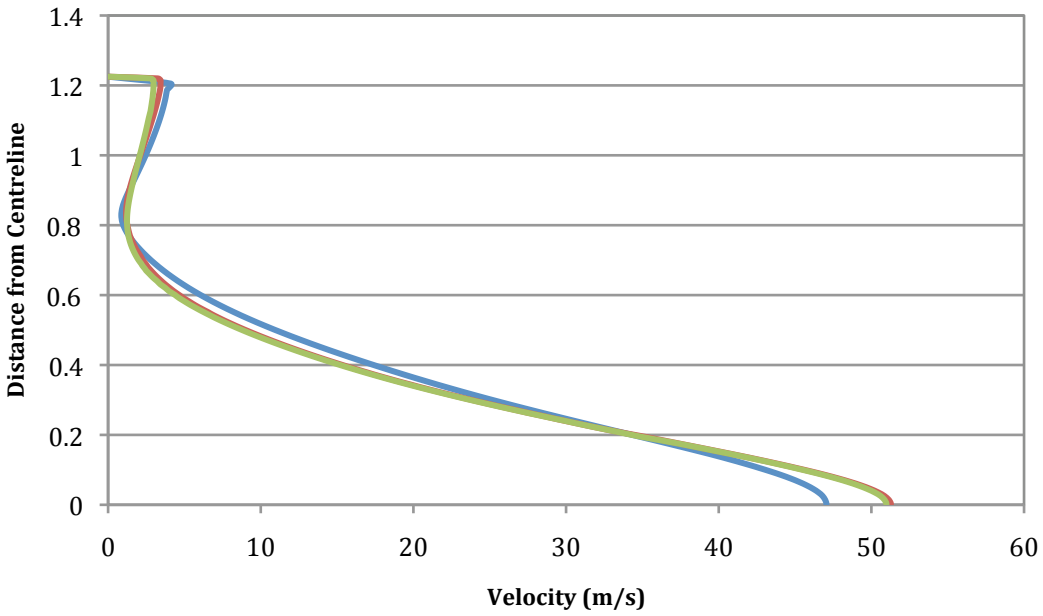

Figure 43: Velocity profiles at Line 1 for the 64,000 cell (■), 98,000 cell (■), and 124,000 cell (■) meshes.

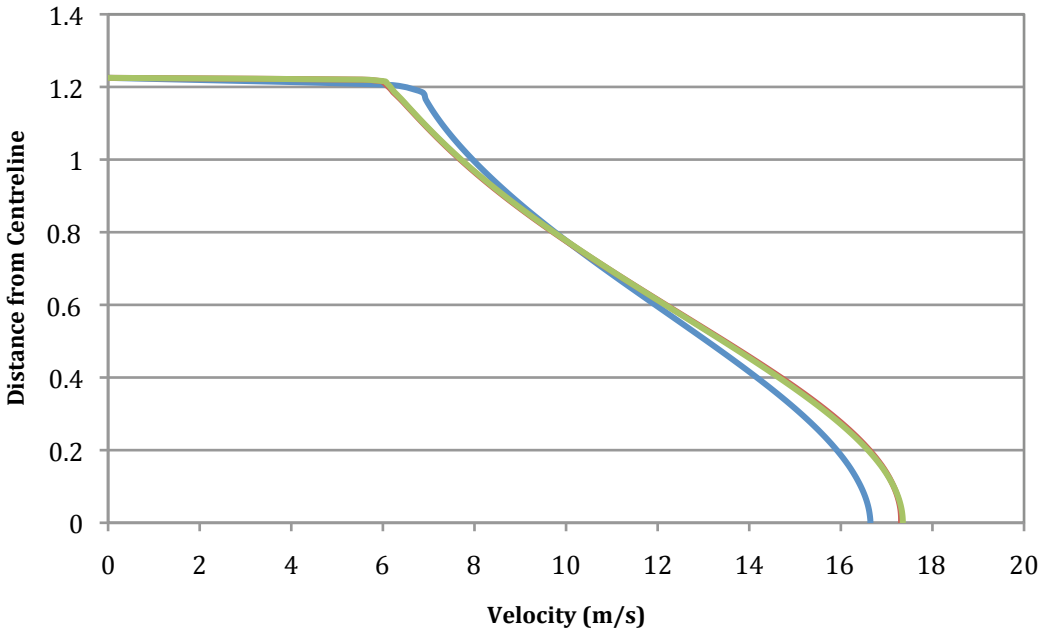

Figure 44: Velocity profiles at Line 2 for the 64,000 cell (■), 98,000 cell (■), and 124,000 cell (■) meshes.

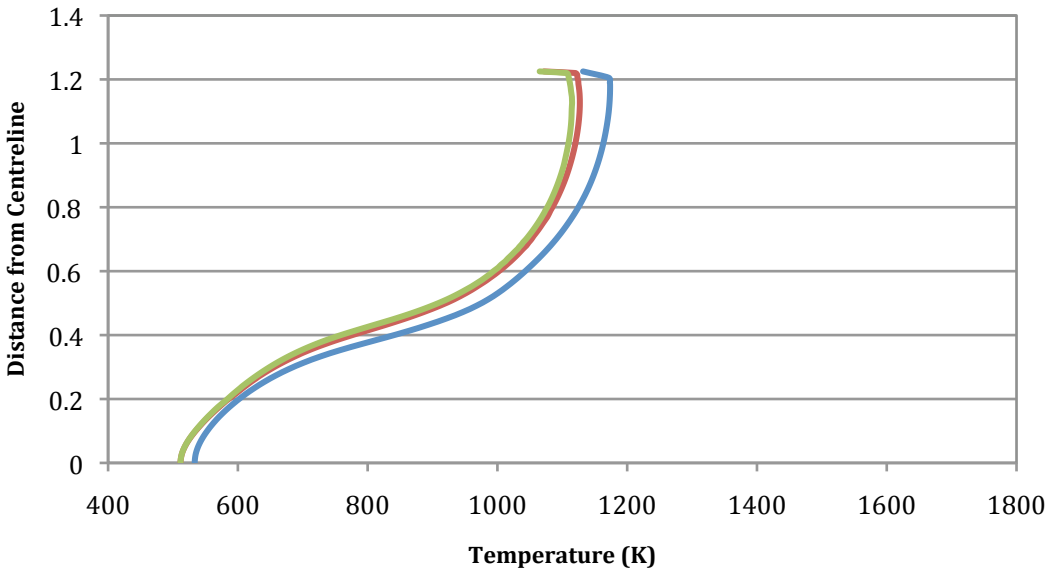

Figure 45: Temperature profiles at Line 1 for the 64,000 cell (■), 98,000 cell (■), and 124,000 cell (■) meshes.

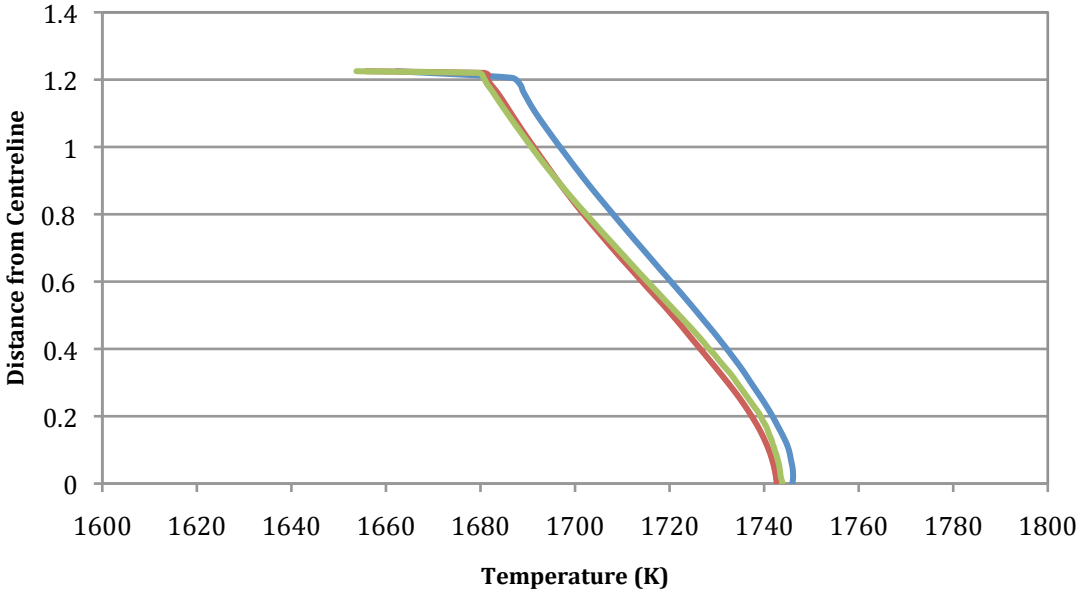

Figure 46: Temperature profiles at Line 2 for the 64,000 cell (■), 98,000 cell (■), and 124,000 cell (■) meshes.

Table 23: Mass imbalance of three different sized 2D meshes.

Mesh Size	Mass Imbalance	Energy Imbalance
60,000 cells	0.007%	0.04%
98,000 cells	0.001%	0.02%
124,000 cells	0.01%	0.08%

Figure 43 and Figure 44 show velocity profiles of each mesh at Lines 1 and 2. Once again, refinements of the original mesh are seen to have a notable effect on the profiles, however there is little difference between the two larger meshes. The same situation arises for the temperature profiles shown in Figure 45 and Figure 46. Once again the mass and energy imbalances of the three two-dimensional meshes are all of an acceptable value. The mesh independence study has shown that the 98,000 cell two-dimensional mesh is the most suitable for the modelling of Kiln Two, providing accurate results while being computationally efficient.

7.2.1 Performance of chosen 2D mesh

The three two-dimensional meshes were solved on dual-core desktop PC's. Simulations using the chosen 98,000 cell mesh took approximately eight hours for the control coal case and 12 hours for the control oil case. 8000 and 9000 iterations were required to ensure convergence of the coal and oil simulations respectively. The transport equation residuals for a control coal simulation are shown in Figure 47.

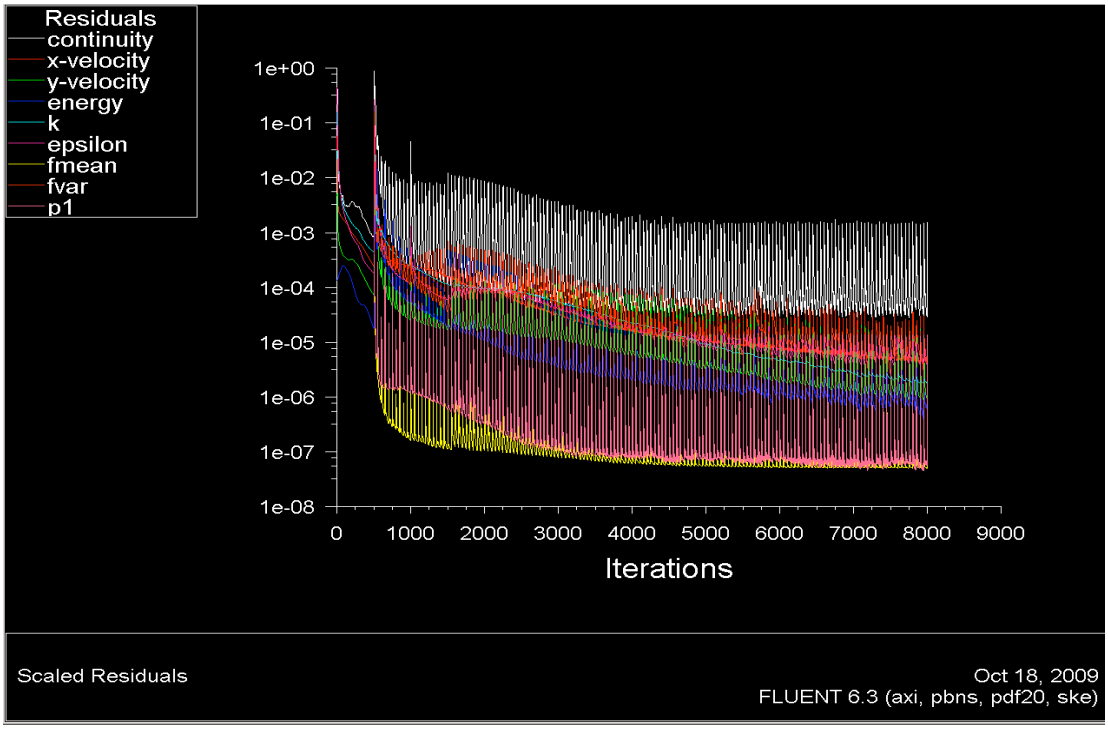

Figure 47: Transport equation residuals of the 2D 98,000 mesh.

7.3 Comparison of the 2D and 3D Axisymmetric Models

The following section aims to investigate the validity of using 2D axisymmetric modelling as an alternative to the much more complex and time consuming 3D modelling. This will determine whether it is acceptable to investigate the combustion characteristics of Kiln Two using the two-dimensional approach. Figure 48 shows the centre line temperature profiles for the two different approaches, while Figure 49 analyses the wall heat flux profiles.

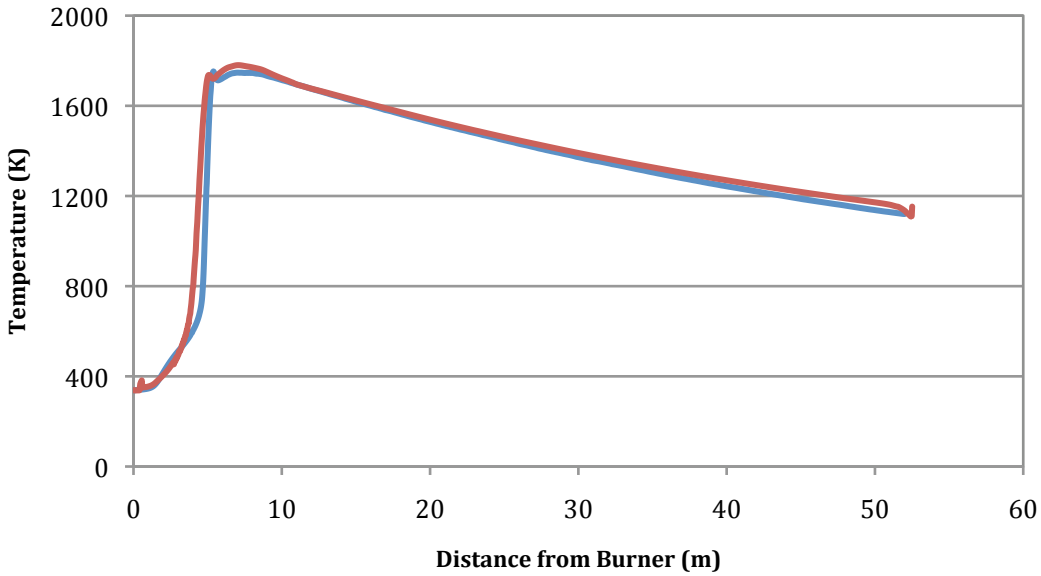

Figure 48: Comparison of the centre line temperature profile of the two-dimensional (■), and three-dimensional (■) meshes.

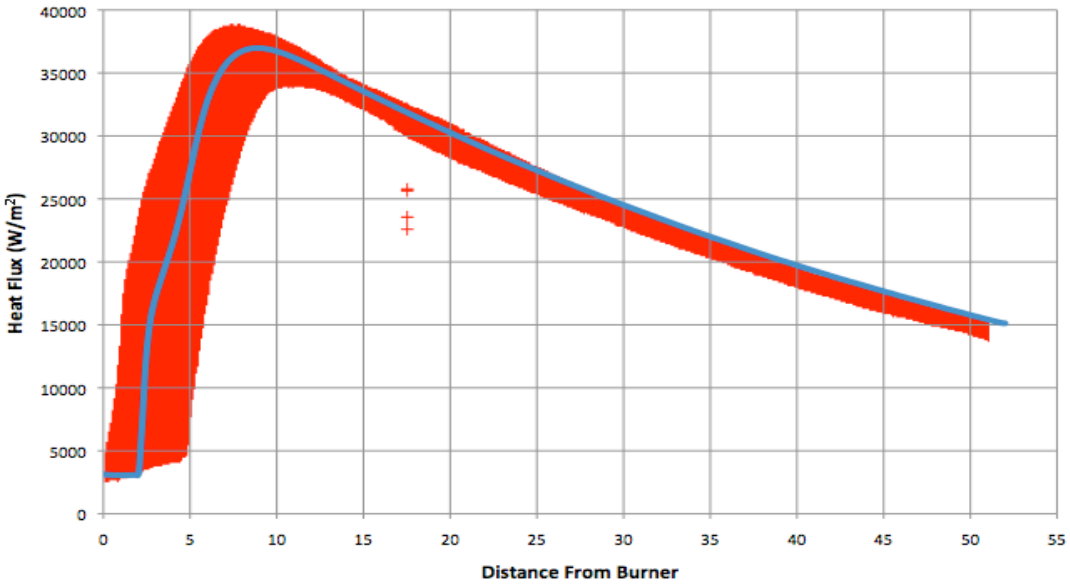

Figure 49: Comparison of the wall heat flux profiles of the two-dimensional (■), and three-dimensional (■) meshes.

The centre-line temperature profiles for the two cases have excellent agreement, and while initially appearing quite different, the two wall flux profiles also agree with each other respectably.

The 3D wall heat flux plot provides a flux value for every node at the wall boundary and thus the plot consists of many thousand data points. The reason for having the thick line, especially in the near burner region, is that the temperature profile is not axisymmetric. Figure 50 demonstrates this with the flow in the upper section increasing in temperature sooner than the lower section of the kiln. This causes a radial variation in heat flux to the kiln wall and consequently the wide heat flux profile. Further downstream, outside of the flame region, there is less radial variation in the wall heat flux and the profile narrows. Because the 2D profile lies within the bounds of the 3D profile it is believed that there is suitable agreement between the two.

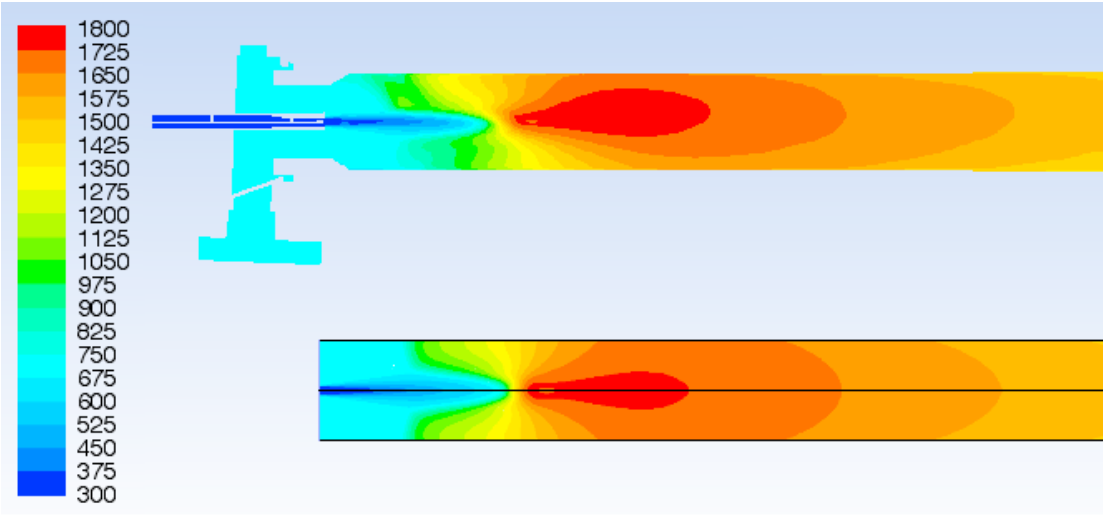

Figure 50: A comparison of mid-plane temperature contours in the flame region between the three-dimensional domain (above) and two dimensional domain (below).

Overall it is felt that 2D modelling is an excellent alternative to 3D modelling, providing desirable accuracy while being much more computationally efficient. Consequently all the results presented from this point onward have been obtained using the two-dimensional approach. If further aspects of the kiln were to be investigated other than heat flux and temperature then it may be necessary to perform further comparisons between the two and three-dimensional models.

8 Coal Combustion

After developing a working numerical model of Kiln Two based on the average, or control, operating conditions, the next task is to investigate how the combustion characteristics react when there are small deviations from the control conditions. The following chapter takes five operating parameters of Kiln Two and compares how features such as temperature, wall flux and species concentration are affected when each parameter is adjusted from its control value, to both a higher and lower value. The five parameters that are investigated and the conditions under which they are adjusted are as follows:

- Compare different primary air momenta, while keeping the excess air constant at 10%.
- Compare different excess air levels, while keeping the primary air portion of stoichiometric air constant at 36.5%.
- Compare different primary air temperatures, while keeping the excess air constant at 10% and the primary air portion of stoichiometric air constant at 36.5%.
- Compare different secondary air temperatures, while keeping the excess air constant at 10% and the primary air portion of stoichiometric air constant at 36.5%.
- Compare different coal flow rates, while keeping the excess air constant at 10% and the primary air portion of stoichiometric air constant at 36.5%.

In addition swirling primary air was investigated and compared to the control case which has purely axial primary air.

8.1 Primary Air Momentum

As was explained in Chapter Three, primary air momentum is a significant factor in controlling the recirculation of combustion gases and the subsequent prevention of flame impingement on the refractory wall. In the interest of

reducing ash ring formation, a phenomenon promoted by flame impingement, it was felt that the effects of varying the primary air inlet velocity, and consequently its momentum, should be investigated. Table 24 lists the primary air portion of the total stoichiometric air for the control case and the two additional simulations.

Table 24: Settings for differing PA momentum simulations

Control PA% of Stoichiometric	36.5%
High PA% of Stoichiometric	42.5%
Low PA% of Stoichiometric	30.3%

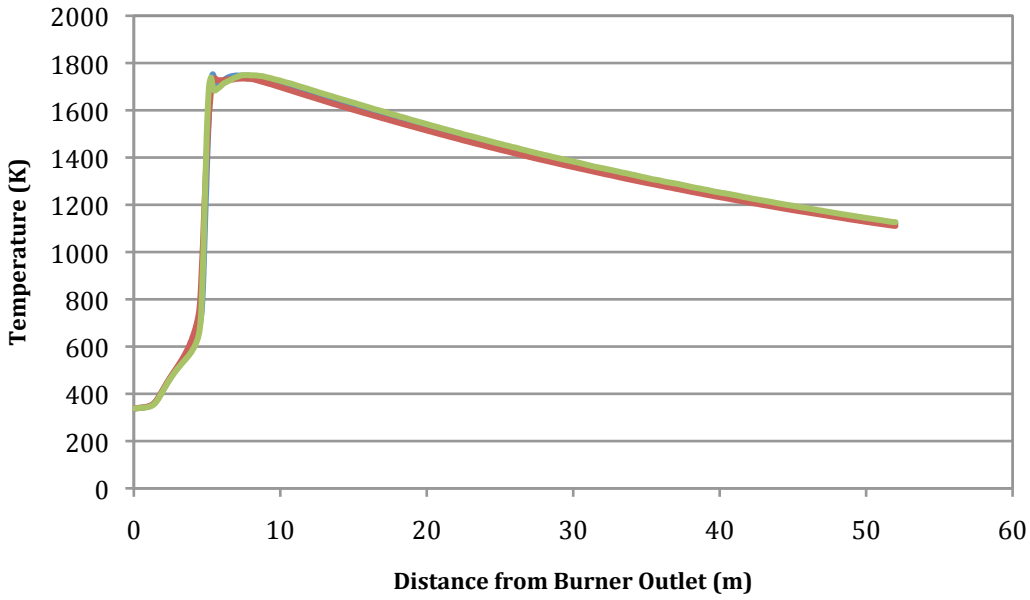

Figure 51: Centre line temperature profiles of Kiln Two for the control case (■), high primary air momentum (■) and low primary air momentum (■).

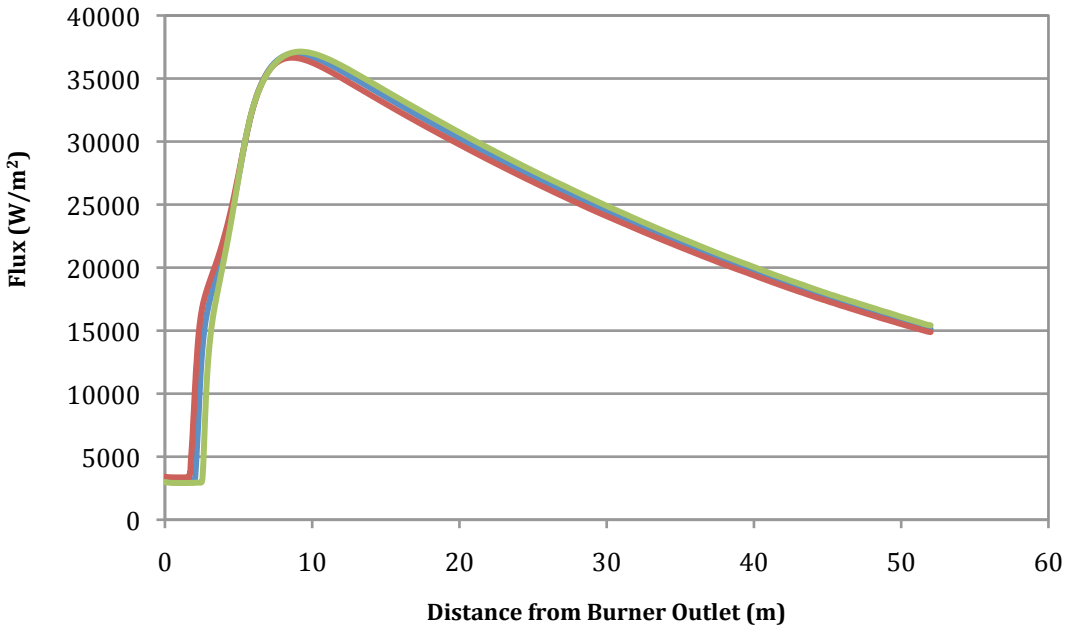

Figure 52: Wall heat flux profiles of Kiln Two for the control case (■), high primary air momentum (■) and low primary air momentum (■).

Figure 51 and Figure 52 show the centre line temperature profiles and wall heat flux profiles respectively for the three different cases. While the differences are minimal it does appear that increasing the primary air momentum slightly decreases both the centre line temperature and the wall heat flux. This is further supported by Figure 53 which show the exit gas temperature and peak kiln temperature to increase for a higher primary air momentum. For a lower primary air momentum the opposite effect occurs for all features.

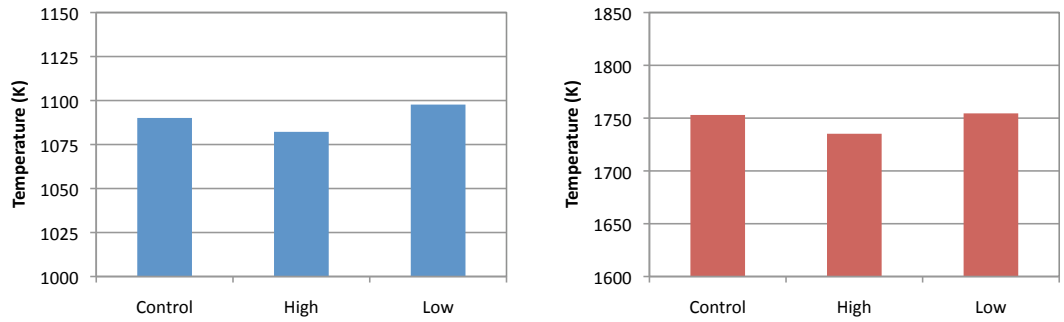

Figure 53: Comparison of exit gas temperatures (left) and peak kiln temperatures (right) for varying levels of primary air momentum.

The operators of Kiln Two support the conclusions drawn above noting that the exit gas temperature does in fact decrease when the speed of the firing fan, which controls primary air momentum, is increased. The operators believe this

results from the shorter flame that is produced when there is greater primary air momentum (and vice versa). This is also evident from analysing the temperature contours of the numerical model shown in Figure 54.

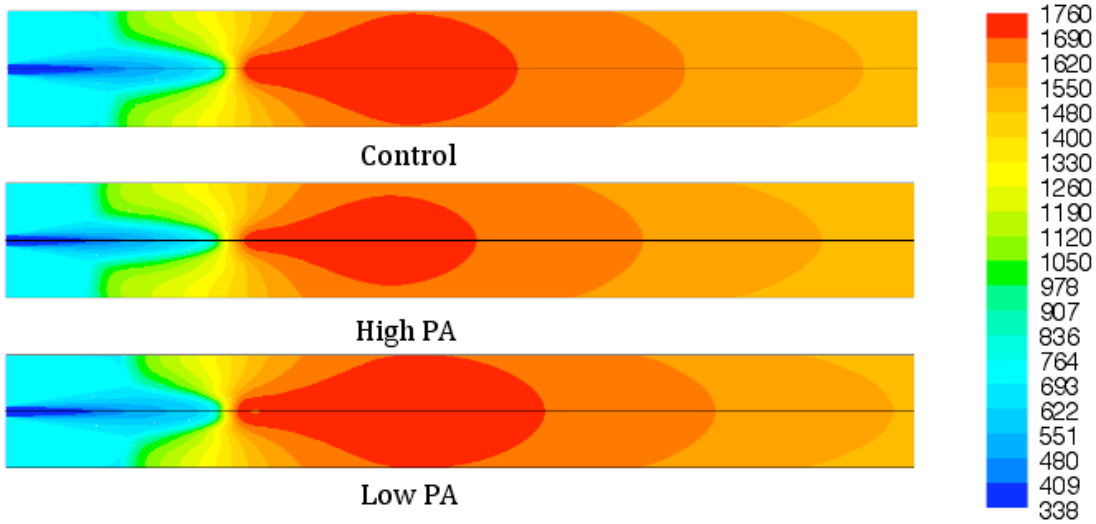

Figure 54: Comparison of temperature (K) profiles in the first 20 metres of kiln two for differing primary air momentums.

To investigate the effects of primary air momentum on the recirculation of combustion gases, contours of stream function were plotted to highlight the recirculation regions. Figure 55 shows the stream function contours for the control, high momentum and low momentum cases, as well as an optimised primary air case. This optimised case represents the recommendations of FCT, wherby to ensure optimum recirculation and prevent flame impingement the burner should operate with a Craya-Curtet parameter of 2.46 at 31.5% primary air. FCT also suggest that the burner tip should be level edge of the dam ring throat, which is the case for the simplified two-dimensional mesh.

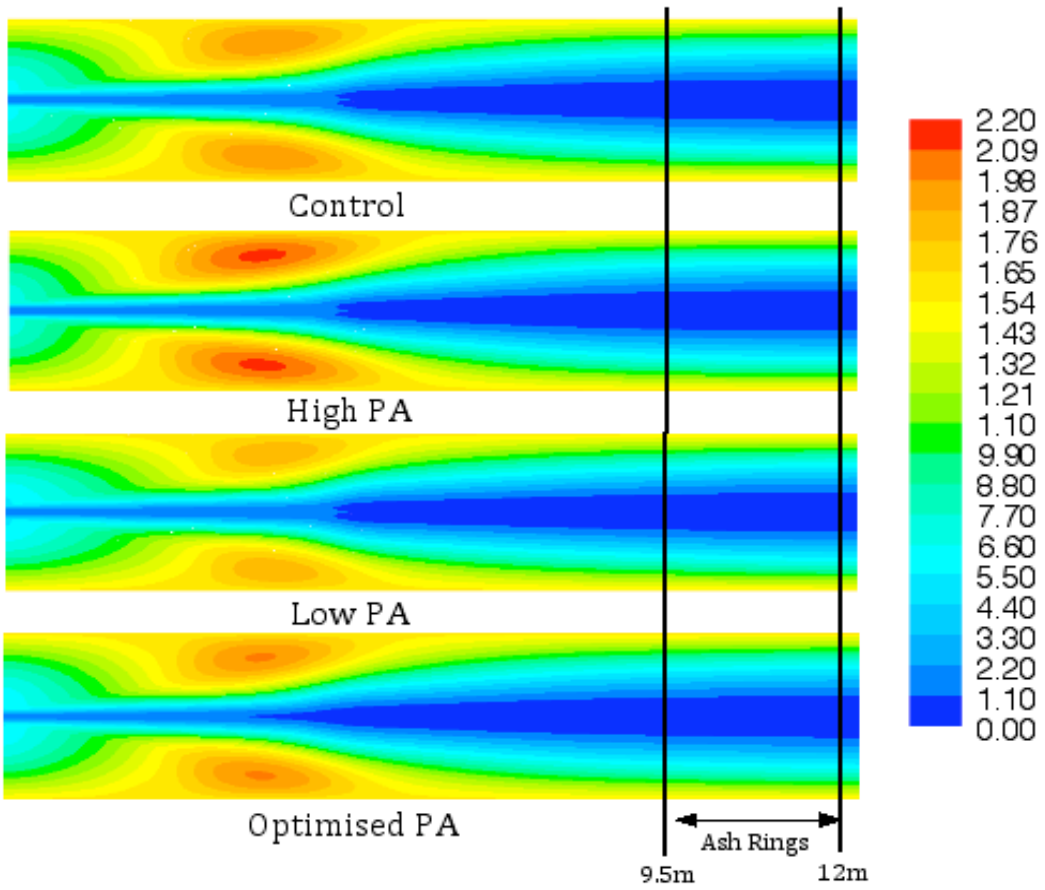

Figure 55: Stream function (m^2/s) contours in the flame region for a range of different primary air setups.

When analysing the contour plots in Figure 55 it is clear that increasing the primary air momentum does increase the size of the recirculation region, and vice versa, however increasing the recirculation region is unlikely to help reduce ash ring formation. The numerical study shows that recirculation occurs approximately two to five metres from the burner outlet, while FCT reports the ash rings to form between 9.5 and 12 metres from the burner outlet. The optimised primary air case does increase the amount of recirculation slightly in comparison to the control case, however the recirculation is still located outside of where the ash rings form.

The above findings are further supported by recent operation of Kiln Two in, during which there has been an extended period without any ash ring formation, yet the operators have been running the kiln with a lower than average primary air momentum. This emphasizes the conclusion that the primary air momentum does not influence ash ring formation.

8.2 Excess Air Level

As was explained in Chapter Six, quantifying the exact amount of secondary combustion air passing through Kiln Two was a difficult task and therefore, upon discussion with McDonald's Lime staff, it was decided that the 'control' case would operate with 10% excess air. For that reason it is considered important to investigate how the combustion characteristics of Kiln Two change when the quantity of excess air is either increased or decreased.

Table 25: Settings for differing excess air simulations

Control Excess Air	10%
High Excess Air	15%
Low Excess Air	5%

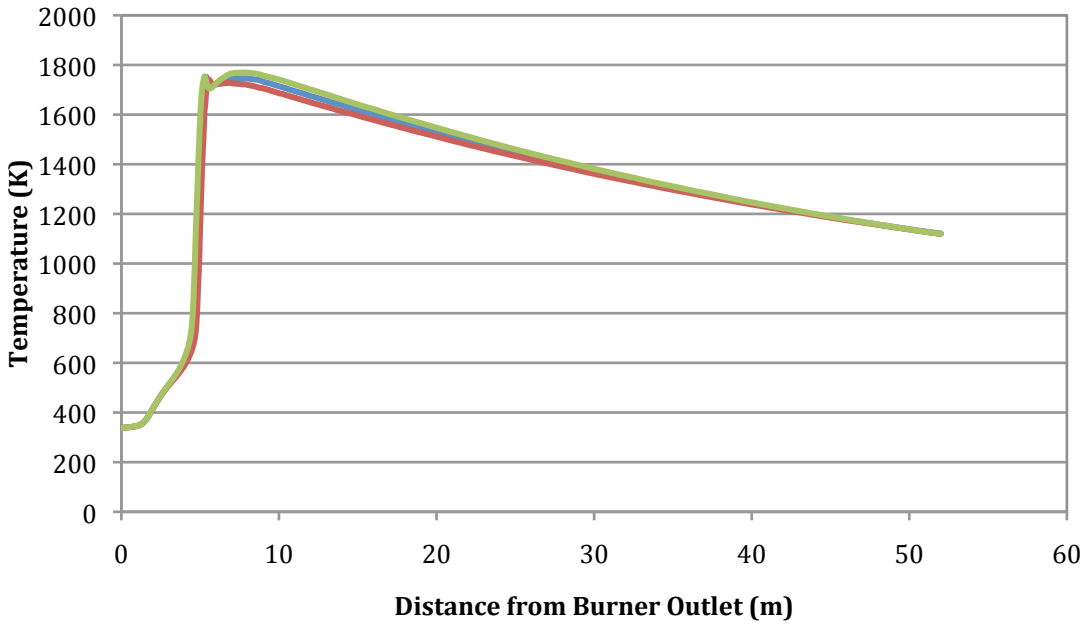

Figure 56: Centre line temperature profiles of Kiln Two for the control case (■), high levels of excess air (■) and low levels of excess air (■).

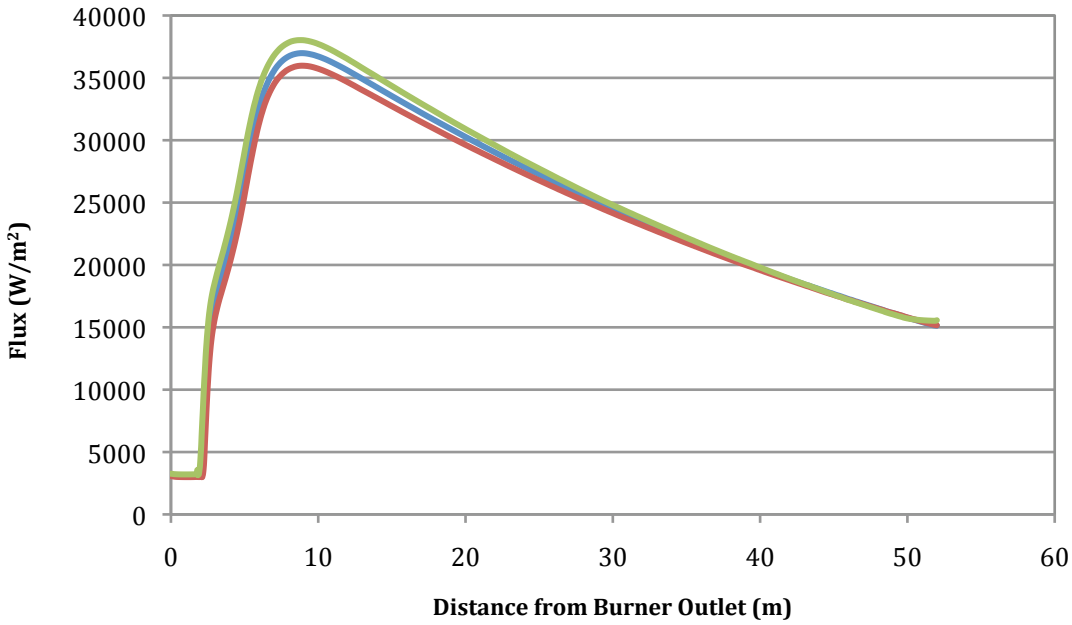

Figure 57: Wall heat flux profiles of Kiln Two for the control case (■), high levels of excess air (■) and low levels of excess air (■).

Figure 56 and Figure 57 show that the centre line temperature and wall heat flux reduce in the flame region if the level of excess air is increased, and vice versa, however there is little change to either features further downstream. The plots in Figure 58 showing the peak temperature to be more affected by changes to the excess air than the exit temperature, further support this conclusion. As is explained in Chapter Four it is important that adequate oxygen is supplied to ensure complete combustion, however as additional air is supplied, it must be heated up to the back end temperature, reducing temperatures in the kiln and the overall efficiency.

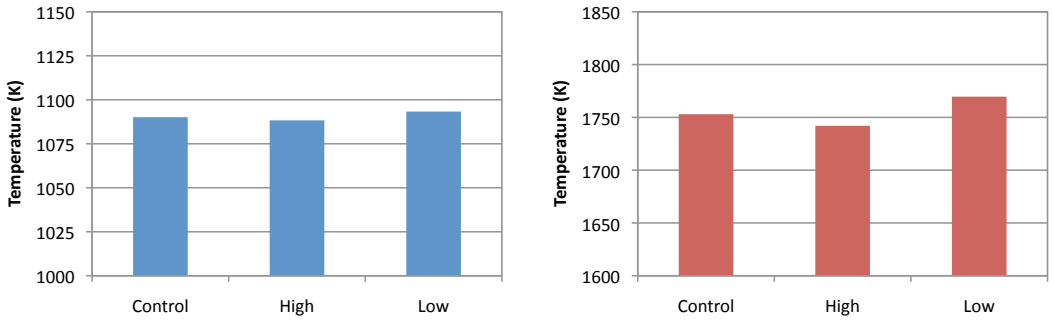

Figure 58: Comparison of exit gas temperatures (left) and peak kiln temperatures (right) for varying levels of excess air.

Adjusting the level of excess air affects the amount of oxygen present in the gases leaving the rotary kiln. The numerical study found that for the control case with 10% excess air, there is 3.8% oxygen in the exit gases. Increasing the excess air by 5% increases the oxygen at the exit by 0.6%, and vice versa. Meanwhile the Kiln Two operators aim to operate the kiln with 0-1% oxygen for steel-grade production and 2-4% oxygen for high-grade production, meaning there is relatively good agreement between the actual kiln and the numerical modelling. It is believed however that accurately quantifying the amount of excess air passing through Kiln Two would be beneficial and lead to a more precise numerical model.

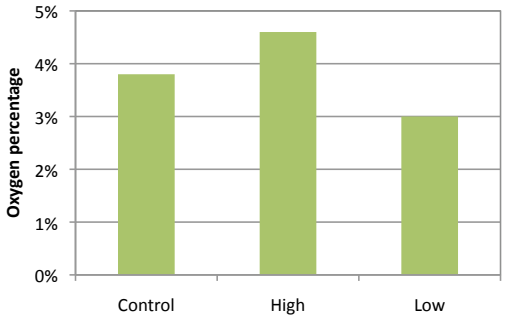

Figure 59: Level of oxygen at the kiln outlet.

8.3 Secondary Air Temperature

The secondary air temperature was another variable for which it was difficult to obtain a specific value. A number of measurements of the gas temperature at the top of the cooler were made, however the temperature of air extracted from the firing hood was found to be much cooler, most likely due to the cold air leaked in through the firing hood door. It was decided that the temperature of the air extracted from the firing hood best represented the temperature of air travelling up the kiln, and thus the secondary air temperature was set at 712K. However it was felt important to investigate how the kiln reacts when the secondary air temperature is both increased and decreased.

Table 26: Settings for differing secondary air temperature simulations

Control SA Temperature	712 K
High SA Temperature	1012 K
Low SA Temperature	412 K

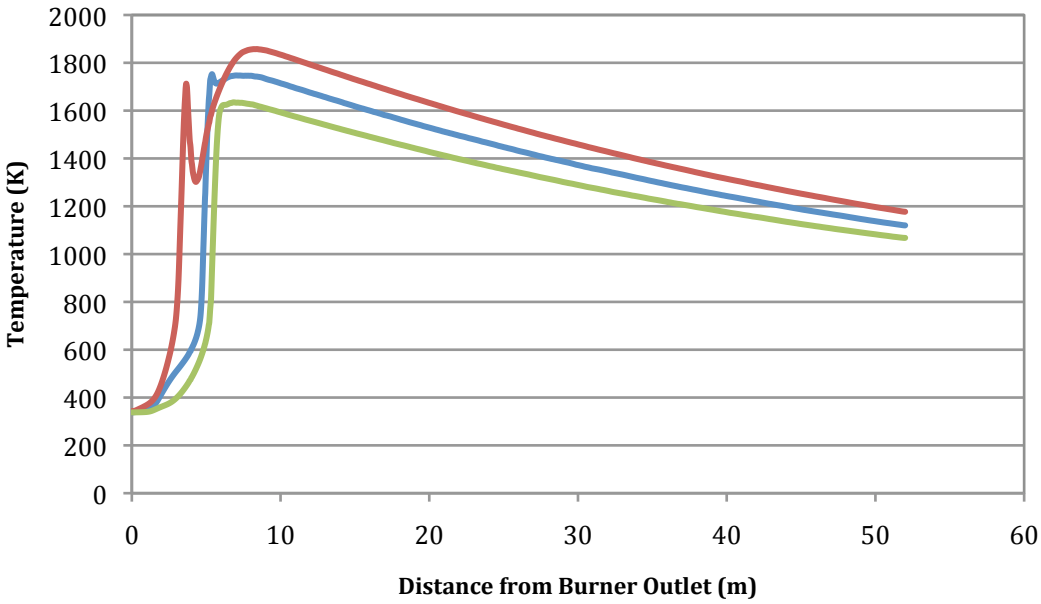

Figure 60: Centre line temperature profiles of Kiln Two for the control case (■), high secondary air temperature (■) and low secondary air temperature (■).

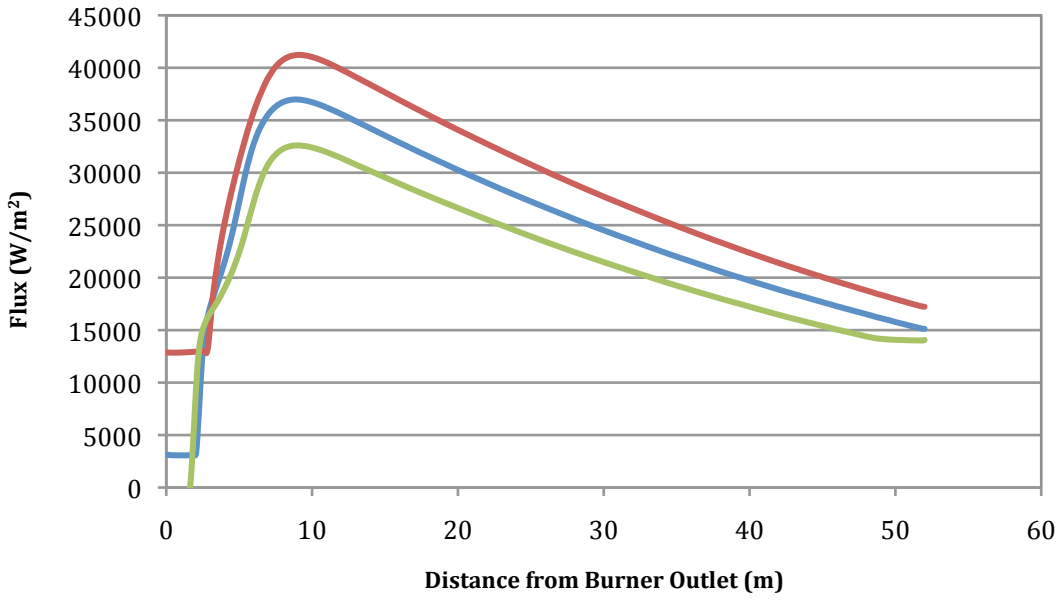

Figure 61: Wall heat flux profiles of Kiln Two for the control case (■), high secondary air temperature (■) and low secondary air temperature (■).

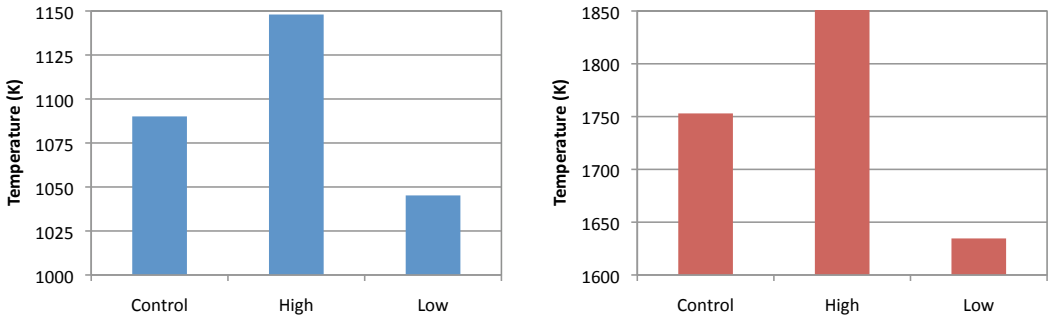

Figure 62: Comparison of exit gas temperatures (left) and peak kiln temperatures (right) for varying secondary air temperatures.

Increasing the secondary air temperature by 300K was found to significantly increase the temperatures in the kiln and consequently the heat flux to the wall. This conclusion suggests that McDonald's Lime should look closely at reducing the amount of cold air leaking in through the firing hood door in order to increase the secondary air temperature and ultimately improve their operating efficiencies.

8.4 Primary Air Temperature

The previous section recommended that McDonald's Lime reduce air leakage through the firing hood door in order to increase the temperature of the secondary combustion air. Because the primary air originates from the firing hood, adjustments to the secondary air temperature are likely to influence the primary air temperature. The literature review also explains that the primary air temperature may affect the kiln efficiency. Consequently the effects of differing primary air temperatures on the kiln system have been investigated.

Table 27: Settings for differing primary air temperature simulations

Control PA Temperature	337.7 K
High PA Temperature	377.4 K
Low PA Temperature	298 K

Numerical simulations ultimately showed that the above adjustments to the primary air temperature of Kiln Two have negligible effect on both the centreline temperature profile and the wall flux. Nevertheless there is a small difference in

the peak flame temperatures as is shown in Figure 63. The variability in exit gas temperatures is negligible.

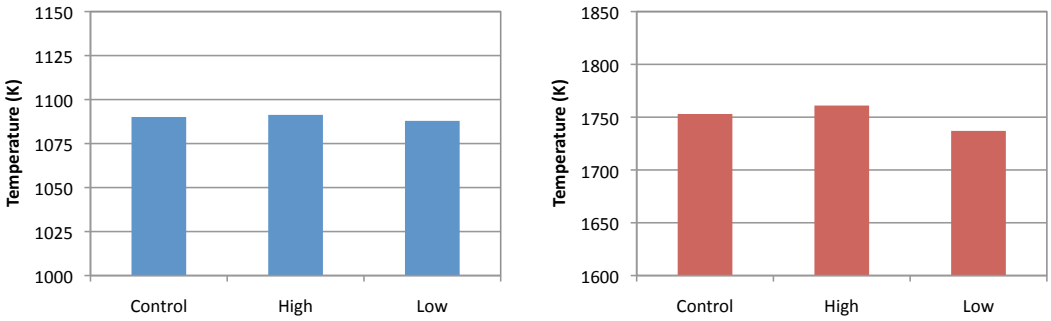

Figure 63: Comparison of exit gas temperatures (left) and peak kiln temperatures (right) for varying primary air temperatures.

8.5 Coal Flow Rate

Coal is the primary source of energy entering Kiln Two and therefore it was considered important to investigate the temperatures and wall fluxes for differing flow rates. Table 28 lists the coal flow rate for the control case and the two additional simulations, which are 11.6% higher and lower than the control flow rate respectively.

Table 28: Settings for differing coal flow rate simulations.

Control Coal Flow Rate	0.8594 kg/s (dry)
High Coal Flow Rate	0.9594 kg/s (dry)
Low Coal Flow Rate	0.7594 kg/s (dry)

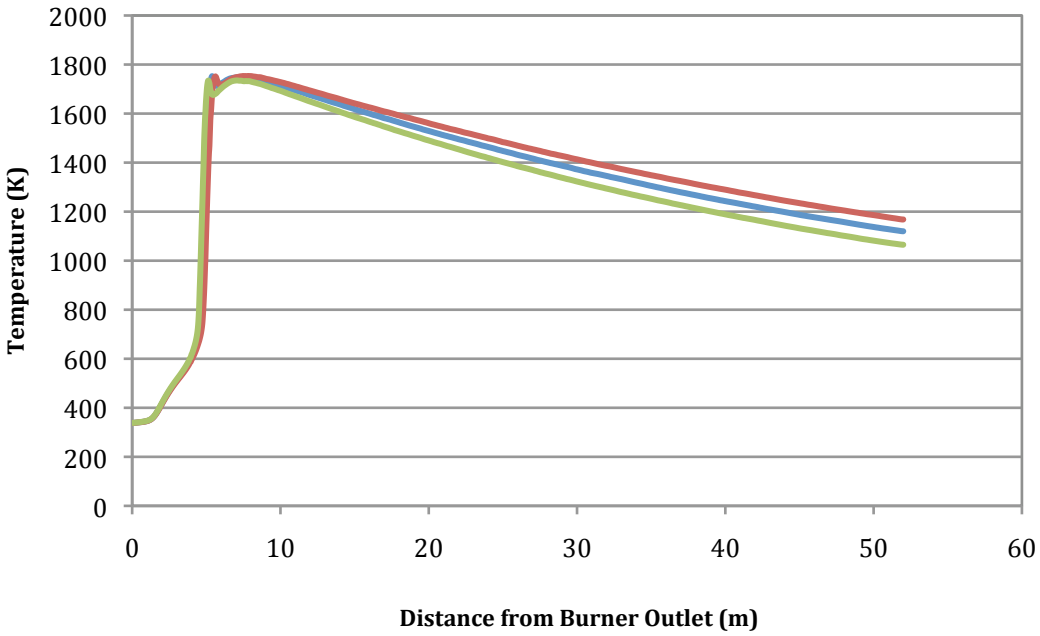

Figure 64: Centre line temperature profiles of Kiln Two for the control case (■), high coal flow rate (■) and low coal flow rate (■).

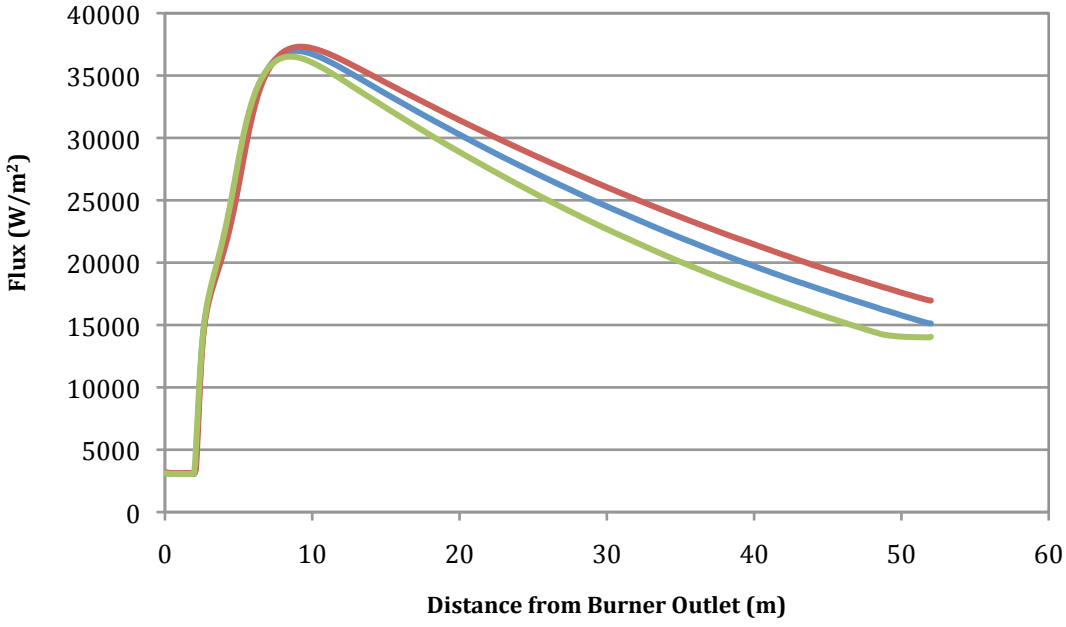

Figure 65: Wall heat flux profiles of Kiln Two for the control case (■), high coal flow rate (■) and low coal flow rate (■).

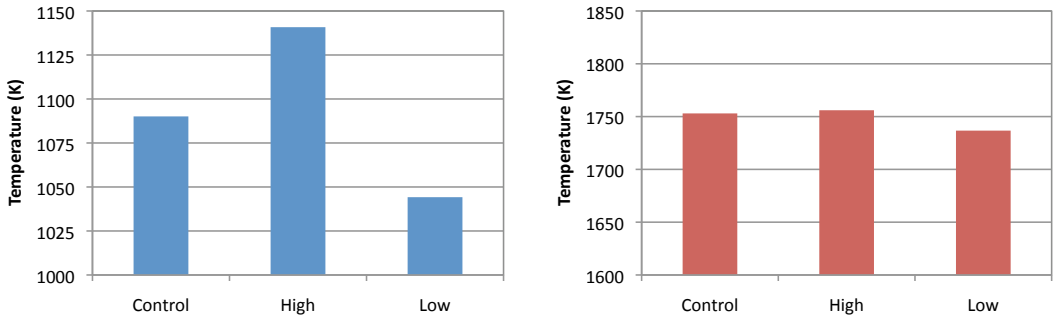

Figure 66: Comparison of exit gas temperatures (left) and peak kiln temperatures (right) for varying coal flow rates.

As is expected the coal flow rate affects both the temperature and wall heat flux within Kiln Two. The effects are seen to be most prominent towards the back end of the kiln with Figure 66 showing there to be minimal change in the peak temperature for differing coal flow rates, yet more noticeable change in the exit gas temperature. The above results were of significant interest to McDonald's Lime. Recently the kiln operators were having issues raising the burning zone temperature of Kiln Two and their immediate response was to increase the coal flow rate. However all the operators managed to achieve was an increased back end temperature, as is supported by the numerical modelling. In future the kin operators would have greater success increasing the firing zone temperature by increasing the temperature of the secondary air.

8.6 Swirl Air

As was explained in the literature review, swirling air is often used in rotary kiln burners to promote turbulent mixing of fuel and air and prevent flame impingement. This concept was therefore investigated by modifying the control coal combustion case by adding a swirl component of 15° to the incoming primary air. This translates to a tangential (swirl) velocity of 21.8 m/s.

The addition of swirling primary air was seen to move the peak temperature and wall flux closer to the burner, indicating that the swirling air has promoted faster mixing of fuel and air and thus the combustion processes have occurred earlier. The differences, as seen in Figure 67 and Figure 68, are rather minimal however

and it is not thought that McDonald's Lime would obtain any great benefits from adding swirl air to their current burners. There may however be benefits from adding additional channels and combining swirl and axial air. This could be investigated in future work. The effects of swirling air on recirculation were also investigated but once again there were no significant changes to the control case.

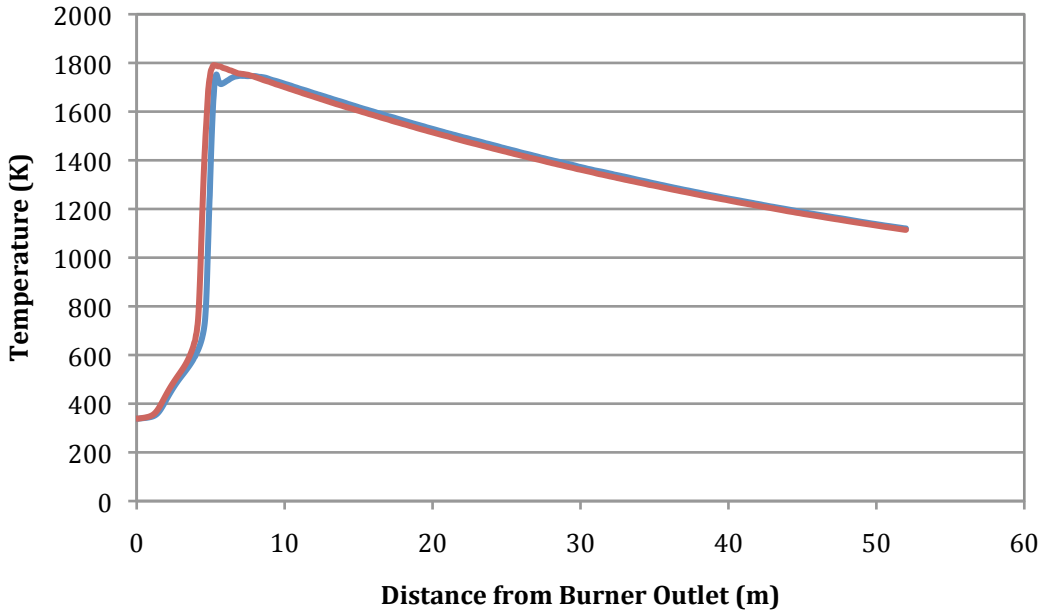

Figure 67: Wall heat flux profiles of Kiln Two for the control case (■) and swirling primary air case (■).

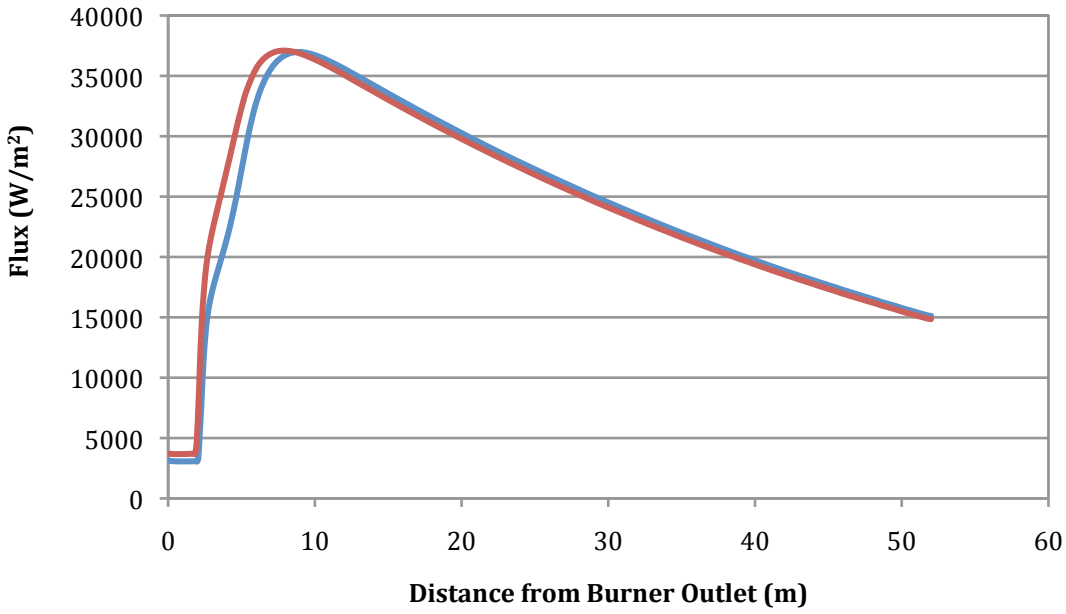

Figure 68: Centre line temperature profiles of Kiln Two for the control case (■) and swirling primary air case (■).

9 Oil Combustion

McDonalds Lime Ltd has recently added a waste oil firing system to Kiln Two in an attempt to reduce their fuel costs. As explained earlier this addition involved placing a lance down the centre of the single tube burner pipe, which sprays vaporised waste oil into the kiln in addition to pulverised coal. This section of the thesis investigates the performance of the waste oil firing system in comparison to the control coal firing system. As in the previous chapter, all modelling has been undertaken using the two-dimensional axisymmetric mesh and comparisons between different set-ups have focussed on analysing temperatures and heat fluxes within the kiln.

The initial stage of the oil combustion modelling involved comparing the control coal case to a control oil case as shown in Figure 69. The control oil case was set as a 25% thermal substitution of waste oil for pulverised coal.

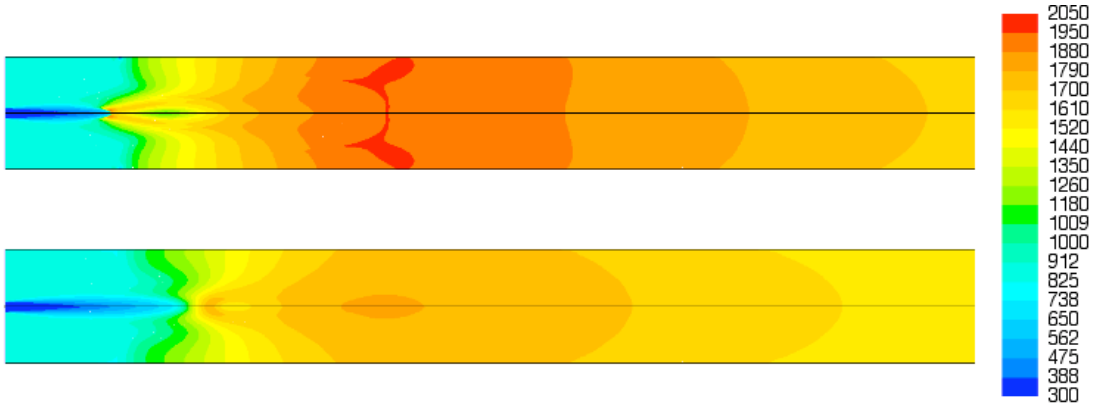

Figure 69: Comparison of temperature profiles in the flame region for the control oil (top) and coal (bottom) cases.

The coal and oil temperature profiles are seen to be rather different in the near burner region, a characteristic that arises as a result of the different devolatilisation temperatures of coal and oil. Because oil volatalises at a much lower temperature than coal (589K compared to 773K), the combustion process begins much sooner providing the spike in temperature close to the burner outlet. There is then a decrease in temperature before the coal begins to volatalise and combust further downstream. In the presented case the oil will

volatalise early due to the high temperature of the secondary combustion air, while the coal relies on heat from the actual flame further downstream for devolatilisation to occur.

The other significant difference between the two cases is the overall hotter temperature profile for the waste oil system compared to the coal only system. This phenomenon will be analysed further in the subsequent sections of this chapter that investigate the effects of different waste oil and primary airflow rates.

9.1 Waste Oil Flow Rates

In addition to the control oil case, 15 and 40 percent thermal substations of waste oil have been investigated. Centreline temperature and wall heat flux profiles are compared for the three oil combustion cases and the control coal combustion case.

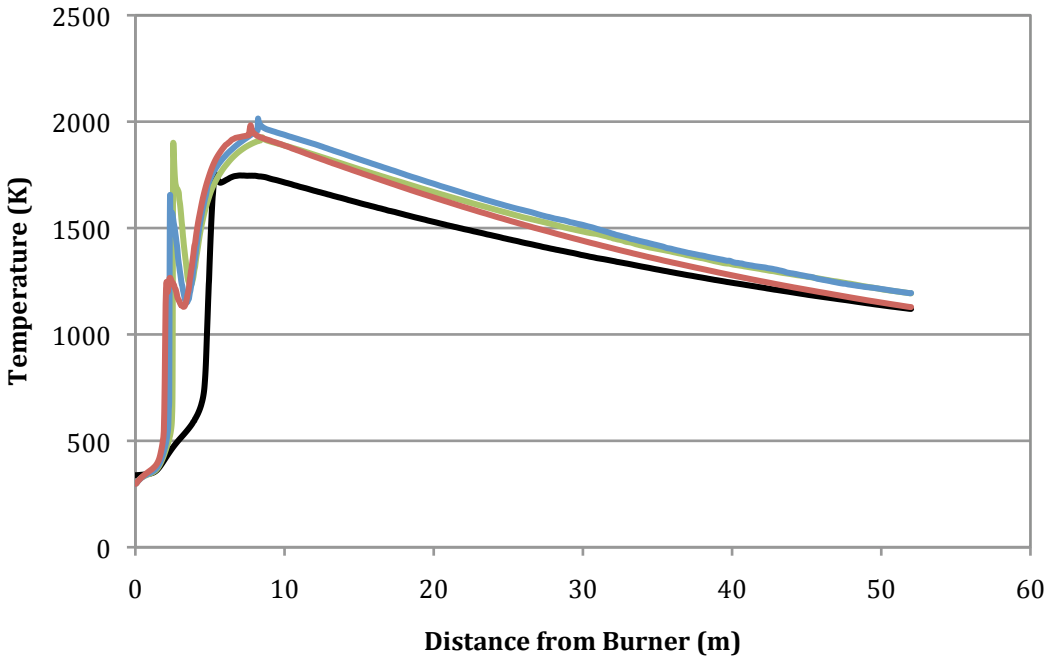

Figure 70: Graph showing the centreline temperature profile for the control coal case (■) and 15% (■), 25% (■) and 40% (■) thermal substitutions of oil.

As was seen in the contour plot above the temperature increases much sooner when oil is used as a partial fuel substitute due to the more rapid devolatilisation. As the oil flow rate increases the magnitude of the temperature spike close to the burner decreases. It is thought that this occurrence may be due to a greater competition for oxygen as the oil flow decreases, thus leading to incomplete combustion taking place and consequently a lower heat output. Further downstream the oil combustion cases all have a higher temperature than the coal combustion case, with the 25% thermal substitution providing the highest temperature. Figure 71 shows that the oil combustion simulations have a much higher peak temperature than the control case. The exit temperatures vary a lot less however with the control coal and 40% thermal oil substitution cases having very similar values.

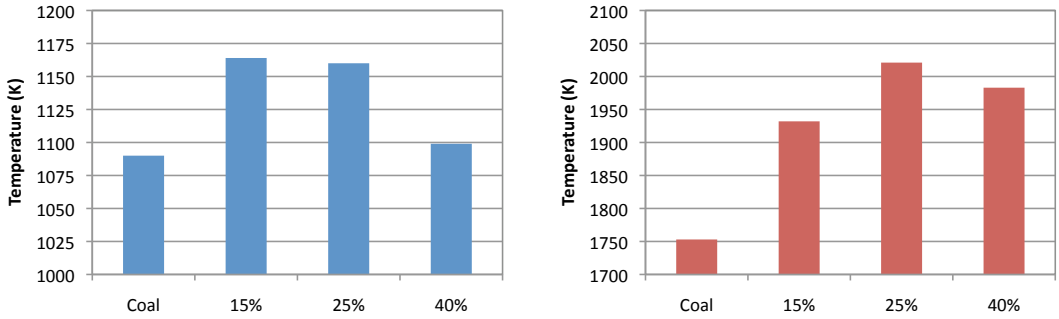

Figure 71: Comparison of exit gas temperatures (left) and peak kiln temperatures (right) for coal and oil fired setups.

As a consequence of higher temperatures in the kiln, the heat flux to the wall is also much higher when oil is partially substituted for coal. Figure 72 shows that operating the kiln with a 25% thermal substitution is the most efficient setup. This setting provides the greatest wall heat flux and thus allows the overall fuel input to be decreased by the greatest amount in order to achieve the same heat flux to the walls and bed as the original coal fired system provided. It is suggested that the lower kiln temperatures generated with a higher oil flow rate are a result of the larger oil particles produced by the laval nozzle being less efficient. It is a recommendation that future work investigates the effects of different oil flow rates for a uniform droplet size.

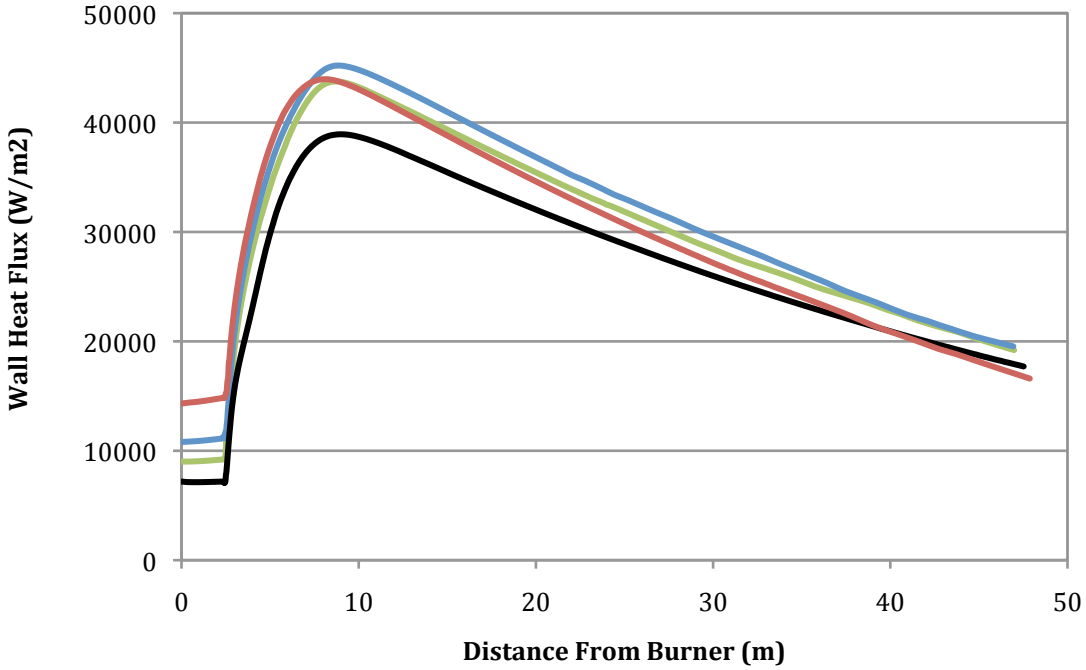

Figure 72: Graph showing the wall heat flux profiles for the control coal case (■) and a 15% (■), 25% (■) and 40% (■) thermal substitution of oil respectively.

9.2 Primary Air Flow Rate

The waste oil lance uses compressed air in the vaporisation process, which is subsequently released into the rotary kiln. As a result of this additional air, and the decrease in flow rate of pulverised coal, the operators at McDonald's Lime reduce the flow rate of primary air entering the kiln through the burner pipe when waste oil is fired. As no data was available on the adjustments to the primary air flow the waste oil numerical models used the assumption that the total primary air portion of stoichiometric air, including compressed air, stayed the same as the control coal cases (36.5%). The following section investigates whether the kiln would operate any differently if the burner airflow was left unadjusted, increasing the primary air portion of stoichimetric air to approximately 41.1% when the compressed air is added to the system.

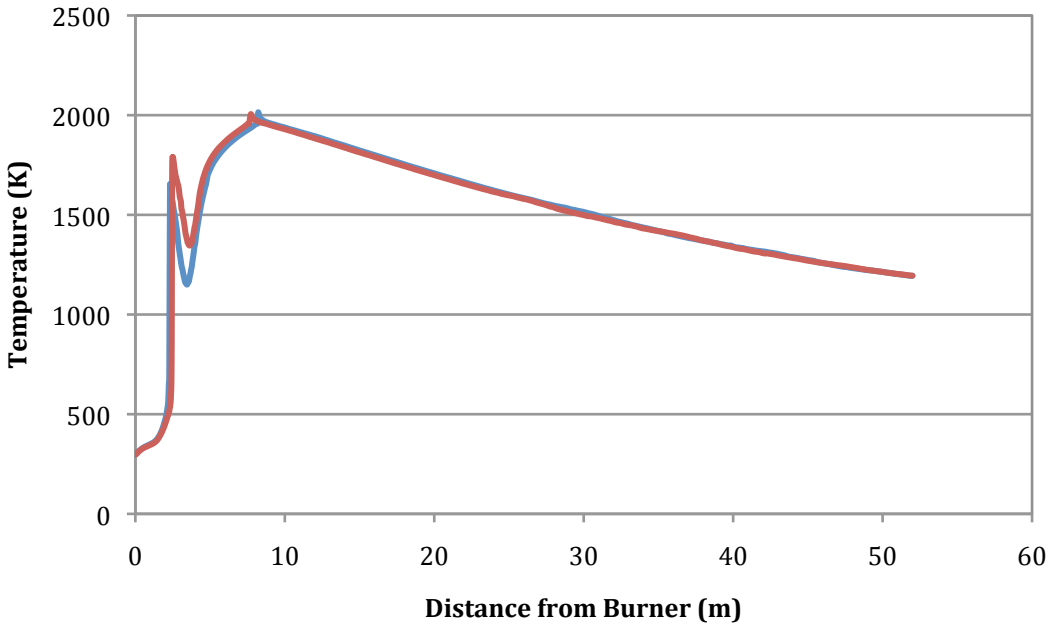

Figure 73: Temperature profiles for 36.5% (■) and 41.1% (■) total primary air.

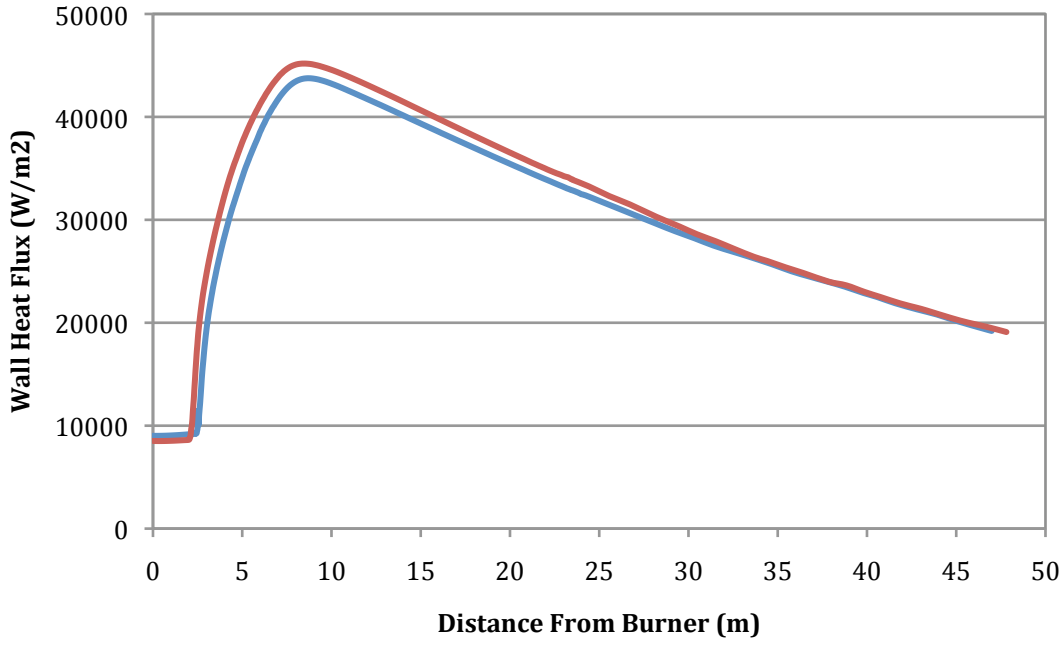

Figure 74: Wall heat flux profiles for 36.5% (■) and 41.1% (■) total primary air.

The temperature profiles are very similar throughout the kiln, however, there is a increase of approximately 200K in the temperature spike close to burner created by the early oil combustion. This increase in temperature close to the burner appears to have assisted the flame in providing a greater heat flux to the walls in the first half of the kiln. Ultimately it appears that leaving the airflow through the burner pipe unchanged is the most efficient mode of operation.

10 Conclusions and Recommendations

McDonalds Lime operate two large scale rotary lime kilns at their production site in Otorohanga, New Zealand. The work presented in this thesis investigates the performance of Kiln Two using Computational Fluid Dynamics. For many years Kiln Two has been fired solely with pulverised coal, however a waste oil firing system has recently been added in an attempt to reduce fuel costs and the environmental impact of the operation. McDonalds Lime felt CFD was an ideal tool for investigating the performance of this new system and ultimately improving the operating efficiencies of both the oil and coal fired systems. CFD allows for an in depth study of the combustion characteristics in Kiln Two while leaving everyday operations completely unaffected.

Prior to investigating the combustion characteristics of Kiln Two at McDonald's Lime a validation study was undertaken to investigate the performance of the commercial CFD code, FLUENT, for numerically modelling combustion applications. The validation study was based on the International Flame Research Foundations No.1 Furnace, with comparisons made between measured and numerical data. More specifically, the validation study focussed on the performance of different combustion chemistry, devolatilisation, and particle size distribution sub-models.

The validation study found that the species transport approach to combustion chemistry better replicated the measured data of the IFRF Furnace than the Mixture Fraction/PDF approach. The Mixture Fraction/PDF approach was, however, chosen as the model of choice for future modelling due to its computational efficiency. The constant rate devolatilisation model was found to be more accurate than the single rate model, and injecting multiple uniform sized injections was superior to using a Rosin Rammler particle size distribution. Overall, however, it was felt that FLUENT would be a suitable model for investigating the combustion characteristics of Kiln Two.

The first stage of the modelling for McDonald's Lime involved the creation of an accurate CAD model of Kiln Two, and the compilation of all the necessary operating parameters needed to perform a numerical simulation. This involved the extraction of data from existing production logs, as well as installation of new equipment for measuring various temperatures and pressures. It was initially intended that all modelling would be undertaken using a three-dimensional domain, however it soon became apparent that this was an unrealistic aim given the time available. Three-dimensional simulations require a lengthy computational time and divergence of some models was also encountered. As a result, two-dimensional modelling was investigated as an alternative. After considering the accuracy of the results, and with the focus of the work being on analysing trends as opposed to quantitative numbers, it was felt that two-dimensional modelling would be a much wiser alternative.

10.1 Coal Combustion

The initial task required by McDonald's Lime was to investigate aspects of the original coal fired system. This work involved simulating the average, or control, operating conditions, before making slight adjustments to a specific parameter and then analysing the affect this has on the combustion characteristics, specifically temperature and heat flux. While some results simply supported existing theories and observations presented in the literature review, a series of conclusions were drawn and are listed below.

- The recirculation of combustion gases, generated by a high primary air momentum, takes place much closer to the burner outlet than where ash rings form. Consequently, optimising the primary air momentum to prevent flame impingement will not assist in the reduction of ash rings.
- Cold air that leaks in through the firing hood, and lowers the secondary air temperature, has a negative impact on the overall kiln efficiency.
- Small changes to the primary air temperature are unlikely to have any significant impact on the operation of Kiln Two.

- A higher coal flow rate will increase the back end temperature, however changes to the peak flame temperature will be minimal.

10.2 Oil Combustion

The second task was to investigate the performance of the waste oil firing system recently added to Kiln Two. Here different oil flow rates were compared to the original coal fired system and the effects of different primary air rates were also analysed. The conclusions from the oil combustion investigations are as follows:

- The waste oil burns with a much higher peak temperature than pulverised coal.
- Operating the kiln with a 25% thermal substitution of waste oil provides the highest kiln temperature and heat flux to the limestone bed.
- As the oil flow rate is increased above 25% the efficiency drops. It is thought this is caused by significant competition for oxygen in the near burner region and the large droplets generated by the Laval nozzle.
- When the pulverised coal flow rate is lowered for the introduction of waste oil, the kiln operates most efficiently when the primary air flow through the bruner pipe is left at is original value.

10.3 Recommendations

To assist McDonald's Lime utilise the findings of the presented research project, a number of recommendations have been made to the company.

- The seal around the firing hood door should be improved in an effort to stop leakage of ambient air into the system. This will increase the secondary air temperature meaning less coal is required to achieve the same heat flux to the limestone bed.
- When the need arises to increase the firing zone temperature, the kiln operators should focus their efforts on increasing the secondary air

temperature, rather than increasing the coal flow rate which will simply increase the back end temperature.

- The true amount of excess air passing through the kiln should be quantified and the kiln operators should then focus on operating the kiln at the optimum level. This will provide adequate air ensuring that complete combustion occurs, without the loss of energy through the heating of unnecessary air.
- Investigations into the cause of ash ring formation should focus on aspects other than primary air momentum.
- A 25% thermal substitution of waste oil is the most efficient way in which to operate Kiln Two.
- McDonald's Lime should continue researching the operation of Kiln Two using Computational Fluid Dynamics. It is felt that there are many more improvements that could be made.

11 Future Work

The project presented in this thesis has involved a significant amount of time learning how to perform CFD simulations that include the combustion of pulverised coal and oil. As this project was also the first step in CFD modelling for McDonald's Lime, and involved the initial compilation of operating conditions, there is significant scope for further work investigating the operation of Kiln Two using Computational Fluid Dynamics. Some suggestions for future work are listed below:

- Investigate further why inaccuracies were seen when using a Rosin Rammler particle size distribution.
- Perform additional modelling using the three-dimensional domain. This will allow greater investigation into the impact of the firing hood, cooler and transfer chute on the kiln aerodynamics. It would also be beneficial to compare the results of two and three dimensional oil combustion simulations.
- Investigate the combustion characteristics of differing oil flow rates, while keeping the droplet size constant.
- Investigate the effects of firing Kiln Two using other waste fuels such as plastic and biomass.
- Investigate the characteristics of burners that include both axial and swirling air and see if these have any benefits over a burner that has simply one or the other, as was investigated in the current project.
- Develop a model that incorporates both the physical and chemical presence of the reacting limestone bed.
- Perform additional validation of the numerical results against operating conditions of the real kiln. A greater amount of validation will be possible as the complexity of the model increases.
- Perform an investigation to determine the waste oil firing setup required to match the temperature and heat flux profiles of the original coal firing system.

12 References

Alyaser, A. H. (1998). *Fluid Flow and Combustion in Rotary Kilns.* Thesis. University of British Columbia.

ANSYS, I. Gambit.

ANSYS, I. (2008). Tutorial: Coal combustion with Eddy Break Up (EBU) Model.

Badzioch, S., & Hawksley, P. G. W. (1970). Kinetics of Thermal Decomposition of Pulverized Coal Particles. *Ind. Eng. Chem. Process Des. Develop. , 9*(4), 521-530.

Barr, P. V., Watkinson, A. P., & Brimacombe, J. K. (1989). A heat transfer model for the rotary kiln .1. Pilot kiln trials. *Metallurgical Transactions B, Proces Metallurgy, 20*(3), 391-402.

Baum, M. M., & Street, P. J. (1971). Predicting the Combustion Behaviour of Coal Particles. *Combustion Science and Technology, 3*(5), 231-243.

Borghi, R., & Destriau, M. (1998). *Combustion and Flames: Chemical and Physical Principals* (R. Turner, Trans.). Paris: Editions Technip.

Bosoaga, A., Panoiu, N., Mihaescu, L., Backreedy, R. I., Ma, L., Pourkashanian, M., et al. (2006). The combustion of pulverised low grade lignite. *Fuel, 85*, 1591-1598.

Bui, R. T., Simard, G., Charette, A., Kocaefe, Y., & Perron, J. (1995). Mathematical Modelling of the Rotary Coke Calcining Kiln. *The Candian Journal of Chemical Engineering, 73*(August 1995), 534-545.

Burgerscentrum, J. M. 2005, personal communication,2005.

Craya, A., & Curtet, R. (1955). On the Spreading of a Confined Jet. *Comptes-Rendus Acad. des Sciences*(241), 611-622.

Cresswell, A. (1970). Flame shape control in rotary cement kilns. *Cement Technology, May/June*, 92-93.

Eastwick, C. N., Pickeing, S. J., & Aroussi, A. (1999). Comparisons of two commercial computational fluid dynamics codes in modelling pulverised coal combustion for a 2.5 MW burner. *Applied Mathematical Modelling, 23*, 437-446.

FCT. (1997a). *McDonald's Lime Limited Kiln Two Coal Firing System Assesment*.

FCT. (1997b). *McDonald's Lime Limited Physical and Mathematical Model Study of Rotary Lime Kiln*.

Field, M. A. (1969). Rate of Combustion of Size-Graded Fractions of Char from a Low Rank Coal between 1200K - 2000K. *Combustion and Flame, 13*, 237-252.

FLUENT, I. (2006). *Fluent 12.0 User Guide*: ANSYS.

Garnick, R. H. (1963). Gas and Oil Firing of Rotary Kilns. *Materials Processing, 4*(6), 29-32.

Genetti, D., & Fletcher, T. H. (1999). Development and Application of a Correlation of C NMR Chemical Structural Analyses of Coal Based on Elemtntal Composition and Volatile Matter Content. *Energy & Fuels, 13*, 60-68.

Georgallis, M. (2004). *Mathematical Modelling of Lime Kilns.* Thesis. University of British Columbia.

Gorog, J. P., & Adams, T. N. (1987, January 11-16 1987). *Design and Performance of Rotary Lime Kilns in the Pulp and Paper Industry Part 3: How Flame Characteristics and Product Coolers Affect Lime Kiln Performance.* Paper presented at the Kraft Recovery Operations, Orlando, FL.

He, P., Salcudean, M., Gartshore, I., & Nowak, P. (1996). Multigrid Calculation of the Fluid Flows in Complex 3D Geometries using Curvilinear Grids. *Computers and Fluids, 25*(4), 395-419.

Helton, D. (1996). Appendix C: Oil Behaviour, Pathways, and Exposure. In: Injury Assessment Guidance Document for Natural Resource Damage Assessment Under the Oil Pollution Act of 1990. In N. D. A. a. R. Program (Ed.). Silver Spring, MD.

Kocaefe, Y., Simard, G., Bui, R. T., Charette, A., Perron, J., & Potocnik, V. (1992). Anallyzing the Heat Transfer in a Coke Calcining Kiln. *Light Metals*, 627-632.

Launder, B. E., & Sharma, B. I. (1974). Application of the energy-dissipation model or turbulence to the calculation of flow near a spinning disc. *Letters in Heat and Mass Transfer, 1*(2), 131-138.

Magnussen, B. F., & Hjertager, B. H. (1976). On mathematical models of turbulent combustion with the special emphasis on soot formation and combustion. In *International Symposium on Combustion*. Vol. 16, (The Combustion Institute).

Malalasekera, W., & Versteeg, H. K. (1995). *An Introduction to Compuational Fluid Dynamics*. Harlow: Pearson Education Limited.

Moles, F. D., Watson, D., & Lain, P. B. (1973). Paper 6: The aerodynamics of the rotary cement kiln. *Journal of the Institute of Fuel, 389*, 353-361.

Mullinger, P. J. (1987). Rotary kiln coal firing part II: Burner design. *ZKG International, 40*(5), 259-294.

Pai, B. R., Richter, W., & Lowes, T. M. (1975). Flow and Mixing in Confined Axial Flows. *Journal of the Institute of Fuel*, 185-196.

Peters, A. A. F., & Weber, R. (1996). Mathematical Modelling of a 2.4MW Swirling Pulverized Coal Flame. *Combustion Science and Technology, 122*, 131-182.

Polacsek, R. (1992). Advantages of Co-Firing Gas and Pulverized Solid Fuel in a Rotary Lime Kiln. *Industrial Heating*, 24-27.

Pugmire, R. J., Solum, M. S., & Grant, D. M. (1992). Chemical Percolation Model for Devoaltilization. 3. Direct Use of C NMR Data To Predict Effects of Coal Type. *Energy & Fuels, 6*, 414-431.

Ruhland, W. (1967). Investigatin of flames in the cement rotary kiln. *Journal of the Institute of Fuel, 40*(313), 69-75.

Sahajwalla, V., Eghlimi, A., & Farrell, K. (1997). Numerical Simulation of Pulverised Coal Combustion. In *Inter Conf on CFD in Mineral and Metal Processing Generation*. `.

SHARC. Harpoon. Manchester.

Wang, S., Lu, J., Li, W., Li, J., & Hu, Z. (2006). Modelling of pulverised coal combustion in cement rotary kilns. *Energy & Fuels, 20*(6), 2350-2356.

Weber, R., Dugue, J., Sayre, A., & Visser, B. M. (1992). *Quarl Zone Flow Field and Chemistry of Swirling Pulverized Coal Flames: Measurements and Computations.* Paper presented at the Tweenty-Fourth Symposium (International) on Combustion.

Weber, R., Peters, A. A. F., Breithaupt, P. P., & Visser, B. M. (1995). Mathematical Modelling of Swirling Flames of Pulverised Coal: What Can Combustion Engineers Expect From Modeling? *Journals of Fluids Engineering, 117*, 289-297.

Wikipedia (2009). *Rotary Kiln*. Retrieved 16th March. 2008

Williams, A., Pourkashanian, M., & Jones, J. M. (2001). Combustion of pulverised coal and biomass. *Progress in Energy and Combustion Science, 27*, 587-610.

13 Appendices

13.1 Appendix A1: Primary Air Mass Flow Calculation

Primary Air Mass Flow		
Diff Pressure	474.1	mm H_20
D_1	437	mm
D_2	199	mm
Air Temp	64.72	ºC
Water Temp	25	ºC
Vapour Flow Rate	0.1702	kg/s
Velocity	19.53	m/s
Density Vapour	0.058103803	kg/m^3
Density Air	1.0358	kg/m^3
Denisty air & vapour	1.093903803	kg/m^3
Density Water	998	kg/m^4
A_1	0.149986702	m^2
A_2	0.031102553	m^3
P	4641.619158	pa
V_1	19.52755638	m/s
FOW RATE AIR ONLY m	**3.033727459**	**kg/s**

13.2 Appendix A2: Stoichiometric Combustion Analysis

Stoichiometric Combustion Analysis

Proximate Analysis -Environ Landfill coal

	Wt% wet	Wt% dry	Wt% DAF
Volatiles	39.30	49.2%	54.1%
Char	33.30	41.7%	45.9%
Ash	7.20	9.0%	
Moisture	20.20		
		Gross CV	21.62 MJ/kg

Ultimate Analysis

	Wt % (DAF)
C	74.88%
H	5.23%
O	18.31%
N	1.27%
S	0.32%

Stoichiometric Air/Fuel Ratio

	Mass / kg coal	Equation	Required O_2 (kg)
C	0.748774982		1.997
H	0.052276606		0.418
O	0.183064472		-0.183
N	0.012663106		to products
S	0.003220834		0.003

Oxygen to completely combust 1 kg coal 2.235 kg

Mass fraction O_2 in air

	Vol. fraction	Weight 1 mole air	Mass Fraction
O2	0.21	6.72	0.233
N2	0.79	22.12	0.767

Air Required 9.592314886 kg

Stoich Air/Fuel Weight Ratio 9.59 : 1

Burnout Stoichiometric Ratio

In 1kg Coal	34.344638%	Char
	0.343446376	kg
Oxygen Required	0.916	kg
Ratio	2.667	:1

13.3 Appendix A3: Flow Characteristics

Flow Characteristics			
Coal Flow Rate	**Mass Flow Rate - RAW**	1.077	kg/s
	DRY	0.859	kg/s
Primary Air	**Mass Flow Rate**	3.006	kg/s
	Temperature	337.72	K
	Inlet Area	0.08895	m^2
	Density Air	1.0358	kg/m^3
	Velocity	32.625	m/s
	Sensible Heat Addition	0.120	MW
Cold Air Inflow	**Velocity**	0	m/s
	Temperature	298	K
	Density	1.17	kg/m^3
	Area	0.196	m^2
	Mass Flow Rate	0	kg/s
Hot Air Outflow	**Mass Flow Rate**	2.500	kg/s
Cooler Inflow	**Total Cooler Flow Rate**	8.56	kg/s
	Temperature	712	K
	Density	0.4895	
	Area	8.76	m^2
	Velocity	2.00	m/s
Secondary Air	**Mass Flow Rate**	6.060	kg/s
	Temperature	712	K
	Sensible Heat Addition	2.7863	MW
	Total Air through Kiln	9.066	kg/s
	Stoichiometric Air	8.244	kg/s
	Excess Air	10.0%	
	PA% of Stoiciometric Air	36.5%	

13.4 Appendix A4: Water Vapour Effects

Water Vapour Effects		
Primary Air	3.006	kg/s
Secondary Air	6.06	kg/s
Raw Coal Rate	1.077	kg/s
Firing Pipe	337.72	K
Back End	1281	K
Cp vapour	2.08	kJ/kg
Cp liquid	4.1813	kJ/kg
Initial coal moisture	20.20%	
Moisture removed by mill	15.82%	
Moisture remaining	4.38%	
Moisture in dried coal	5.20%	
Vapour Flow Rate	0.170	kg/s
Liquid Flow Rate	0.047	kg/s
Vapour Heating Energy	334.2921233	kW
Liquid Heating Energy	186.0551812	kW
Total	520.3473045	kW
% Total Energy Output	2.54%	